KONSTANTINA-MARIA TRIANTAFYLLOU

SCHOOL OF MECHANICAL ENGINEERING

Development of a computer code for the calculation of efficiency correction factors due to self-attenuation in γ-spectroscopic analysis of NORM

Section: Nuclear Engineering

Supervisor: Prof. Marios J Anagnostakis

Athens 2024

ΚΩΝΣΤΑΝΤΙΝΑ-ΜΑΡΙΑ ΤΡΙΑΝΤΑΦΥΛΛΟΥ

ΣΧΟΛΗ ΜΗΧΑΝΟΛΟΓΩΝ ΜΗΧΑΝΙΚΩΝ

Ανάπτυξη μεθοδολογίας και λογισμικού για τη διόρθωση αυτοαπορρόφησης κατά τη γ-φασματοσκοπική ανάλυση δειγμάτων NORM

Τομέας: Πυρηνικής Τεχνολογίας

Επιβλέπων: Μάριος Ι. Αναγνωστάκης, Καθηγητής ΕΜΠ

Αθήνα 2024

--- κενή σελίδα ---

Solemn Declaration for plagiarism and copyright theft:

I have read and understood the plagiarism rules and how to properly cite the sources contained in the Diploma Thesis writing guide. I declare that, as far as I know, the content of this Thesis is the product of my work and there are references to all the sources I have used.

The views and conclusions contained in this Thesis are those of the author and should not be construed as representing the official positions of the School of Mechanical Engineering or the National Technical University of Athens.

Full Name: Konstantina-Maria Triantafyllou

Υπεύθυνη δήλωση για λογοκλοπή και για κλοπή πνευματικής ιδιοκτησίας:

Έχω διαβάσει και κατανοήσει τους κανόνες για τη λογοκλοπή και τον τρόπο σωστής αναφοράς των πηγών που περιέχονται στον οδηγό συγγραφής Διπλωματικών Εργασιών. Δηλώνω ότι, από όσα γνωρίζω, το περιεχόμενο της παρούσας Διπλωματικής Εργασίας είναι προϊόν δικής μου εργασίας και υπάρχουν αναφορές σε όλες τις πηγές που χρησιμοποίησα.

Οι απόψεις και τα συμπεράσματα που περιέχονται σε αυτή τη Διπλωματική εργασία είναι του συγγραφέα και δεν πρέπει να ερμηνευθεί ότι αντιπροσωπεύουν τις επίσημες θέσεις της Σχολής Μηχανολόγων Μηχανικών ή του Εθνικού Μετσόβιου Πολυτεχνείου.

Ονοματεπώνυμο: Τριανταφύλλου Κωνσταντίνα-Μαρία

ΠΡΟΛΟΓΟΣ

Η Διπλωματική Εργασία εκπονήθηκε στον Τομέα Πυρηνικής Τεχνολογίας της Σχολής Μηχανολόγων Μηχανικών του ΕΜΠ. Θα ήθελα να ευχαριστήσω τον Δρ. Μ.Ι. Αναγνωστάκη, Καθηγητή του ΕΜΠ, για την καθοδήγηση και την διάθεση να μοιραστεί την εμπειρία και τις γνώσεις του καθ' όλη την διάρκεια της έρευνας που πραγματοποιήθηκε για την περάτωση της παρούσας Διπλωματικής Εργασίας. Επίσης, θα ήθελα να ευχαριστήσω τους Υποψήφιους Διδάκτορες του Τομέα Πυρηνικής Τεχνολογίας Κωνσταντίνο Κανούτο και Αναστασία Μηλιώνη για την πολύτιμη βοήθειά τους με τις γνώσεις τους πάνω σε θέματα ακτινοβολίας και προσομοιώσεων Monte-Carlo με τον κώδικα PENELOPE.

Table of Contents

List of Abbreviations

NEL-NTUA	Nuclear Engineering Laboratory of the National Technical University of Athens
ECF	Efficiency Correction Factor
EID	Effective Interaction Depth
NORM	Naturally Occurring Radioactive Material
LEGe	Low Energy Germanium Detector
PENELOPE	PENetration and Energy Loss of Positrons and Electrons
GUI	Graphical User Interface
Soil 3%	Soil with 3% moisture
RM	Red Mud
FA	Fly Ash
PG	Phosphogypsum
LS	Lead Slag
GS	Granulated Slag
SFS	Shaft Furnace Slag
4M HCl	4M HCl solution (calibration material)
ΔΕ	Διπλωματική Εργασία

Abstract

The main objective of this thesis has been the calculation of self-absorption correction factors in gamma-spectroscopy analysis of Naturally Occurring Radioactive Materials (NORM). The research focused on the upgrade of a Matlab code for the calculation of the Efficiency Correction Factor (ECF) for NORMs, with the "Integral Method". Several parameters affecting this correction factor were studied, with the most important being the Effective Interaction Depth (EID), inside the detector, which is considered crucial for calculating the ECF.

Environmental radioactivity analysis with gamma-spectroscopy remains a complex procedure due to the numerous parameters that affect the detectors' efficiency. Some of these parameters include the - often unknown - sample composition, as well as the sample's volume and density. The major obstacle, however, is the self-absorption phenomenon, which is particularly intense for NORMs due to their high density and the large percentage of high-Z elements they contain. Therefore, an ECF for the accurate analysis of these samples is necessary.

This study investigated thoroughly the value of the Effective Interaction Depth (EID) and its variation with energy for the XtRa detector, operating at NEL-NTUA[1], using Monte Carlo simulations. The plot created was integrated into the Matlab code. Moreover, Monte Carlo simulations were conducted to calculate the ECFs and to compare the results with the outcomes from the Matlab code. The Matlab code calculates the ECF with the "Integral Method", which from previous studies showed promising results. This method relies on calculating two integrals proportional to the detector's efficiency: one for the calibration standard material and another for the analyzed sample material. The ratio of these two integrals gives us the ECF, which accounts for the differing self-absorption properties between the calibration source material and the sample material being analyzed. Moreover, the standalone application of the Matlab code that had been previously developed was upgraded to make it more user-friendly.

The entire endeavor led to significant improvements in the code. More specifically, the percentage differences between the results derived from the Matlab code and the PENELOPE simulations for most of the materials, especially in the low energy range below 200 keV, are almost negligible, while the highest percentage difference is 15% at 1000 keV for the highest density material Lead Slag.

[1] Nuclear Engineering Laboratory – National Technical University of Athens

Εκτενής Περίληψη

Η παρούσα Διπλωματική Εργασία (ΔΕ), εκπονήθηκε στο Εργαστήριο Πυρηνικής Τεχνολογίας του Εθνικού Μετσοβίου Πολυτεχνείου (ΕΠΤ-ΕΜΠ), και το θέμα που πραγματεύεται είναι η ανάπτυξη ενός κώδικα σε Matlab για την εύρεση συντελεστών διόρθωσης λόγω του φαινομένου της αυτοαπορρόφησης των φωτονίων, τα οποία εκπέμπονται από ένα δείγμα, κατά τη γ-φασματοσκοπική ανάλυση. Συγκεκριμένα, η γ-φασματοσκοπία αποτελεί μία μη-καταστροφική μέθοδο ανάλυσης που πραγματοποιεί ποιοτικό και ποσοτικό προσδιορισμό των ραδιενεργών ισοτόπων που περιέχονται σε ένα δείγμα, ανάλογα με τις ακτίνες-γ που εκπέμπουν. Ωστόσο, παρά την ευκολία που προσφέρει αυτή η μέθοδος ανάλυσης, παρουσιάζει και προβλήματα τα οποία χρήζουν ιδιαίτερης προσοχής, προκειμένου να επιτευχθεί υψηλή ακρίβεια κατά την ανάλυση του δείγματος. Ένα από τα βασικότερα εμπόδια στην ανίχνευση των φωτονίων που εκπέμπονται από το δείγμα, ιδιαίτερα στις χαμηλές ενέργειες, είναι η υψηλή εξασθένιση που παρουσιάζουν, λόγω της απορρόφησης τους από το ίδιο το δείγμα [1].

Το φαινόμενο της αυτοαπορρόφησης που αναφέρθηκε παραπάνω, έχει ως αποτέλεσμα κάποια φωτόνια να μην φθάνουν ποτέ στον ανιχνευτή προς ανίχνευση. Αυτή η εξασθένιση εξαρτάται από ποικίλους παράγοντες, όπως είναι η σύσταση και η πυκνότητα του δείγματος, ο όγκος του, η ενέργεια των φωτονίων που εκπέμπει, καθώς και η απόσταση του δοχείου που περιέχει το δείγμα, από τον ανιχνευτή. Όπως γίνεται αντιληπτό, το ποσοστό των φωτονίων που απορροφούνται ή σκεδάζονται μέσα στο δείγμα διαφέρουν σημαντικά, ανάλογα με την προέλευση του δείγματος. Επομένως, η πειραματικά προσδιορισμένη απόδοση του ανιχνευτή βάσει της πηγής βαθμονόμησης, είναι διαφορετική από την απόδοση του ανιχνευτή για ένα άλλο δείγμα διαφορετικής σύστασης. Το γεγονός αυτό οδηγεί στην ανάγκη της εύρεσης ενός συντελεστή διόρθωσης της απόδοσης ανίχνευσης των φωτονίων (Efficiency Correction Factor, ECF), ο οποίος θα υπολογίζεται για κάθε διαφορετικό δείγμα προς ανάλυση. Έτσι, συνδυαστικά με την απόδοση του ανιχνευτή που έχει προσδιοριστεί για την πηγή βαθμονόμησης, υπολογίζεται η εκάστοτε απόδοση του ανιχνευτή για το δείγμα.

Στην παρούσα ΔΕ δόθηκε έμφαση στον υπολογισμό συντελεστών διόρθωσης λόγω της αυτοαπορρόφησης για φυσικά ραδιενεργά υλικά τύπου NORM (Naturally Occurring Radioactive Materials). Φυσικά ραδιενεργά υλικά υπάρχουν παντού στο περιβάλλον, όπως στο έδαφος, στα πετρώματα, στο νερό, στον αέρα και τη βλάστηση. Στις περισσότερες ανθρώπινες δραστηριότητες που περιλαμβάνουν ορυκτά υλικά τύπου NORM, τα επίπεδα έκθεσης στα φυσικά ραδιενεργά ισότοπα δεν είναι σημαντικά υψηλότερα σε σχέση με τα φυσιολογικά επίπεδα. Ωστόσο, ορισμένες βιομηχανικές διεργασίες, όπως είναι η εξόρυξη και η καύση λιγνίτη, η εξόρυξη και επεξεργασία βωξίτη για την παρασκευή αλουμινίου, η βιομηχανία φωσφορικών λιπασμάτων και η οικοδομική βιομηχανία μπορούν να οδηγήσουν σε επαύξηση της ραδιοβιολογικής επιβάρυνσης των εργαζομένων ή του κοινού πληθυσμού. Αυτό έχει ως αποτέλεσμα, να είναι αναγκαίος ο ακριβής προσδιορισμός των

ραδιενεργών ισοτόπων στα δείγματα αυτά, καθώς τα επίπεδα της ραδιενέργειας τους υπόκεινται σε κανονισμούς και συγκεκριμένη νομοθεσία [2]. Ένα εμπόδιο στην ακριβή ανάλυση αυτών των δειγμάτων αποτελεί η έντονη αυτοαπορρόφηση που παρουσιάζουν τα φωτόνια που εκπέμπουν. Αυτό οφείλεται στην μεγάλη πυκνότητα και την υψηλή περιεκτικότητά τους σε στοιχεία με μεγάλο ατομικό αριθμό Z, καθώς και στον μεγάλο όγκο που συνήθως έχουν αυτά τα δείγματα. Επομένως, κρίνεται απαραίτητος ο υπολογισμός συντελεστών διόρθωσης λόγω της αυτοαπορρόφησης των φωτονίων κατά την ανάλυση δειγμάτων υλικών τύπου NORM.

Για τον υπολογισμό των συντελεστών διόρθωσης λόγω αυτοαπορρόφησης κατά την ανάλυση περιβαλλοντικών δειγμάτων, έχει αναπτυχθεί στο ΕΠΤ-ΕΜΠ από το 2017 [3] ένας κώδικας σε Matlab στα πλαίσια ΔΕ που πραγματοποιήθηκε – η μελέτη αυτή συνεχίστηκε σε επόμενη ΔΕ, που πραγματοποιήθηκε το 2021 [4]. Η μέθοδος που χρησιμοποιήθηκε για τον υπολογισμό των συντελεστών διόρθωσης έχει προταθεί από τον [5] και στηρίζεται σε εκτίμηση συντελεστή αναγωγής της απόδοσης από το υλικό της πηγής βαθμονόμησης στο υλικό του αναλυόμενου δείγματος, λόγω της διαφορετικής αυτοαπορρόφησης που παρουσιάζουν. Η μέθοδος βασίζεται στον υπολογισμό ενός διπλού ολοκληρώματος (“Integral Method”) που υπολογίζεται τόσο για την πηγή βαθμονόμησης όσο και για το υπό ανάλυση δείγμα. Ο λόγος των δύο ολοκληρωμάτων είναι ο ζητούμενος συντελεστής διόρθωσης (ECF). Απαραίτητη προϋπόθεση για την εφαρμογή αυτής της μεθόδου είναι η γνώση της γεωμετρίας πηγής-ανιχνευτή, του ολικού γραμμικού συντελεστή εξασθένησης (μ) των υλικών της πηγής και του δείγματος, της γεωμετρίας του κυλινδρικού δοχείου του δείγματος, καθώς και του ενεργού βάθους αλληλεπίδρασης των φωτονίων μέσα στον ανιχνευτή (Effective Interaction Depth, EID). Το ενεργό βάθος αλληλεπίδρασης είναι προσέγγιση ότι ο συνολικός όγκος του ανιχνευτή υποκαθίσταται από ένα ιδεατό σημειακό ανιχνευτή που βρίσκεται μέσα στον πραγματικό ανιχνευτή, και εκεί απορροφώνται όλα τα φωτόνια μίας συγκεκριμένης ενέργειας. Επομένως, αυτό το μέγεθος αλλάζει ανάλογα με την ενέργεια των φωτονίων και για αυτό απαιτείται μελέτη για τον προσδιορισμό του.

Συγκεκριμένα, η πρώτη ΔΕ επικεντρώθηκε στο ενεργειακό εύρος από 40 έως 400 keV, καθώς οι ενέργειες πολλών χαρακτηριστικών φωτονίων που εκπέμπονται από τα υλικά NORM είναι κάτω από 400 keV, όπως ^{210}Pb (46.52 keV), ^{241}Am (59.54 keV), ^{234}Th (63.29 keV), ^{212}Pb (238 keV), ^{214}Pb (295 και 352 keV) και ^{228}Ac (338 keV). Το πρώτο βήμα αυτής της μελέτης ήταν ο υπολογισμός του μαζικού συντελεστή εξασθένισης (μ_m) για όλα τα υλικά NORM που μελετήθηκαν, τα οποία είναι: χώμα με 3% υγρασία, ερυθρά ιλύς (παραπροϊόν της επεξεργασίας βωξίτη), ιπτάμενη τέφρα, φωσφογύψος, τρία διαφορετικά είδη σκωρίας και νερό. Αυτός ο υπολογισμός έγινε με την βοήθεια του κώδικα MUPLOT[2], ο οποίος έχει αναπτυχθεί στο πανεπιστήμιο της Μπολόνια. Για τις ενέργειες για τις οποίες δεν υπολογίστηκε ο μαζικός συντελεστής εξασθένισης, αυτές υπολογίζονται μέσω μίας σχέσης της μορφής:

[2] Είναι διαθέσιμος στο website: http://shape.ing.unibo.it/html/muplot.htm

$$\boldsymbol{ln(\mu_m) = A \cdot (lnE)^2 + B \cdot ln(E) + C} \quad (1)$$

Όπως φαίνεται όμως και στο παρακάτω διάγραμμα η προσαρμογή της συνάρτησης αναδρομής στα δεδομένα που έχουν ληφθεί μέσω του κώδικα MUPLOT για το υλικό 4M HCl, δεν είναι ιδιαίτερα ικανοποιητική. Αντίστοιχες σχέσεις υπολογίστηκαν για όλα τα υλικά που αναλύθηκαν.

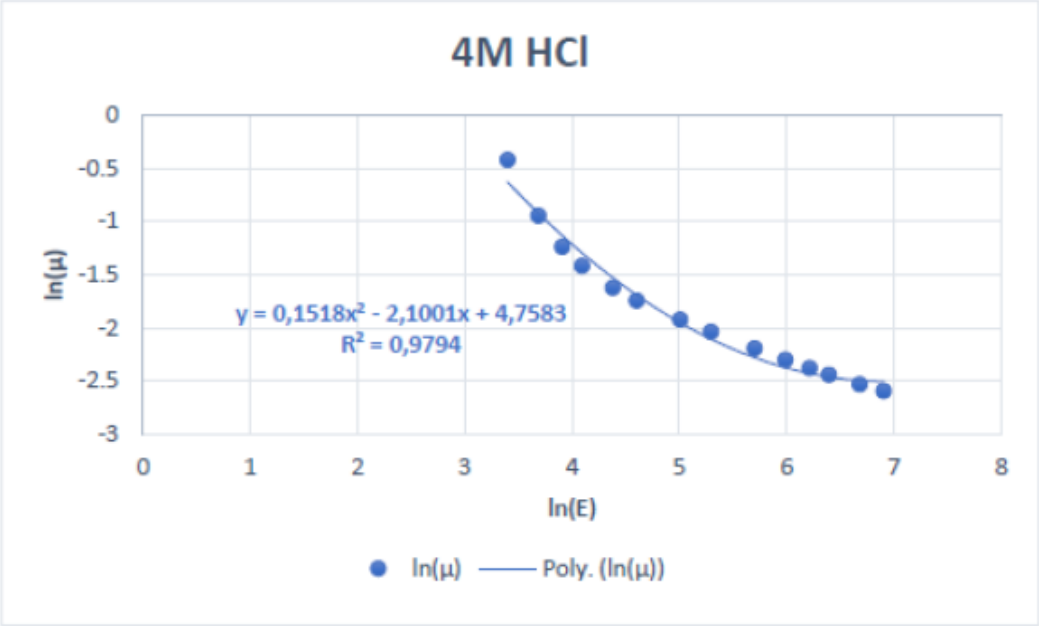

Σχήμα 1 Σχέση αναδρομής για το 4M HCl [3]

Στη συνέχεια, αναπτύχθηκε ο κώδικας σε Matlab για τον υπολογισμό των συντελεστών διόρθωσης ECF για τον ανιχνευτή του ΕΠΤ-ΕΜΠ LEGe[3]. Σε αυτή την έκδοση του κώδικα, ο χρήστης καλείται να δώσει τρία δεδομένα εισόδου, τα οποία είναι: η γεωμετρία του δείγματος, η ενέργεια των φωτονίων και το υλικό του δείγματος προς ανάλυση. Αναφορικά με την γεωμετρία του δείγματος, οι επιλογές που δίνει ο κώδικας είναι δύο τυποποιημένες κυλινδρικές γεωμετρίες που χρησιμοποιούνται στο ΕΠΤ-ΕΜΠ, οι γεωμετρίες “2” και “8”. Επιπλέον, η απόσταση από το δείγμα έως τον «ιδεατό σημειακό ανιχνευτή» θεωρείται σταθερή και ίση με 2 cm. Επομένως, αφού ο χρήστης εισάγει τα δεδομένα, το πρόγραμμα υπολογίζει μέσω των σχέσεων που προαναφέρθηκαν τους κατάλληλους μαζικούς συντελεστές εξασθένισης, και στη συνέχεια τα διπλά ολοκληρώματα που θα οδηγήσουν εν τέλει στον υπολογισμό του επιθυμητού συντελεστή διόρθωσης ECF.

Οι συντελεστές διόρθωσης λόγω αυτοαπορρόφησης ECF, εκτός του κώδικα Matlab, υπολογίστηκαν και μέσω προσομοιώσεων Monte-Carlo, και συγκεκριμένα με τον κώδικα

[3] **L**ow **E**nergy **Ge**rmanium detector

PENELOPE[4]. Με αυτό τον τρόπο ήταν εφικτό να συγκριθούν τα αποτελέσματα μεταξύ τους και να βγουν χρήσιμα συμπεράσματα σχετικά με την ακρίβεια του κώδικα Matlab. Στο παρακάτω διάγραμμα παρουσιάζονται οι αποκλίσεις που υπήρξαν από την σύγκριση των δύο μεθόδων για την κυλινδρική γεωμετρία “8” ύψους 1cm. Ειδικότερα στις χαμηλές ενέργειες και για τα υλικά υψηλής πυκνότητας, οι ποσοστιαίες διαφορές αγγίζουν το 60%. Επομένως, η διαδικασία υπολογισμού που ακολουθήθηκε σε αυτή την εργασία έχει αρκετά περιθώρια βελτίωσης. Συγκεκριμένα, ένας βασικός λόγος στον οποίο αποδόθηκαν οι μεγάλες αποκλίσεις μεταξύ των δύο μεθόδων, ήταν ότι οι βάσεις δεδομένων για τον υπολογισμό του μαζικού συντελεστή εξασθένισης (μ_m), που χρησιμοποιούν οι δύο μέθοδοι διαφέρουν μεταξύ τους. Επομένως, οι τιμές των συντελεστών αυτών που εν τέλει χρησιμοποιήθηκαν για τον υπολογισμό των συντελεστών διόρθωσης ECF, ήταν διαφορετικές. Ταυτόχρονα, έπρεπε να βελτιωθεί και η προσαρμογή της καμπύλης $\mu_m=f(E)$, καθώς όπως φαίνεται από το Σχήμα 1, δεν ήταν ιδιαίτερα επιτυχημένη. Ένα σημαντικό αποτέλεσμα που προέκυψε από αυτή την μελέτη είναι ότι συντελεστές διόρθωσης της εξασθένισης χρειάζονται και για ενέργειες μεγαλύτερες των 400 keV, καθώς οι τιμές που υπολογίστηκαν διαφέρουν της μονάδας για όλες τις ενέργειες και όλα τα υλικά.

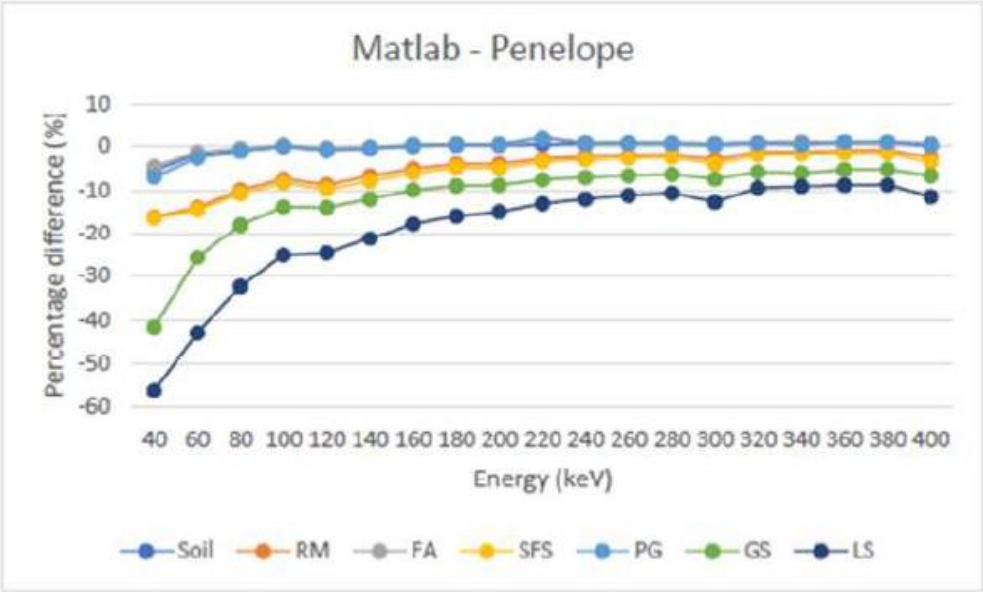

Σχήμα 2 Ποσοστιαίες διαφορές μεταξύ των αποτελεσμάτων από Matlab και PENELOPE[3]

Η ΔΕ που ακολούθησε [4], επικεντρώθηκε στις αδυναμίες που παρουσίαζε ο αρχικός κώδικας Matlab, καθώς και στην αναβάθμισή του. Αρχικά, υπολογίστηκαν οι τιμές των γραμμικών και μαζικών συντελεστών εξασθένισης για όλα τα υλικά που μελετήθηκαν με την βοήθεια του κώδικα προσομοιώσεων PENELOPE. Στη συνέχεια, οι τιμές που

[4] Τα αποτελέσματα που υπολογίζονται για τον συντελεστή διόρθωσης μέσω της προσομοίωσης θεωρούνται ακριβέστερα και για το λόγο αυτό θεωρούνται ως τιμές αμαφοράς.

υπολογίστηκαν χωρίστηκαν σε δύο ενεργειακές υπό-περιοχές, και σε κάθε μία προσαρμόστηκε μία συνάρτηση αναδρομής της ακόλουθης μορφής:

$$\boldsymbol{ln(\mu_m) = A \cdot (lnE)^3 + B \cdot (lnE)^2 + C \cdot \ln(E) + D} \quad (2)$$

Στο παρακάτω διάγραμμα φαίνονται ενδεικτικά οι συναρτήσεις που υπολογίστηκαν για το υλικό Lead Slag. Με τον παραπάνω υπολογισμό, έγινε εφικτή η πιο άμεση σύγκριση των αποτελεσμάτων του κώδικα Matlab με τις προσομοιώσεις που έγιναν με τον κώδικα PENELOPE, καθώς πλέον χρησιμοποιούν τα ίδια δεδομένα για τον μαζικό συντελεστή εξασθένισης (μ_m).

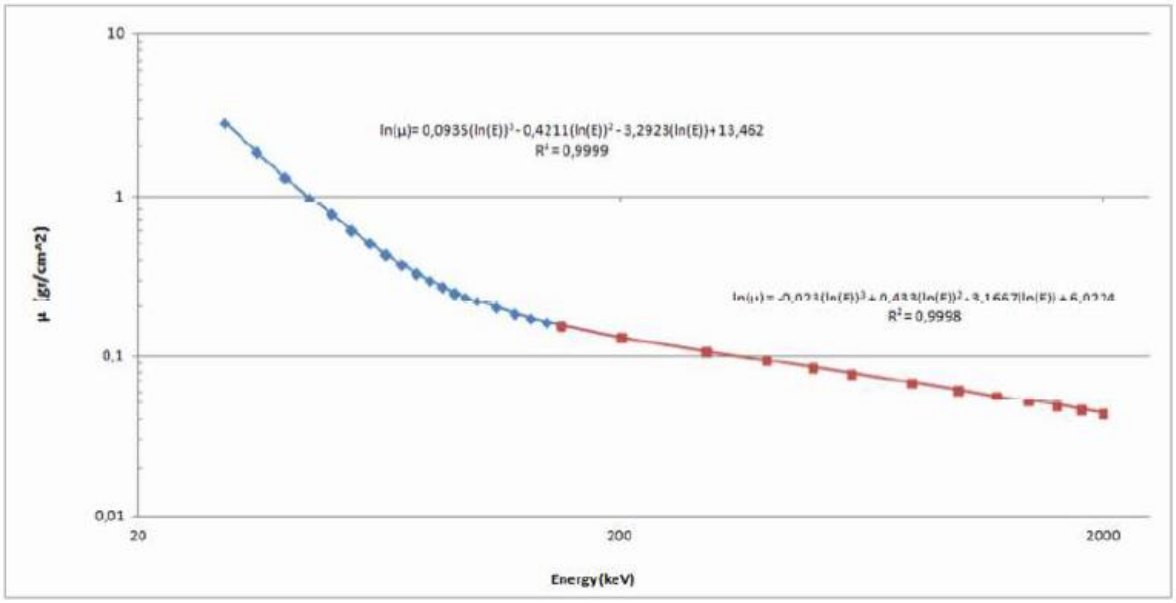

Σχήμα 2 Σχέση αναδρομής για την εύρεση του μαζικού συντελεστή εξασθένισης [4]

Μία άλλη αλλαγή που είχε γίνει στην ΔΕ αυτή ήταν η επέκταση της ενεργειακής περιοχής μέχρι τα 2000 keV. Στη συνέχεια, έγιναν αναβαθμίσεις στον κώδικα Matlab προκειμένου να παρέχει περισσότερη ελευθερία και ευελιξία στα δεδομένα που εισάγει ο χρήστης. Συγκεκριμένα, ο χρήστης πλέον έχει την δυνατότητα να επιλέξει την τιμή του ενεργού βάθους αλληλεπίδρασης d_e, καθιστώντας έτσι εύκολη την μελέτη της επίδρασης που έχει η τιμή αυτή στον υπολογισμό του ECF. Ταυτόχρονα, εκτός της επιλογής των τυπικών γεωμετριών “2” και “8”, υπάρχει η δυνατότητα κατασκευής οποιασδήποτε κυλινδρικής γεωμετρίας, με τον καθορισμό της ακτίνας και του ύψους αυτής. Επιπλέον, μία εξαιρετικά χρήσιμη αναβάθμιση του κώδικα ήταν η μετατροπή του σε “standalone” εφαρμογή, γεγονός το οποίο δίνει την δυνατότητα στον χρήστη να έχει την εφαρμογή για τον υπολογισμό του συντελεστή ECF, χωρίς να έχει εγκατεστημένο το Matlab στον υπολογιστή του, καθώς και χωρίς να διαθέτει γνώσεις προγραμματισμού. Το γραφικό περιβάλλον της εφαρμογής (GUI), παρουσιάζεται στην παρακάτω εικόνα.

Σχήμα 3 Το γραφικό περιβάλλον της "standalone" εφαρμογής Matlab [4]

Επομένως, στην ανανεωμένη έκδοση του κώδικα, ο χρήστης είχε τη δυνατότητα επιλογής της γεωμετρίας του δείγματος, της απόστασης μεταξύ του ιδεατού σημειακού ανιχνευτή και του δείγματος d, του υλικού προς ανάλυση, της πυκνότητας του υλικού, καθώς και της ενέργειας των φωτονίων. Αφού εισαχθούν αυτά τα δεδομένα, ο κώδικας υπολογίζει και εμφανίζει τον συντελεστή διόρθωσης της αυτοαπορρόφησης ECF, καθώς και τον ολικό μαζικό συντελεστή εξασθένησης των φωτονίων μ_m του υλικού του δείγματος προς ανάλυση.

Όσον αφορά τα αποτελέσματα που είχαν προκύψει από το βελτιωμένο κώδικα Matlab, αυτά παρουσίαζαν αισθητή βελτίωση σε σχέση με τα αποτελέσματα του αρχικού κώδικα. Πιο συγκεκριμένα, στο Σχήμα 4 παρουσιάζονται οι ποσοστιαίες διαφορές των αποτελεσμάτων που προέκυψαν από τον κώδικα Matlab και τις προσομοιώσεις Monte Carlo για την γεωμετρία "8" και τον ανιχνευτή LEGe. Διαπιστώνεται ότι η διαφορά για το υλικό με την μεγαλύτερη πυκνότητα (Lead Slag) στις χαμηλές ενέργειες, από 60% έπεσε στο 21%. Ομοίως και για τα υπόλοιπα υλικά, οι διαφορές είχαν μειωθεί αρκετά. Επιπλέον, επιβεβαιώνεται η ανάγκη ύπαρξης συντελεστή διόρθωσης για υψηλές ενέργειες, καθώς οι συντελεστές διόρθωσης ECF που υπολογίστηκαν δεν ήταν ίσοι με την μονάδα για κανένα υλικό και ενέργεια μέχρι τα 2000 keV. Επομένως, οι τροποποιήσεις που είχαν γίνει

κρίνονται επιτυχημένες, αφήνοντας ωστόσο περιθώρια βελτίωσης μέσω της μελέτης και άλλων παραμέτρων από τις οποίες επηρεάζεται ο υπολογισμός του συντελεστή διόρθωσης ECF.

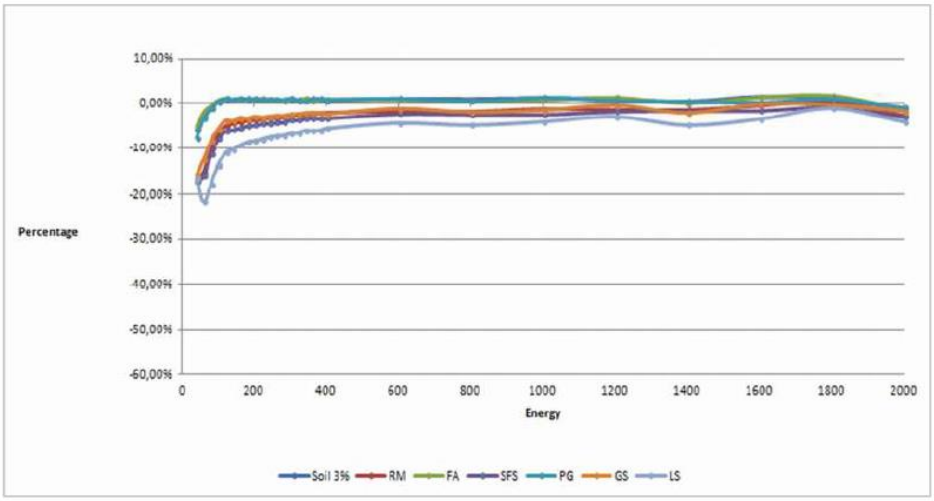

Σχήμα 4 Ποσοστιαίες διαφορές μεταξύ των αποτελεσμάτων από Matlab και PENELOPE [4]

Δεδομένης της ευκολίας που προσέφερε η ανάπτυξη της εφαρμογής για παραμετρική μελέτη των διαφόρων παραμέτρων, είχε διερευνηθεί και η επίδραση που έχει το ενεργό βάθος αλληλεπίδρασης (EID). Στο παρακάτω σχήμα παρουσιάζονται τα αποτελέσματα αυτής της μελέτης για E=1000 keV. Είναι φανερό ότι ειδικά για τα βαρύτερα υλικά η επίδραση είναι αρκετά έντονη, επομένως πρόκειται για μία παράμετρο που απαιτεί περαιτέρω διερεύνηση.

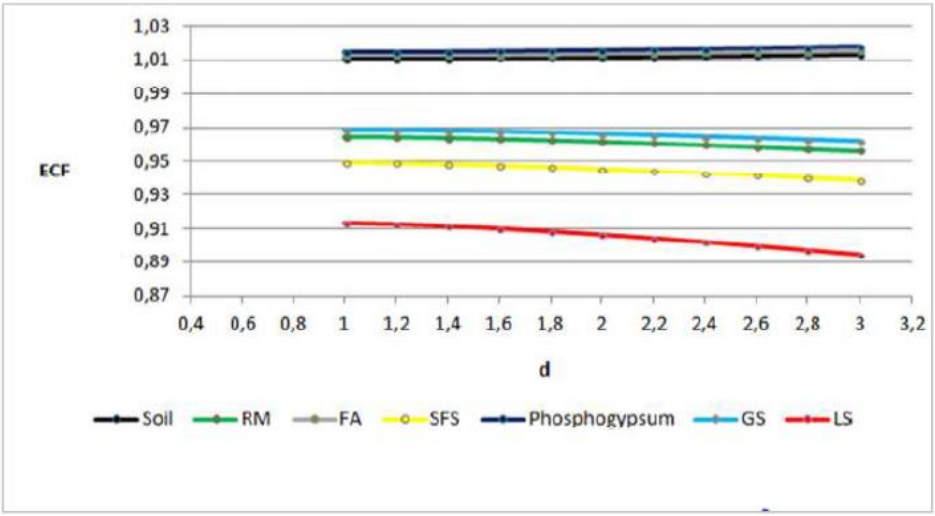

Σχήμα 5 Επίδραση του ενεργού βάθους αλληλεπίδρασης στον υπολογισμό του ECF για E=1000 keV [4]

Στην παρούσα Διπλωματική Εργασία, στο πλαίσιο της προσπάθειας για περαιτέρω βελτίωση του κώδικα, η έρευνα επικεντρώθηκε στην διερεύνηση της τιμής του ενεργού βάθους αλληλεπίδρασης (EID) για τον ανιχνευτή XtRa, ο οποίος είναι εγκατεστημένος στο ΕΠΤ-ΕΜΠ. Η μέθοδος που ακολουθήθηκε για τη μελέτη αυτή περιγράφεται αναλυτικά στα [1], [5]. Βασίζεται στην αρχή ότι ο ρυθμός **n** των καταμετρουμένων φωτονίων ενέργειας **E**, όταν η πηγή απέχει απόσταση **d** από το σημειακό ανιχνευτή, θα είναι ανάλογος του $\mathbf{1/d^2}$. Συγκεκριμένα, η τιμή του ενεργού βάθους αλληλεπίδρασης υπολογίστηκε με την βοήθεια προσομοιώσεων Monte-Carlo (κώδικας PENELOPE), για δέκα διαφορετικές ενέργειες: 40 keV, 50 keV, 100 keV, 150 keV, 200 keV, 250 keV, 300 keV, 350 keV, 500 keV, και 1000 keV. Για κάθε μία ενέργεια έγιναν εννιά προσομοιώσεις, σε κάθε μία εκ των οποίων η σημειακή πηγή τοποθετούνταν σε διαφορετική απόσταση από τον ανιχνευτή. Στη συνέχεια, έγινε κατάλληλη επεξεργασία των αρχείων των αποτελεσμάτων των προσομοιώσεων και προέκυψαν διαγράμματα της μορφής που φαίνεται στην παρακάτω εικόνα για την ενέργεια των 50 keV.

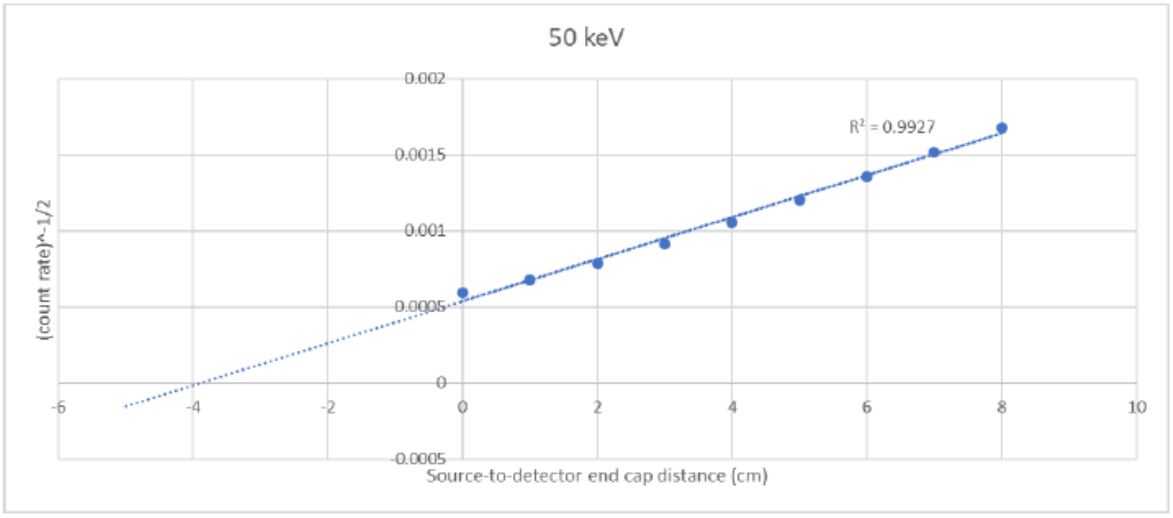

Σχήμα 6 Διάγραμμα για τον υπολογισμό του ενεργού βάθους αλληλεπίδρασης-50 keV

Το σημείο που η επέκταση της ευθείας αναδρομής τέμνει τον άξονα των τετμημένων αντιστοιχεί στην απόσταση του ιδεατού σημειακού ανιχνευτή από το σημείο αναφοράς που στην προκειμένη περίπτωση θεωρήθηκε η επιφάνεια από το καπάκι προπυλενίου του ανιχνευτή. Επομένως, αφαιρώντας την απόσταση από το σημείο αναφοράς έως την επιφάνεια του ανιχνευτή που είναι γνωστή για τον ανιχνευτή XtRa, προκύπτει η τιμή του ενεργού βάθους αλληλεπίδρασης d_e. Για την ενέργεια των 50 keV, αυτή υπολογίστηκε 2.97 cm. Ακολουθήθηκε η ίδια διαδικασία για όλες τις ενέργειες, και από τις τιμές του ενεργού βάθους αλληλεπίδρασης που προέκυψαν για κάθε ενέργεια, δημιουργήθηκε το ακόλουθο διάγραμμα συναρτήσει της ενέργειας.

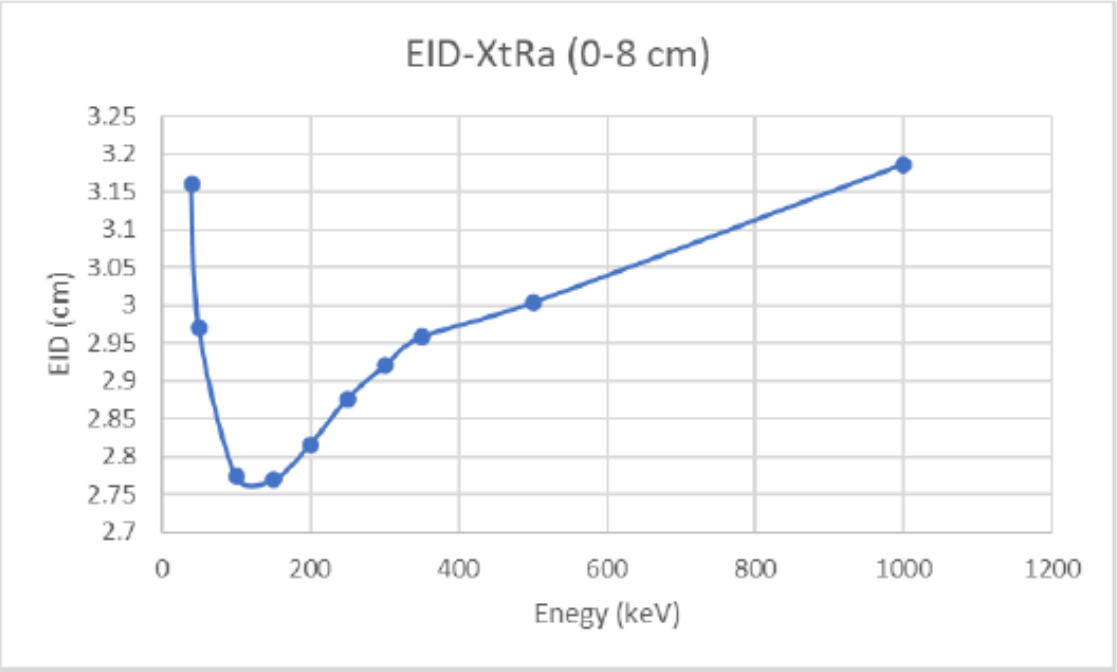

Σχήμα 7 Διάγραμμα του ενεργού βάθους αλληλεπίδρασης συναρτήσει της ενέργειας

Η μορφή του διαγράμματος στις χαμηλές ενέργειες είναι μη αναμενόμενη σε σχέση με αντίστοιχα διαγράμματα που έχουν βρεθεί στη βιβλιογραφία, τα οποία ωστόσο επικεντρώνονται ως επί το πλείστο σε ενέργειες μεγαλύτερες των 60 keV. Σύμφωνα με τη δημοσίευση [6], αυτή η συμπεριφορά προκύπτει εξαιτίας του πάχους του νεκρού στρώματος (dead layer) του ανιχνευτή, του οποίου η επιλογή, ιδιαίτερα στις χαμηλές ενέργειες, επηρεάζει πολύ την ανίχνευση των φωτονίων. Αυτό είναι ένα σημείο που αξίζει περαιτέρω διερεύνησης σε μελλοντική εργασία.

Προκειμένου να επαληθευτούν τα αποτελέσματα των προσομοιώσεων πραγματοποιήθηκε και πειραματικός προσδιορισμός του ενεργού βάθους αλληλεπίδρασης για τον ανιχνευτή XtRa. Η διαδικασία αυτή έγινε με σημειακή πηγή Αμερικίου-241 (^{241}Am) που εκπέμπει φωτόνια ενέργειας 59.54 keV, η οποία τοποθετήθηκε σε διάφορες αποστάσεις από τον ανιχνευτή. Για κάθε απόσταση συλλέχθηκε το αντίστοιχο φάσμα και εκτιμήθηκε ο ρυθμός των φωτονίων που καταγράφηκαν. Το διάγραμμα που προέκυψε παρουσιάζεται παρακάτω στο Σχήμα 8. Η τιμή του ενεργού βάθους αλληλεπίδρασης που υπολογίστηκε με την πειραματική μέθοδο είναι 1.8 cm και βοήθησε στον να προσδιορισθεί το πλήθος σημείων που απαιτείται να προσομοιωθεί, ώστε τα αποτελεσμάτων των προσομοιώσεων να προσεγγίσουν καλύτερα τις πειραματικές τιμές.

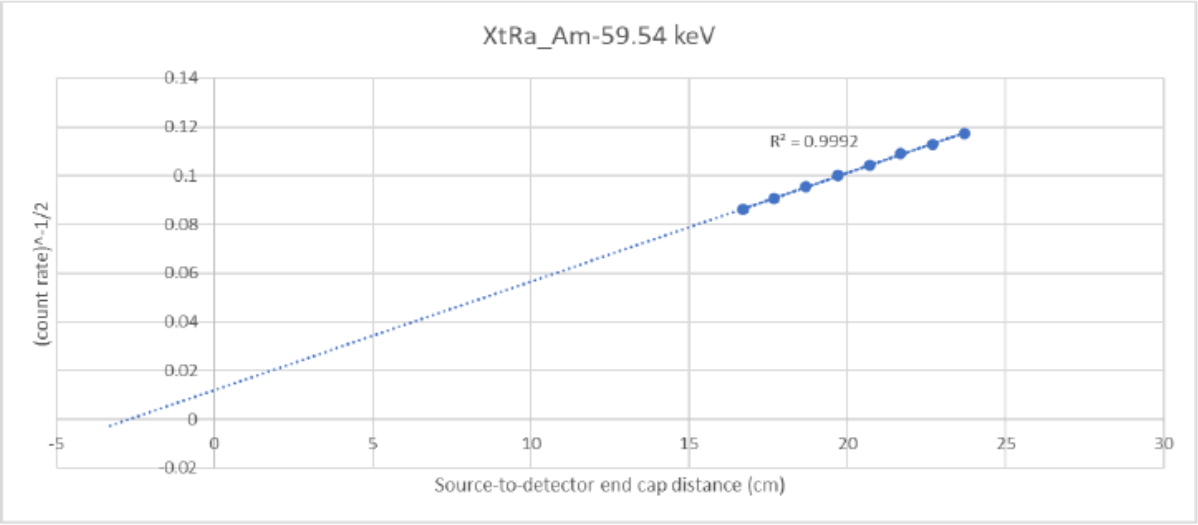

Σχήμα 8 Διάγραμμα για τον πειραματικό υπολογισμό του ενεργού βάθους αλληλεπίδρασης με σημειακή πηγή Αμερικίου-241

Μετά από μερικές δοκιμές βρέθηκε ότι όταν τα σημεία που λαμβάνονται υπόψιν για τον υπολογισμό του ενεργού βάθους αλληλεπίδρασης είναι σε απόσταση μεγαλύτερη των 4 cm από το σημείο αναφοράς, τότε οι ευθείες αναδρομής για όλες τις ενέργειες παρουσιάζουν καλύτερη ακρίβεια, όπως φαίνεται και στο παρακάτω διάγραμμα για τα 50 keV. Στην περίπτωση αυτή για την ενέργεια 59.54 keV προέκυψε 1.84 cm, που είναι πολύ κοντά στην πειραματική τιμή, κάτι το οποίο είναι και το ζητούμενο.

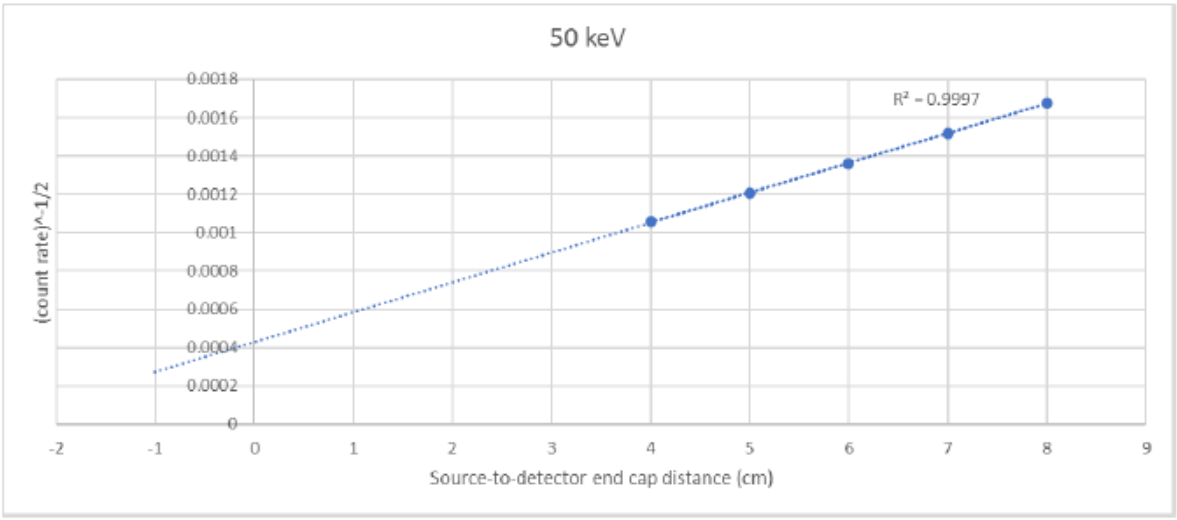

Σχήμα 9 Διάγραμμα για τον υπολογισμό του ενεργού βάθους αλληλεπίδρασης για απόσταση 4-8 cm από το καπάκι προπυλενίου

Με εφαρμογή της διαδικασίας προσομοίωσης που υιοθετήθηκε, παρήχθη νέο διάγραμμα για τις τιμές του ενεργού βάθους αλληλεπίδρασης συναρτήσει της ενέργειας, το οποίο παρουσιάζεται στο Σχήμα 10, ενώ οι αντίστοιχες συναρτήσεις αναδρομής που παρήχθησαν από τα πειραματικά σημεία ενσωματώθηκαν στον κώδικα Matlab, με αποτέλεσμα όταν ο χρήστης επιλέγει την επιθυμητή ενέργεια, ο κώδικας να χρησιμοποιεί την αντίστοιχη τιμή του ενεργού βάθους αλληλεπίδρασης για τον ανιχνευτή XtRa. Συγκεκριμένα, η απόσταση από το δείγμα μέχρι τον ιδεατό σημειακό ανιχνευτή που στην προηγούμενη έκδοση του κώδικα ήταν ενιαία, πλέον έσπασε σε δύο ξεχωριστές αποστάσεις. Η μία αφορά την απόσταση από το δείγμα μέχρι την επιφάνεια του ανιχνευτή που είναι γνωστή για κάθε γεωμετρία πηγής-ανιχνευτή και η άλλη είναι το ενεργό βάθος αλληλεπίδρασης μέσα στον ανιχνευτή, που προσδιορίζεται μέσω προσομοιώσεων ή πειραματικά, όπως ακριβώς περιγράφεται στην παρούσα ΔΕ.

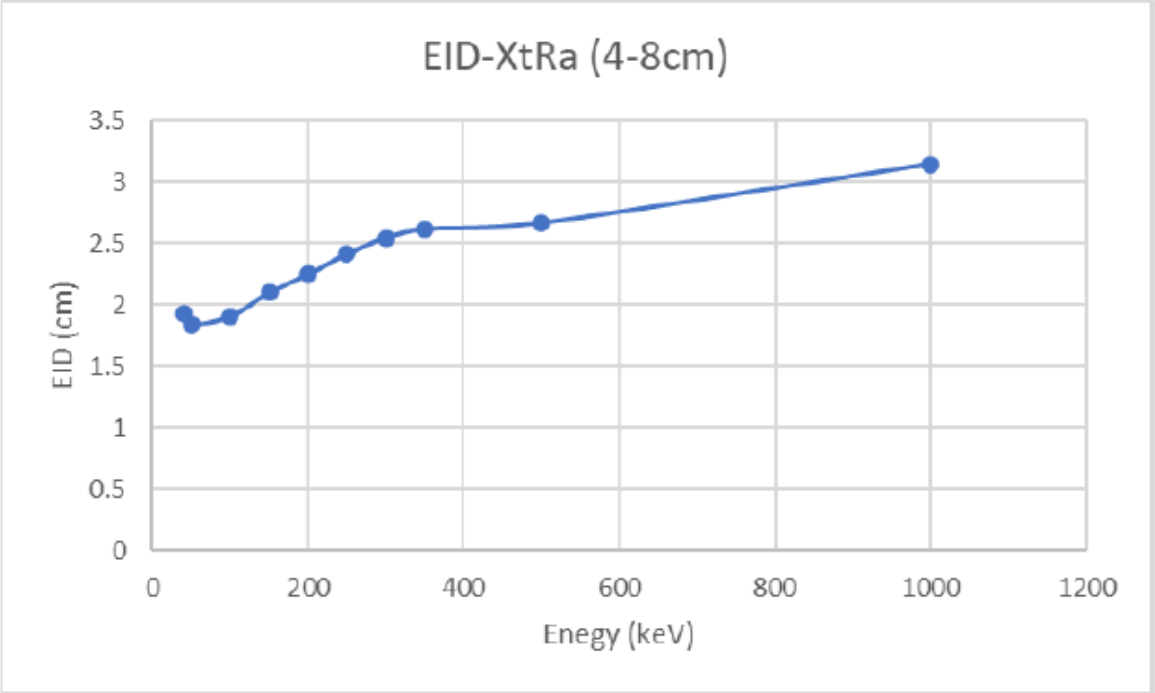

Σχήμα 10 Διάγραμμα του ενεργού βάθους αλληλεπίδρασης συναρτήσει της ενέργειας

Αφότου διερευνήθηκε σε βάθος ο υπολογισμός της τιμής του ενεργού βάθους αλληλεπίδρασης στον ανιχνευτή, η εργασία αυτή επικεντρώθηκε στην αναβάθμιση της “standalone” εφαρμογής, ώστε να βελτιωθεί η ευλιξία και η ευκολία χρήσης της. Το νέο γραφικό της περιβάλλον παρουσιάζεται στην παρακάτω εικόνα.

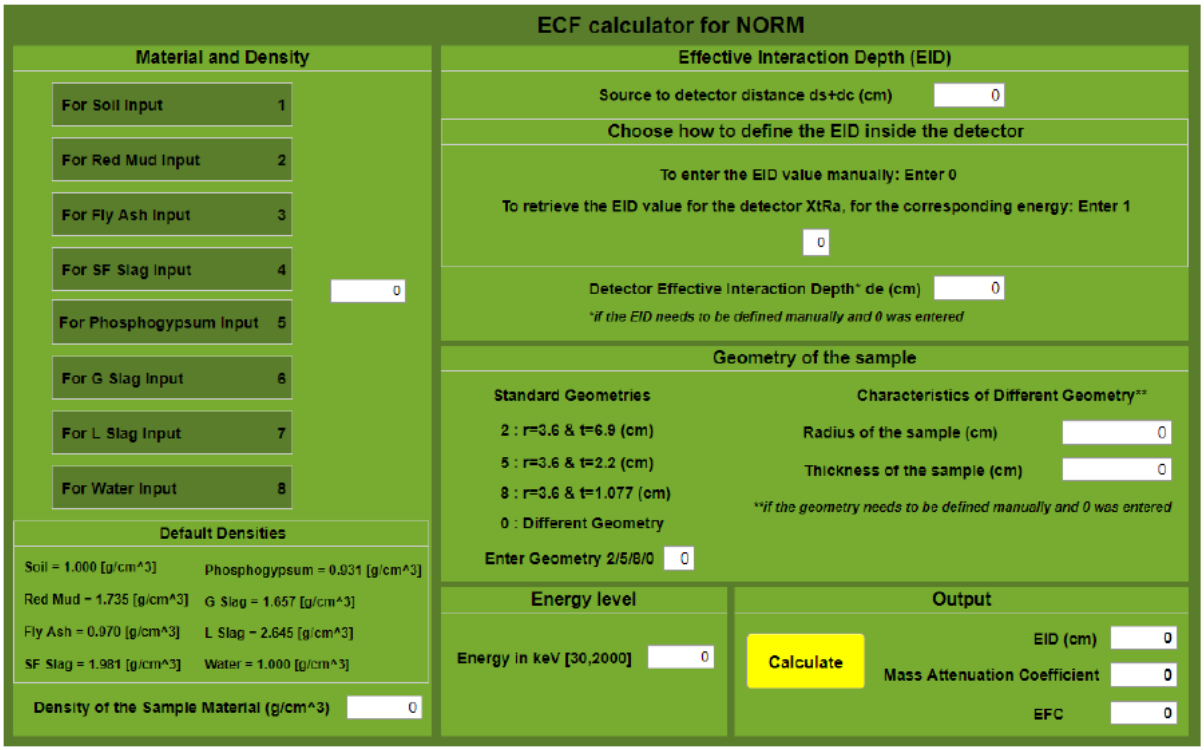

Σχήμα 11 Το γραφικό περιβάλλον της νέας έκδοσης της "standalone" εφαρμογής σε Matlab

Για την σύγκριση των αποτελεσμάτων που δίνει ο κώδικας Matlab με αυτά των προσομοιώσεων Monte-Carlo, λήφθηκε υπόψιν το χειρότερο δυνατό σενάριο[5] για το φαινόμενο της αυτοαπορρόφησης που είναι η μεγαλύτερη γεωμετρία δείγματος, στην προκειμένη περίπτωση η γεωμετρία "2". Γενικά η όλη προσπάθεια κρίθηκε ιδιαίτερα επιτυχημένη, ειδικότερα στις χαμηλότερες ενέργειες κάτω των 200 keV, όπου οι ποσοστιαίες διαφορές μεταξύ των δύο μεθόδων είναι αμελητέες κυρίως για τα υλικά με την μικρότερη πυκνότητα. Οι μεγαλύτερες διαφορές υπολογίστηκαν για το πυκνότερο υλικό (Lead Slag), όπου στα 1000 keV, έφτασαν το 15%, όπως φαίνεται στο Σχήμα 12.

Από την άλλη πλευρά, οι μικρότερες ποσοστιαίες διαφορές εμφανίστηκαν για το υλικό χώμα, που είναι από τα υλικά με τις χαμηλότερες πυκνότητες που μελετήθηκαν. Όπως φαίνεται και στο διάγραμμα του Σχήματος 13, η μέγιστη διαφορά μεταξύ των μεθόδων βρέθηκε μόλις 3% στα 1000 keV.

Αν και η όλη μελέτη έχει προχωρήσει σε μεγάλο βαθμό, ακόμα υπάρχουν περιθώρια βελτίωσης και αναβάθμισης στην διαδικασία υπολογισμού των συντελεστών διόρθωσης της αυτοαπορρόφησης ECF. Για παράδειγμα, θα ήταν χρήσιμο να γίνει η μελέτη που περιγράφεται στην παρούσα Διπλωματική Εργασία και για άλλους ανιχνευτές. Επιπλέον,

[5] Αφορά στις συνήθεις αναλύσεις που γίνονται στο ΕΠΤ-ΕΜΠ

είναι σημαντικό να γίνει ενδελεχής μελέτη και άλλων παραμέτρων που επηρεάζουν τον υπολογισμό του συντελεστή διόρθωσης, όπως είναι η πυκνότητα του υλικού. Τέλος, θα είχε ενδιαφέρον η μελέτη του νεκρού στρώματος του ανιχνευτή στις προσομοιώσεις, καθώς φαίνεται να επηρεάζει σημαντικά τον υπολογισμό του ενεργού βάθους αλληλεπίδρασης.

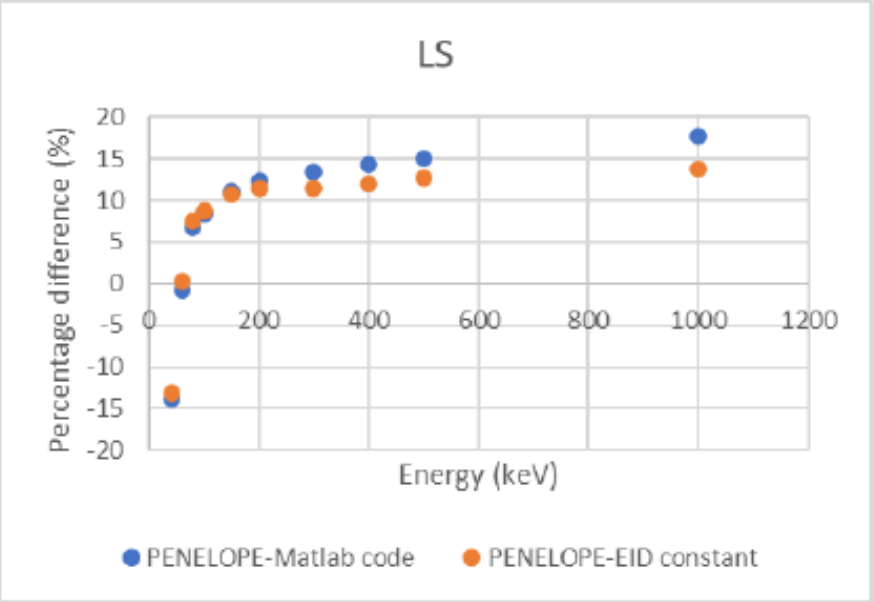

Σχήμα 12 Ποσοστιαίες διαφορές μεταξύ αποτελεσμάτων από Matlab και PENELOPE για το πυκνότερο υλικό (Lead Slag)

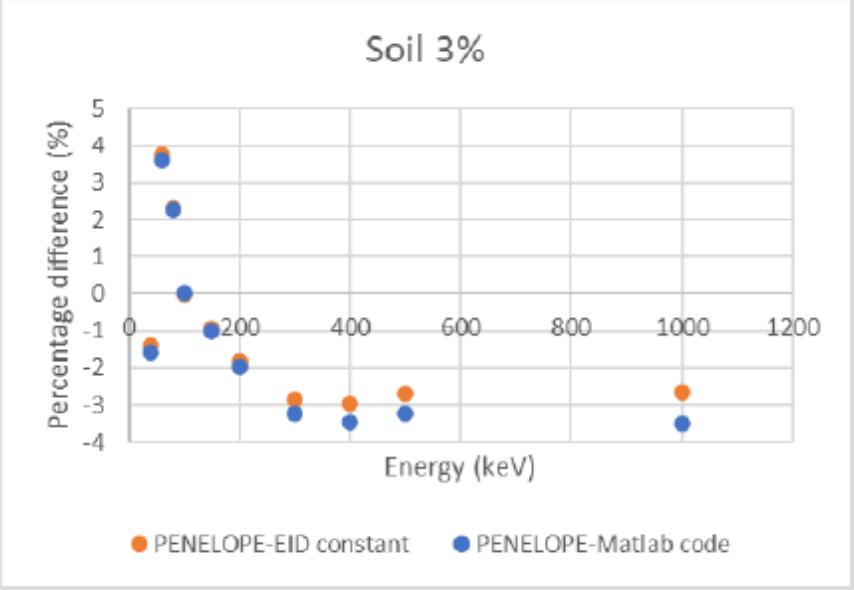

Σχήμα 13 Ποσοστιαίες διαφορές μεταξύ αποτελεσμάτων από Matlab και PENELOPE για το χώμα

1. Introduction

The main goal of this thesis is to explore ways to improve the accuracy of the gamma spectroscopic analysis of environmental samples. Gamma spectrometry is a powerful tool for identifying and quantifying radioactive isotopes based on the characteristic gamma rays they emit. Despite its many advantages, there are critical challenges that require careful attention. One such challenge, which this research addresses, is the difference in absorption properties between the calibration source and the sample to be analyzed, leading to different attenuation of photons between the two. This difference in self-absorption results in a considerable variation in efficiency. Consequently, it is of great importance to introduce an Efficiency Correction Factor (ECF) for the sample analyzed [7]. In the case of Naturally Occurring Radioactive Materials (NORM), which are the primary focus of this study, the problem of self-absorption becomes very evident due to the mainly low-energy photons they emit, such as ^{210}Pb (46.52 keV), ^{234}Th (63.29 keV), ^{241}Am (59.54 keV), ^{212}Pb (238 keV), ^{214}Pb (295 and 352 keV), and ^{228}Ac (338 keV), as well as the large volume of these samples, their large amounts of high Z elements, and their high density. The need to accurately analyze NORMs arises from the fact that these materials are often by-products of industrial activities, and therefore specific regulations apply regarding their radioactivity.

In the literature, several methods have been proposed to resolve the problem of the different self-absorption between the calibration source and the sample to be analyzed. However, the method that has been used in the Nuclear Engineering Laboratory of the National Technical University of Athens (NEL-NTUA) for more than 25 years, and shows promising results, is the “Integral Method”. This method requires the numerical calculation of two integrals, which are proportional to the photons interacting with the detector: one for the calibration source material and the other for the sample material being analyzed. The two integral ratio results in the ECF. By considering the ratio rather than the respective efficiencies, this approach can eliminate inaccuracies caused by the unknown exact geometrical characteristics of the samples.

This work concentrated on upgrading a Matlab code originally developed by [3], and subsequently improved by [4], which calculates the ECF for NORMs using the “Integral Method”. Both of these works were student theses and led to significant conclusions and results. However, given the broad topic with numerous parameters to consider, there were still areas for improvement. Specifically, the first thesis focused on calculating self-absorption correction factors for photon energies up to 400 keV, for the LEGe detector operating at NEL-NTUA. The results obtained from the Matlab code and Monte-Carlo simulations were compared, revealing significant differences (~60%), especially for photon energies below 250 keV. These deviations were mainly attributed to the different linear attenuation coefficients used in the two methods. The second thesis extended the energy range for the calculation of the ECF up to 2000 keV, as it was proved that correction factors are necessary for higher energies as well. Moreover, the issue with the linear attenuation

coefficients was resolved, resulting in substantial improvements and reducing the differences between the Monte Carlo simulations and the MATLAB code to less than 20%. Another important upgrade was the development of the MATLAB code as a standalone application, eliminating the need for MATLAB installation or programming knowledge. However, further improvements were still necessary, especially considering the significant conclusions drawn in this second thesis, such as the great impact of the Effective Interaction Depth (EID) parameter on the calculation of the ECF.

This study advanced previous research by thoroughly investigating the Effective Interaction Depth (EID) and its energy variation for the XtRa[6] detector, opertining at NEL-NTUA, through Monte Carlo simulations and experiments with an ^{241}Am point source. In particular, the plot created from this investigation was fitted with polynomial functions, which were integrated into the Matlab code. This change improved the accuracy of ECF calculations, reducing the differences between MATLAB code results and Monte Carlo simulations, especially in the low energy range, below 200 keV. The study highlighted the significant role of EID in ECF calculations, as well as the impact of material density. Lastly, the standalone application's Graphical User Interface (GUI) was also upgraded to make the program more user-friendly.

The 2nd chapter of this work covers the theoretical background of the study. It starts with the definition and explanation of gamma rays and their interactions with matter and continues with the principles of gamma spectroscopy and germanium detectors. Additionally, a thorough explanation of the phenomenon of self-absorption is provided, along with the method used to calculate the ECF and the definition of the EID. Lastly, the NORMs of interest in this study are described.

The 3rd chapter covers the work done in the previous theses to estimate the ECF using Matlab code. It showcases all the significant results derived and highlights the areas that require improvement.

The 4th chapter thoroughly describes the methodology used to determine the EID values through both Monte Carlo simulations and experimental methods.

The 5th chapter describes all the modifications made to the Matlab code to enhance the results. Moreover, it explains the steps involved in updating the standalone application. Lastly, the results obtained from the new application are presented and compared with those from the simulations.

The 6th chapter presents the results and conclusions of this work, along with ideas for future research in this field.

[6] E**Xt**ended **Ra**nge Germanium detector

2. Gamma-spectroscopic analysis of environmental samples (NORM)

2.1 Gamma-rays

Gamma rays constitute electromagnetic radiation of the shortest wavelength and highest energy. Atomic nuclei have distinct excitation energy levels determined by the number of the protons and neutrons within them. Gamma rays are the photons emitted by the disintegration of the radioactive atomic nuclei. This is the phenomenon where a nucleus undergoes a transition from a high-energy level to a lower-energy level, and a photon or a series of successive photons are emitted to release the surplus energy. Gamma rays of relatively high energies are also generated through the process of pair production and positron annihilation, where an electron and its antiparticle, a positron, annihilate each other, resulting in the creation of two photons. On the other hand, atoms also have discrete excitation energy levels, corresponding to different configurations of orbital electrons. When charged particles (usually electrons) change atomic energy levels or slow down in a Coulomb force field, electromagnetic radiation is emitted which is photons called X-rays. Energy levels in atoms typically range from 1 to 10^5 electron volts (eV), while energy differences within nuclei usually span from 10^3 volts (keV) to 10^7 eV. This is because the nuclear forces that act between nuclear particles are much stronger than the corresponding electrostatic forces acting between electrons and nuclei. Therefore, the characteristic gamma rays emitted from the radioactive decay of atomic nuclei normally range from a few kilo electronvolts (keV) to several megaelectron volts (MeV). However, X-rays that are produced from linear accelerators can have comparable energy to gamma-rays or even higher [8], [9], [10].

2.2 Environmental Radioactivity

Radioactivity constitutes an integral part of the Earth's environment. Nuclei found in nature can be either stable (ground state) or unstable (radioactive). Whether a nucleus is stable or not is directly dependent on its atomic number Z and its neutron number N. A chemical element can have both stable and radioactive isotopes, like Strontium, which has four stable isotopes: ^{84}Sr, ^{86}Sr, ^{87}Sr, and ^{88}Sr, and one radioactive isotope, ^{82}Sr. The graph shown below, which is called the Segre chart, depicts schematically which combinations between atomic number Z, and neutron number N lead to stable nuclei, as well as radioactive ones. When there is an excess or deficiency of neutrons, the nuclei are unstable and thus possible to disintegrate by expelling mass to reach a more energetically stable condition or ground state. This process is called radioactive decay and the Segre chart below (Figure 2-1) indicates the different ways that this can happen.

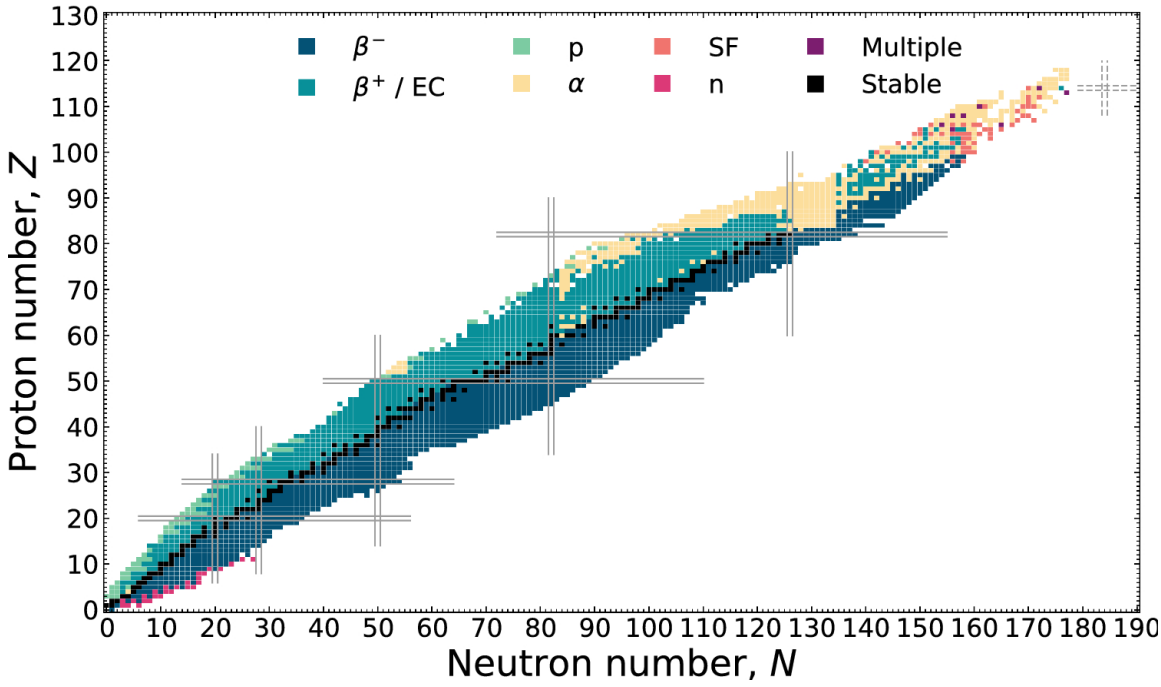

Figure 2-1 Segre chart [11]

During the decay process, ionizing radiation is emitted. This includes particle emissions from various energetic decays, like alpha particles, electrons (including beta- and beta+ particles), as well as electromagnetic radiations in the form of X-rays and gamma rays (photons).

Radioactive isotopes with atomic number greater than 85 typically decay to a radioactive daughter nucleus. This daughter nucleus subsequently undergoes decay to produce a second radioactive daughter nucleus, continuing in this manner until a stable nucleus is formed. This series of consecutive alpha and beta decays is known as a radioactive chain. The figure below (Figure 2-2) depicts one of the most common decay chains, which is the Uranium-238 decay chain, which produces Lead-206 after a series of 14 sequential alpha and beta decay reactions.

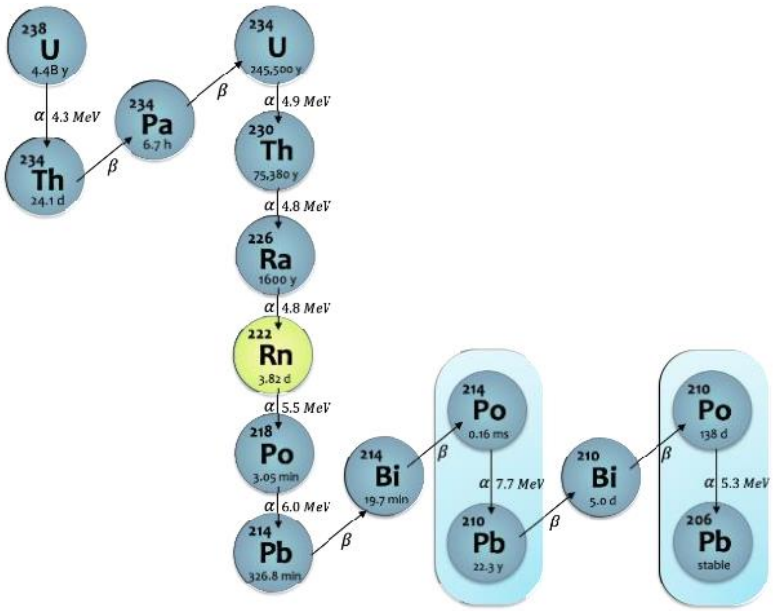

Figure 2-2 U-238 radioactive chain [12]

All radionuclides are characterized by their half-life $T_{1/2}$, which indicates the time required for the number of nuclei of a particular radionuclide, to decrease to half the original number. Its value varies from a fraction of a second to billions of years, i.e. Uranium-238 has a half-life of 4.5 billion years. The decay rate is called radioactivity, and is described by the equation:

$$\boldsymbol{R(t) = \lambda N(t)} \tag{2-1}$$

Where λ is the decay constant that characterizes the radionuclide and is equal to:

$$\boldsymbol{\lambda = \frac{ln\,2}{T_{1/2}}} \tag{2-2}$$

Radioactivity is measured in Curie (Ci) or Becquerel (Bq), which is the SI unit. One 1 Bq equals one decay per second [13].

2.3 Gamma-ray interactions with matter

Gamma radiation is very penetrating and ionizes matter primarily via indirect ionization. The interaction of photons with matter can result in different outcomes, such as large energy transfer, complete absorption of the photon, or the photon can be scattered rather than absorbed and change its direction while keeping most of its initial energy [10]. The mechanisms by which photons can interact with matter are Photoelectric absorption,

Compton scattering, Rayleigh (coherent) scattering, Pair production, and Photodisintegration. The first four are described in more detail below, as they are of more importance.

2.3.1 Photoelectric absorption

Photoelectric absorption is the dominant interaction for low-energy photons, mainly for photon energy E_γ below 0.1 MeV, with matter. Specifically, a photon undergoes an interaction with an electron that is strongly bound in an atom (e.g. a K-shell electron), and the photon completely disappears. During this process, the electron gains sufficient energy to escape from the atom, and it is often called a photoelectron [10]. The kinetic energy of the photoelectron E_{e^-} is equal to the incident photon energy $E_\gamma = h \cdot v$ reduced by the binding energy of the photoelectron in the atom E_b.

$$\boldsymbol{E_{e-} = h \cdot v - E_b} \tag{2-3}$$

For this interaction to occur, the incident photon must have an energy greater than the binding energy of an orbital electron. The probabilities augment when the photon energy is greater than or comparable to the binding energy of the electrons for a specific shell, especially K-shell, and the atoms have a large atomic number Z [8].

After the interaction, the atom is left with a vacancy because of the released electron (Figure 2-3). Subsequently, an electron from a shell with lower binding energy (typically an outer orbit, such as from an L to a K shell) fills this vacancy. The difference between the binding energies of the electrons involved in this filling is emitted in the form of an X-ray photon, termed *fluorescent radiation*. Alternatively, this excess of energy might prompt the ejection of another orbital electron from the atom, known as the Auger electron. This ejected electron creates another vacancy, initiating a cycle of X-ray photon emission or Auger electron release, repeating the process iteratively.

When photoelectric absorption takes place in a detector, it is most likely that the original photon energy will be fully absorbed inside the detector. This is because the penetrating photons are transformed into electrons and X-rays that are easier to stop and therefore are deposited locally inside the detector.

2.3.2 Compton (incoherent) scattering

Compton scattering is the elastic collision between a photon and a free or weakly bound electron of an atom. It generally occurs for high-energy photons, specifically, the energy ranges from 100 keV to 30 MeV for low-Z materials and from 0.5 MeV to 10 MeV for high-Z materials [10]. In Compton scattering, when a photon collides with an electron, it transfers a portion of its energy and momentum to the electron. This electron, typically stationary or nearly so, is called a target electron.

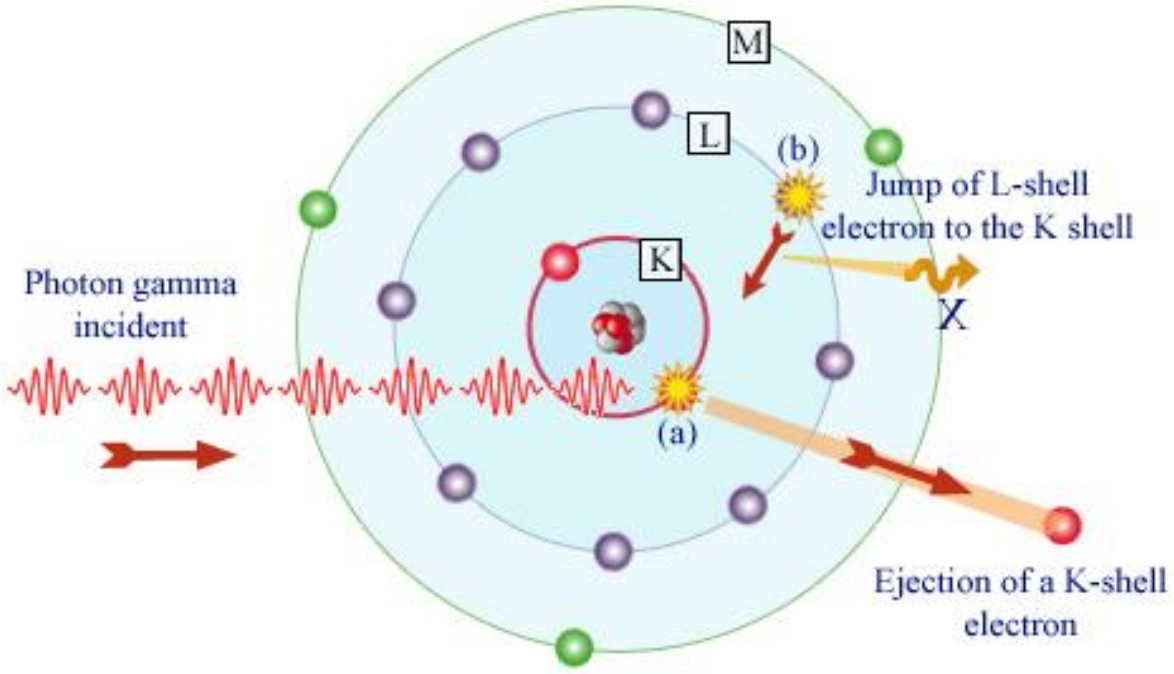

Figure 2-3 Photoelectric absorption [14]

Consequently, the photon scatters with reduced energy and an extended wavelength, moving on a trajectory that forms an angle θ with the trajectory of the original photon. The energy difference between the photon before and after scattering is absorbed by the electron as its kinetic energy, which is called recoil electron. The recoil electron moves on a trajectory that forms an angle ϕ with the trajectory of the original photon, as shown in Figure 2-4 [8]. The amount of energy transferred to the electron can range from zero to a significant portion of the gamma ray's energy. When photon energies are considerably lower than the electron mass, scattering tends to be isotropic, with back-scattering being equally probable as forward scattering. However, if the photon energy greatly exceeds the electron mass, scattering predominantly occurs in the forward direction [15].

Compton scattering is the second dominant way a gamma ray interacts with a detector, after photoelectric absorption. While the transfer of gamma-ray energy to an electron through the photoelectric effect is consistently close to 100%, the energy transfer via the Compton Effect can vary widely, ranging from 0% to nearly 100%, depending on the energy of the gamma-ray and the angle at which it scatters [16].

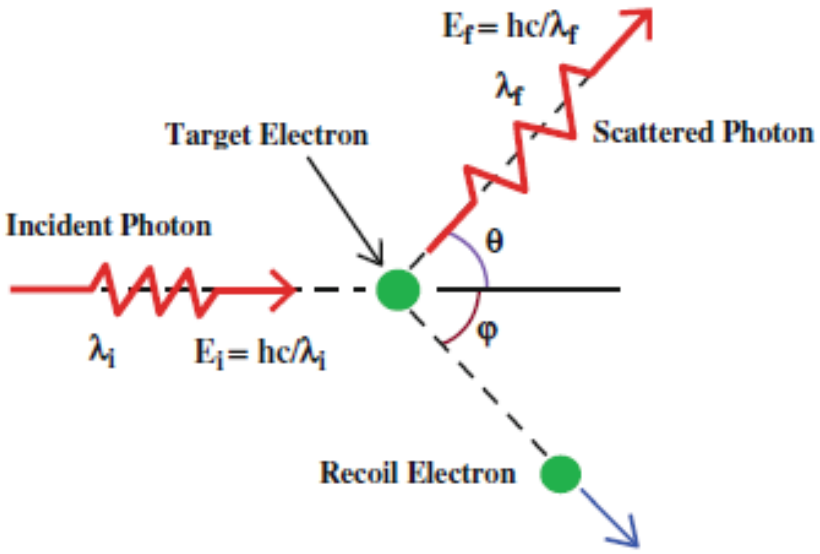

Figure 2-4 Compton scattering [10]

2.3.3 Rayleigh (coherent) scattering

Rayleigh scattering (Figure 2-5) occurs mainly for low-energy photons, below 10 keV, like X-rays. The incident photon excites the atom, and the excess energy due to the excitation is released by the emission of a photon with the same energy and wavelength as the incident one. In this case, the photon does not have enough energy to ionize the atom and therefore there is no energy loss.

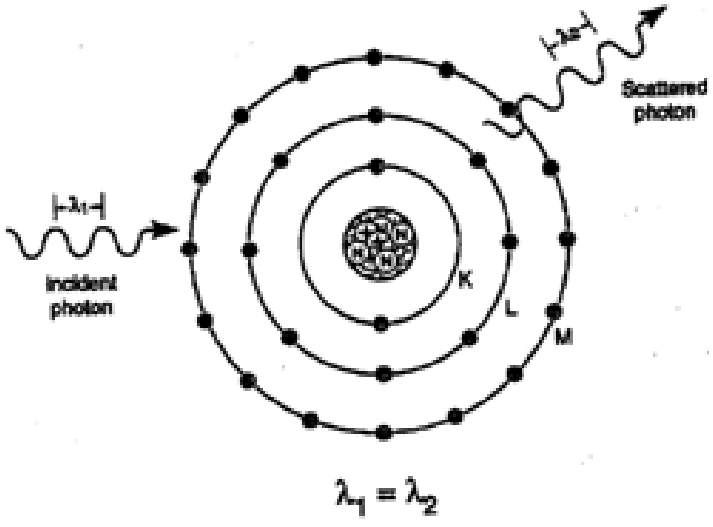

Figure 2-5 Rayleigh scattering [17]

2.3.4 Pair production

Pair production is one of the possible interactions between high-energy photons like gamma rays, and matter. In this process, the incident photon disappears when interacting with the electric field of a nucleus, forming an electron and a positron. For this interaction to occur, the electromagnetic energy of the photon must exceed a threshold energy of approximately 1.022 MeV (which is the sum of the rest mass of an electron and a positron, both equivalent to 0.511 MeV). If the initial photon's energy surpasses 1.02 MeV, any excess energy is distributed between the kinetic energies of the two resulting particles, in accordance with the conservation laws.

Furthermore, since the positron is the antiparticle of the electron, when a positron comes to rest and encounters an electron, both particles interact. This leads to their annihilation, and the total conversion of their rest mass into pure energy, as described by the $E=mc^2$ formula. This energy appears in the form of two oppositely directed 0.511 MeV gamma-rays (photons), as shown in Figure 2-6.

Consequently, the phenomenon of pair production is closely linked with the simultaneous creation and annihilation of matter in a single reaction.

During this interaction in a detector, it is highly likely that the positron will undergo annihilation upon interacting with an electron in the detector material, resulting in the creation of two gamma photons, each with an energy of 0.511 MeV.

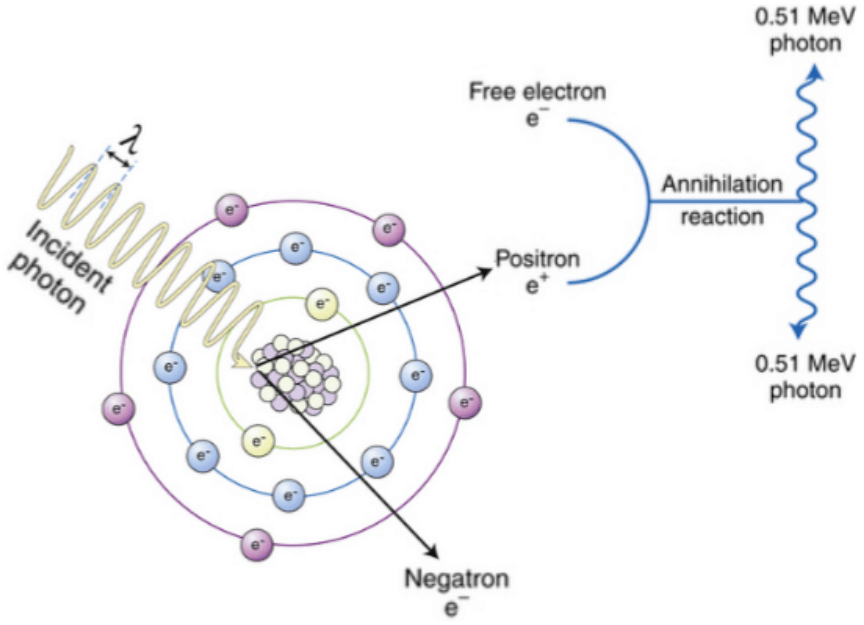

Figure 2-6 Pair production [18]

2.3.5 Linear attenuation coefficient μ and mass attenuation coefficient μ_m

As a photon beam traverses a material it is possible to interact with all possible mechanisms described above. The probability of each interaction mechanism to occur is indicated by a value called cross-section. From the mechanisms mentioned in the previous paragraphs, Rayleigh (coherent) scattering can be omitted in the calculation of the total cross-section σ as its contribution is nonsignificant compared to the others. Therefore, the total cross-section is calculated as follows:

$$\boldsymbol{\sigma = \sigma_f + \sigma_c + \sigma_p} \tag{2-4}$$

Where:

- σ_f is the cross-section for Photoelectric absorption
- σ_C is the cross-section for Compton scattering
- σ_p is the cross-section for Pair scattering

As shown in Figure 2-7, depending on the gamma-ray energy and the material being the absorber, one of the three partial cross-sections may significantly surpass the others. At lower gamma-ray energies, the photoelectric effect takes precedence, while at intermediate energies, Compton scattering becomes dominant. Additionally, Compton scattering becomes more prevalent as the atomic number of the material decreases, resulting in a wider range of dominance for lighter nuclei. Lastly, at higher energies, electron-positron pair production predominates [14].

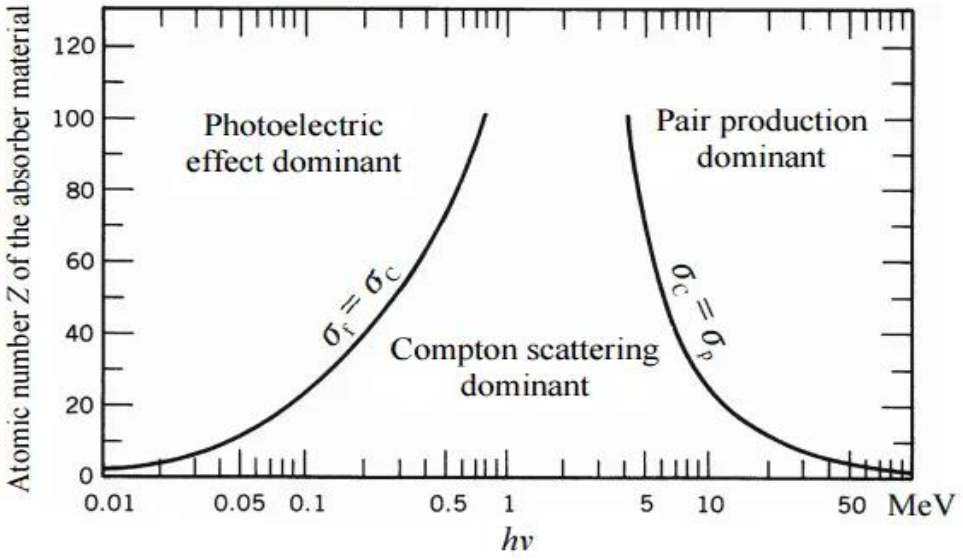

Figure 2-7 The relative importance of various processes of gamma radiation interaction with matter [14]

As photons traverse a medium, the total intensity of the beam diminishes due to absorption and scattering phenomena. The degree of this intensity reduction varies based on both the material the photons pass through and the energy of the radiation. Consequently, these interactions can be defined by a fixed probability of occurrence per unit path length within the absorber. The collective sum of these probabilities is referred to as the **linear attenuation coefficient μ**, and it can be determined by the equation below:

$$\boldsymbol{I = I_0 e^{-\mu x}} \tag{2-5}$$

Where:

- I is the intensity after attenuation
- I_0 is the incident intensity
- μ is the linear attenuation coefficient (cm^{-1})
- x is the physical thickness of the absorber (cm)

Additionally, a value that is also useful, because it takes into account only the atomic composition of the absorber material and not its density, is the **mass attenuation coefficient μ_m** [10]. The mass attenuation coefficient is defined as the ratio of the linear attenuation coefficient and the absorber density, $\mu_m = \mu/\rho$ [cm^2/g].

2.4 Gamma-ray spectroscopy principles

Gamma-ray spectrometry is a non-destructive technique, and powerful tool used to identify and quantify radioactive isotopes, based on the characteristic gamma rays they emit. The basic principle for the qualitative identification of the nuclei is the fact that gamma rays emitted during the de-excitation of the nucleus, constitute its “fingerprint”. The quantitative identification evaluates the sample's radioactivity, meaning the estimation of the number of nuclei that disintegrate per time unit [1].

Gamma-ray spectrometry offers several advantages, some of which are the following:

- Sample preparation for analysis is notably straightforward, often eliminating the need for a radiochemical separation procedure.
- It is very useful for environmental radioactivity analysis and for the analysis of small samples.
- The data acquired by the detection system are highly compatible with computerized data processing, making them ideal for developing automated analysis systems.

- Despite their relatively high cost, gamma-ray spectroscopic devices are offering exceptional standards of performance and quality assurance.

The gamma-ray spectrometer system comprises three distinct parts: a detector, an electronic circuit for pulse management, and facilities for data storage, processing, and display. Specifically, the detector functions as a tool that generates electric signals, or pulses, that are proportional to the energy (wavelength) and quantity of gamma photons detected. This detector is linked to a pulse-handling system, an electronic circuit responsible for shaping, counting, and categorizing these pulses based on their height. Consequently, the electronic signals are transformed into a pulse spectrum, representing both the quantity and distribution of gamma photon energies. This spectrum is stored within a memory system and can undergo additional processing through suitable computer programs. The outcomes are presented through graphical or numerical displays [19].

As mentioned in paragraph 2.3, gamma radiation interacts with matter in different ways. These phenomena also take place during the interaction of gamma rays with the detector; therefore they affect the interpretation of the gamma spectrum. It is important to have a solid knowledge of the three major modes of interaction of gamma-rays with matter, to interpret the gamma-ray spectrum correctly. Firstly, the **full-energy peak** observed in the gamma spectrum is produced by the photoelectrons ejected in the photoelectric effect, as they provide immediate information about the energy of the gamma radiation. Moreover, the **Compton continuum** is observable, caused by the various scattering angles of the Compton electrons that show a distribution of energies over a wide range. The Compton continuum (Compton edge or shoulder) appears with some gap after the full-energy peak, due to the minimum energy that is taken away by a back-scattered gamma photon. Lastly, when pair production takes place for gamma rays of high energy, there are three possibilities. If all the energies of the electron-positron pair including the annihilation photons are dissipated in the detector material, then a **full-energy peak** will be displayed. However, if one of the annihilation photons escapes from the detector, it takes away 0.511 MeV of energy, and a **single escape peak** (full-energy peak minus 0.511 MeV) will be displayed. On the other hand, if both annihilation photons escape from the detector, they take away 1.02 MeV of energy, resulting in a **double escape peak** (full-energy peak minus 1.02 MeV) [19].

As an example, the Figure 2-8 shows the decay scheme of Cobalt-60, that before its stable state, the daughter radionuclide Nickel-60 de-excites by emitting two gamma rays of 1.17 MeV, and 1.33 MeV.

As shown in Figure 2-9 the linear spectrum of Cobalt-60 depicts only the gamma rays emitted during the decay process, while the gamma-spectroscopy spectrum also depicts other phenomena in the detector material.

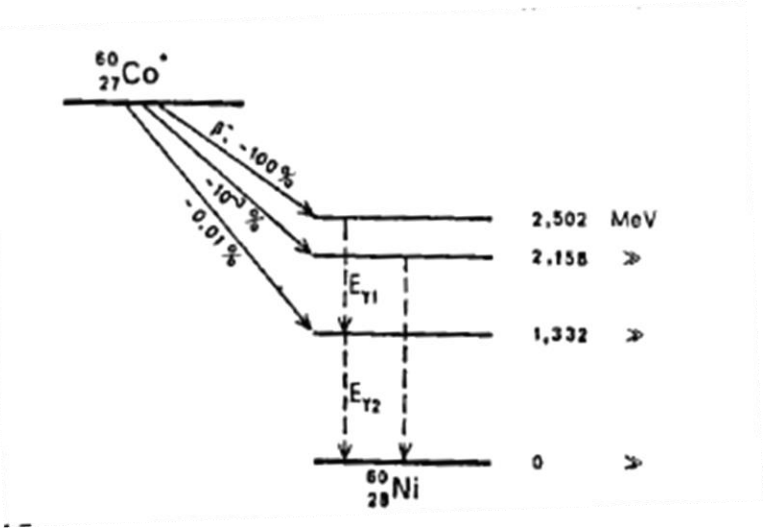

Figure 2-8 Decay scheme of Cobalt-60 [8]

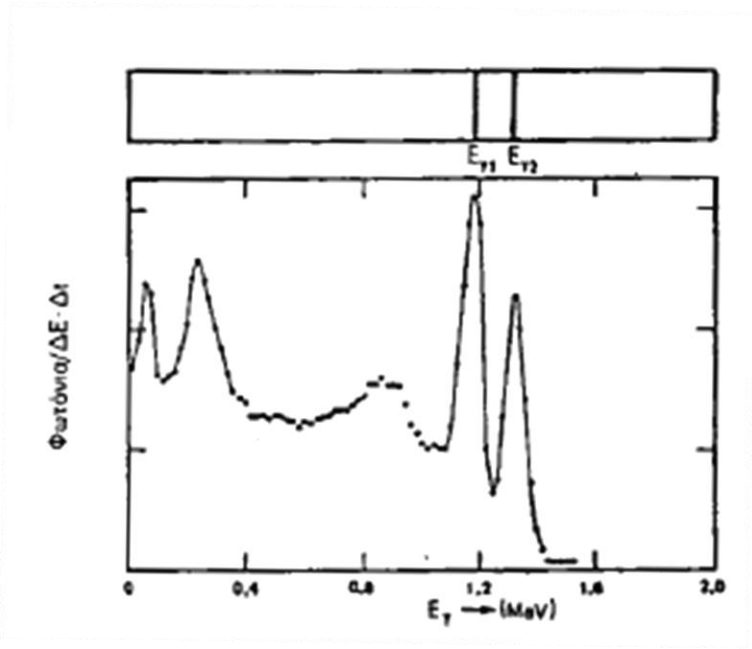

Figure 2-9 The upper figure shows the linear spectrum of Cobalt-60, and the lower figure shows the gamma spectrum of Cobalt-60 taken by a scintillation spectrum [8]

The net area under a photopeak (Figure 2-10), determines the quantitative identification of the radionuclide detected. Then, the activity, measured in Bq (or Bq/kg) of the respective radionuclide is calculated by the following formula:

$$\boldsymbol{activity} = \frac{\boldsymbol{area}}{\boldsymbol{time} \cdot \boldsymbol{yield} \cdot \boldsymbol{efficiency}} \tag{2-6}$$

Where:

- area is the net area under the photopeak
- time is the duration of spectrum collection
- yield is the emission probability of the photons of the specific energy
- efficiency is the full energy peak efficiency of detection of the energy E photons

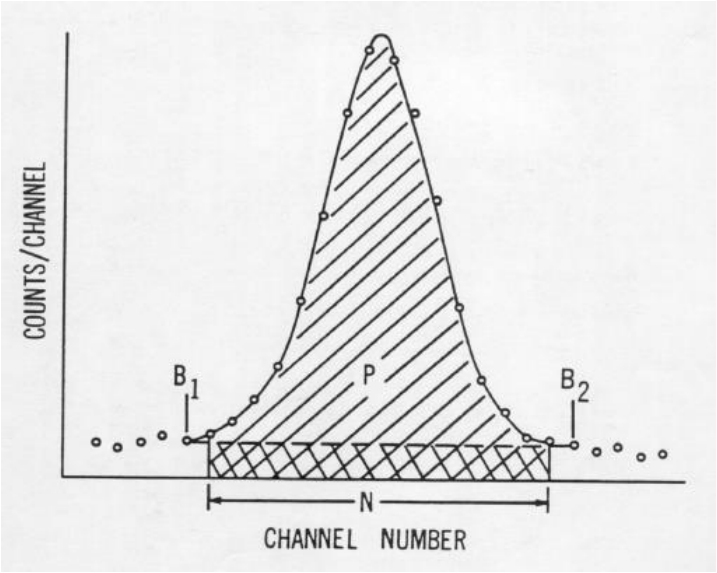

Figure 2-10 The net area under the photopeak

2.5 Detectors

There are different types of detectors, and it is of great importance to use the appropriate one according to the kind of analysis that needs to be conducted. In general, detectors can be categorized into three types:

- Gaseous Ionization Detectors
- Scintillation Detectors
- Semiconductor Detectors (Germanium or Silicon type detectors)

NEL-NTUA is equipped with four (4) high-purity germanium (HPGe) detectors. These are:

- 2 HPGe (High Purity Germanium detector)
- LEGe (Low Energy Germanium detector)
- XtRa (Extended Range Germanium detector)

In the present thesis and the previous ones, two (2) of the above detectors were utilized, these are LEGe and XtRa. These two detectors are capable of effectively detecting and analyzing low energy photons. Therefore, their basic characteristics will be described below.

2.5.1 LEGe detector

The Low Energy Germanium Detector (LEGe) is a planar detector constructed with a thin front and side contact, as well as a thin dead layer, along with a window usually crafted from beryllium or carbon fibers. The rear electric contact area of the detector is smaller than the total detector area, resulting in lower detector capacitance compared to a similarly sized planar detector. As preamplifier noise correlates with detector capacitance, the LEGe detector exhibits reduced noise levels compared to other detector geometries, leading to enhanced energy resolution at low and moderate energies. This feature is particularly significant because the low-energy spectrum typically includes a lot of X-rays from various sources alongside gamma rays, resulting in a complex spectrum. Consequently, LEGe detectors are preferred for low-energy gamma spectroscopy and the detection of radionuclides such as ^{210}Pb (46.52 keV), ^{234}Th (63.29 keV), and ^{241}Am (59.54 keV) [4].

2.5.2 XtRa detector

It is a coaxial semiconductor detector with a window fabricated from carbon fibers and has been installed at NEL-NTUA since 1999. It is characterized as 'coaxial one open end, closed and facing window'. Its crystal's main geometric characteristics are: D=80mm (diameter), and h=78mm (height). It has a relative efficiency of 104.5% for photons of energy 1332.5keV, presenting a resolution of 1.03keV for photons energy 122.06keV, and 2.04keV for 1332.5keV. The peak-to-Compton ratio for energy photons 1332.5keV is 82.2:1. This detection setup is configured for the analysis of samples in the energy range 0-2000keV. It is mounted in a suitable cylindrical front open/split-top type vertical armor of the Canberra company (model 767) and consists of four (4) layers of material. Starting from the inside of the shield, these are: 1.5mm thick copper sheet, 1mm thick tin sheet, 100mm thick lead layer, and a thick steel layer of 9.5mm [20].

2.6 Self-absorption of low-energy photons in gamma spectrometry

An impediment when analyzing samples with gamma spectroscopy is the difference in the absorption properties between the calibration source and the sample that needs to be analyzed. More precisely, this difference in the absorption properties leads to a different attenuation of the photons inside the calibration source and the analyzed sample. The term "self-absorption" expresses this phenomenon, meaning the absorption of photons by the sample emitting them. The count rate detected is significantly affected by the self-absorption of the sample, among other parameters like the source-to-detector geometry used, which in some cases results in a considerable difference in the efficiency. Therefore, it is necessary to introduce an efficiency correction factor (ECF) for the sample analyzed [7],

which multiplied by the already calculated efficiency of the calibration source can surpass the obstacle of the different self-absorptions. Consequently, the new efficiency value can lead to a more accurate calculation of the activity by the formula (2.6).

Self-absorption becomes more evident as the photon energy decreases. Moreover, it is significantly affected by the sample's density, composition, and volume. Specifically, in the case of Naturally Occurring Radioactive Materials (NORM), discussed more elaborately in the next paragraph, the samples often have relatively large volumes [1]. Furthermore, numerous radionuclides detected in environmental samples emit photons with low energy levels below 80 keV, like ^{210}Pb (46.52 keV), ^{234}Th (63.29 keV) (the detection of which leads to the determination of ^{238}U), and ^{241}Am (59.54 keV) [4]. Therefore, self-absorption becomes an important factor in the analysis of these samples. Due to the small inaccuracy, compared to the total error of the calculation, induced when the photon energy is higher than 200 keV, it is generally accepted that the self-absorption difference might be neglected [7]. However, it has been shown in previous work and literature, that correction is also needed for much higher energies, up to 2000 keV [4]. This work also focused on the energy range 40-2000 keV.

2.6.1 Efficiency correction factor (ECF)

Several methods have been proposed in the literature regarding resolving the problem in gamma-spectroscopy caused by the difference in the self-absorption between the calibration source and the sample. These can be categorized as follows [1]:

- Methods based on the preparation of standard calibration sources of the same geometry, and composition which is either the same or similar to that of the analyzed samples. The efficiency for the corresponding geometry, the composition of the sample, the photon energy, and the activity, are estimated according to the respective standard calibration source.

- Methods based on the efficiency calibration with a standard source and the analytical estimation of an efficiency correction factor (ECF) for the sample, due to the difference in their self-absorptions.

- Methods based on directly estimating the efficiency of the geometry and composition of the material of interest, either with Monte Carlo simulation, or numerical calculation. Often, numerical calculation is followed by experimental procedures, which can be very complex.

The current work focused on the calculation of an Efficiency Correction Factor (ECF) "η", which is defined as the ratio:

$$\boldsymbol{\eta = \frac{eff_{sample}}{eff_{cal\_std}}} \tag{2-7}$$

Where:

- eff_{sample} is the efficiency of photon detection for the sample material
- eff_{cal_std} is the efficiency of photon detection for the calibration material

Suppose the detector's efficiency for a given source-to-detector geometry and material is known from previous experimental calibration, and the Efficiency Correction Factor (ECF) is also known. In that case, the actual efficiency during the sample analysis is calculated as follows:

$$\boldsymbol{eff_{sample} = eff_{cal\_std} \cdot \eta} \tag{2-8}$$

If both eff_{sample} and eff_{cal_std} are determined for the same energy in a specific source-to-detector geometry, then ECF is calculated by the formula (2.7). It might be argued that ECF calculation is unnecessary if eff_{sample} is already known. However, it is important to note that if the detector geometry is not accurately known, the ECF, calculated as the ratio of the two efficiencies, helps mitigate inaccuracies introduced by the detector's geometrical characteristics [4].

There are different methods found in the literature used to determine the ECF, a few of which are mentioned below. One of them is the calculation with Monte-Carlo simulations, which can also be compared with other methods' results. Also, the experimental method called the "Spike method" is used, which involves adding a known quantity of a standard solution containing the isotope needed to be analyzed, to the sample under study. Self-absorption correction factors are determined by comparing spiked samples' count rate or activity to those of unspiked samples. However, this method is complex and impractical due to its effect on the chemical composition of the samples [21]. Another method used is the "Parallel beam self-absorption method", introduced by [22]. This method correlates the attenuation of an external photon beam passing through the sample to the self-absorption of photons emitted within the sample. However, its accuracy is limited and only applies to a specific range of sample thicknesses. The method used in the current work was introduced by [5]. It is known as the "Integral method", and more details are given below.

2.6.2 The Integral method for the determination of ECF

This method can be applied to cylindrical samples, without having restrictions regarding the sample's height, unlike the "Parallel beam self-absorption method". According to [5], the

efficiency calibration should be correlated to the self-absorption inside the sample. Therefore, the method proposed is based on the following steps:

- Estimation of the efficiency for a specific source-to-detector geometry
- Estimation of an ECF for the analyzed sample, because of the difference in the attenuation coefficients of the sample and the calibration source

The estimation of the ECF requires the numerical calculation of the double integral J(μ), which is roughly proportional to the fraction of photons interacting with the detector and contributing to the full-energy peak. The formula of J(μ) is:

$$\boldsymbol{J(\mu) = \int_0^R \int_0^t \frac{e^{-\mu \cdot z}}{r^2+(x+d)^2} \cdot r \cdot dx \cdot dr} \quad (2\text{-}9)$$

Where:

- μ is the linear attenuation coefficient of the material (cm^{-1})
- R is the source radius (cm)
- t is the source thickness (cm)
- d is the fictitious source-to-detector distance (cm), which is defined as the distance from the sample's surface facing the detector to a fictitious point within the detector [5]. This distance factors in the interaction of photons that occur inside the detector volume, not only the surface
- z is the distance a photon travels within the source before reaching the detector's active zone, without any prior interaction in the source or adjacent layers, contributing to the full-energy peak through photoelectric absorption. It is calculated by the formula:

$$\boldsymbol{z = x \cdot \sqrt{r^2 + (x+d)^2}/(x+d)} \quad (2\text{-}10)$$

The Efficiency Correction Factor **η** is calculated by evaluating the formula (2.9) twice, once for the calibration source material $\boldsymbol{J(\mu_{Cal\_std})}$ and a second time for the sample's material $\boldsymbol{J(\mu_{sample})}$. Then ECF is calculated as the ratio**:**

$$\boldsymbol{\eta = \frac{J(\mu_{sample})}{J(\mu_{Cal\_std})}} \quad (2\text{-}11)$$

Where:

- μ_{Cal_std} is the calibration source linear attenuation coefficient

- μ_{sample} is the sample source linear attenuation coefficient

According to the formulas used to find ECF with the Integral Method, it is obvious that, for a specific detector, the values needed are: the linear attenuation coefficient of the calibration source, the linear attenuation coefficient of the sample material, the sample-detector geometry characteristics and the fictitious source-to-detector distance, that requires the estimation of the effective interaction depth (EID) d_e inside the detector. More details about this are given in the next paragraph.

2.6.3 The Effective Interaction Depth (EID) inside the detector

As shown in the equations (2.9) and (2.10), a fictitious source-to-detector distance d was introduced. The following formula calculates this distance:

$$\boldsymbol{d = d_s + d_c + d_e(E)} \tag{2-12}$$

Where:

- d_s is the source-to-detector end cap distance (cm)
- d_c is the detector-to-detector end cap distance (cm)
- $d_e(E)$ is the detector's effective interaction depth (cm)

In particular, the distances d_s and d_c are determined by the source and detector geometry, while $\boldsymbol{d_e}$ is the **effective interaction depth (EID)** of the detector [5]. The schematics for these distances are depicted in Figure 2-11.

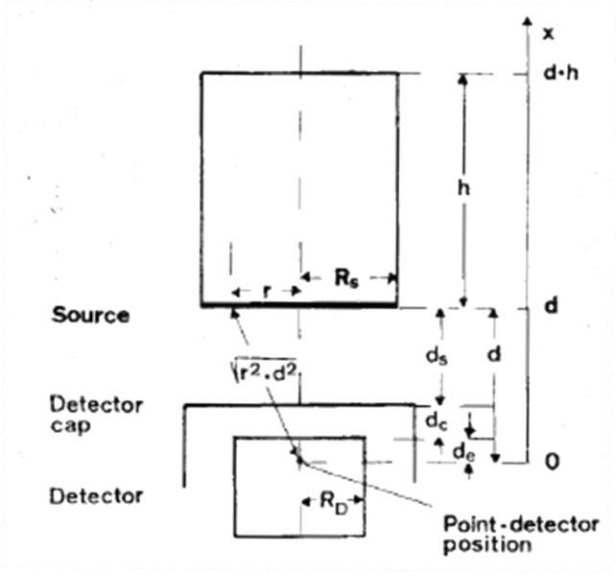

Figure 2-11 Source-to-detector schematics [5]

It is of great importance to estimate the EID, which depends on the type and geometry of the detector, as well as the energy of interest. This need arises from the fact that photons emitted from the volume source are absorbed in different depths inside the volume of the detector, and not just on the surface of it. Thus, the "fictitious" point detector should be located at a position where it would yield results identical to those of the actual detector.

The EID for a specific detector and photon energy can be determined either experimentally, following the procedure defined in [1], or with Monte-Carlo simulations, which is the focus of the current work, and the procedure is described in detail in the fourth chapter. Regarding the experimental procedure, the setup is quite simple. It requires a point source that emits photons of the desired energy, positioned along the axis of the detector at various distances. The count rate of the detected photons is recorded at each distance. The EID can be easily determined by applying the inverse square law and plotting these values for every distance.

The EID for the LEGe detector, which is installed at NEL-NTUA, has been estimated experimentally [1], and is equal to:

- 1.00 cm ± 1.4%, for 59.54 keV photons
- 1.34 cm ± 0.9%, for 122.06 keV photons
- 1.33 cm ± 1.33% for 661.66 keV photons

The next chapters discuss the influence of the EID on ECF determination and how the photon energy affects EID estimation.

2.7 Naturally Occurring Radioactive Materials (NORM)

Naturally **O**ccurring **R**adioactive **M**aterials, commonly called NORM, characterize any radioactive substance that is naturally present in the environment and human activities elevate people's exposure to the ionizing radiation they emit. They exist everywhere in the environment, or are produced due to human activities, like coal burning for electricity production. NORM mainly comprises uranium (^{238}U), thorium (^{232}Th), and potassium (^{40}K), which have existed since the Earth's formation around 4.5 billion years ago. These radionuclides undergo spontaneous decay, resulting in various other radionuclides known as decay products, including radon (^{222}Rn) and radium (^{226}Ra) [23]. In most human activities involving minerals and raw materials, exposure to NORM is typically not much higher than normal background levels and poses no significant radiation protection concern. However, some work activities can lead to substantially increased exposures that may require regulatory control [2].

The term technologically-enhanced NORM (TENORM) is also used to refer to those NORM in which the level of radioactivity has been increased or concentrated due to industrial processes.

Certain industries deal with substantial quantities of NORM, and because of the potential hazards that have been recognized over time, they have increasingly come under monitoring and regulation. These industries include the coal industry (mining and combustion), the oil and gas industry (production), metal mining and smelting, mineral sands (rare earth minerals, titanium, and zirconium), fertilizer (phosphate) industry, the building industry, recycling, and uranium mining. The by-products and waste of these industries characterized as NORM, may have high density and contain substantial amounts of high Z elements. Consequently, when analyzing these materials using gamma spectrometry techniques, the issue of photon self-absorption can become much more pronounced compared to other environmental materials like soil or sediments.

The current work focuses on seven NORMs, regarding their self-absorption properties and the need for ECF when conducting gemma-spectroscopy analysis. These materials are:

- Soil with 3% moisture
- Red Mud (waste generated in the Bayer process for Aluminum production)
- Fly Ash (waste generated in coal burning power plants)
- Phosphogypsum (waste generated in the fertilizer industry)
- Lead Slag
- Granulated Slag
- Shaft Furnace Slag

The calibration source 4M HCl was also examined, as well as water, since water samples are a routine type of analysis at NEL-NTUA.

2.7.1 Soil

Soil is a natural body made up of solids (minerals and organic matter), liquids, and gases that exist on the land surface. It is a fundamental foundation of life on Earth, serving as a reservoir for water and nutrients, a medium for filtering and decomposing harmful wastes, and playing a vital role in the cycling of carbon and other elements throughout the global ecosystem.

The study of soil as a distinct scientific discipline began around the same time as systematic investigations into substances that promote plant growth. This initial research has evolved into understanding soils as complex, dynamic, biogeochemical systems essential to the life cycles of terrestrial plants and soil-dwelling organisms, and ultimately to human life. Radioactivity of soil is of great interest as it may be contaminated due to nuclear or radiological accidents, while elevated soil natural radioactivity may be harmful for human.

2.7.2 Red Mud

Red mud is a by-product of the Bayer process used to produce alumina from bauxite. Typically stored in dams, it poses a risk of accidents. Its composition varies based on the

parent material (bauxite) from which it is derived. Red mud exists as a slurry with 10-30% solid materials and a high pH, and it contains significant amounts of aluminum and iron oxides.

2.7.3 Fly Ash

Fly ash is a by-product of coal combustion and is one of the most abundant waste materials globally. If not collected, it is expelled with flue gas from coal-fired power plants. Composed of tiny, airborne particles, fly ash is considered particulate matter or particle pollution. Its chemical composition can vary depending on the coal's origin. Generally, fly ash is a pollutant containing acidic, toxic, and radioactive substances, including lead, arsenic, mercury, cadmium, and uranium. According to the EPA (United States Environmental Protection Agency), significant exposure to fly ash and other coal ash components increases the risk of cancer and respiratory diseases [24].

2.7.4 Phosphogypsum

Phosphogypsum is a solid waste by-product from processing phosphate ore to produce phosphoric acid, which is used in fertilizer. It contains radium, which decays to form radon gas. Both radium and radon are radioactive and carcinogenic.

The building materials industry appears to be the largest sector capable of reprocessing significant amounts of this industrial by-product. However, only 15% of global phosphogypsum production is recycled in the building materials industry, primarily for the manufacture of Portland cement. The remaining 85% is disposed of without any treatment, typically dumped in large stockpiles that occupy substantial land areas and cause serious environmental damage due to chemical and radioactive contamination.

The primary issue limiting the use of phosphogypsum in construction is its radioactivity, particularly the content of radon, and its potential impact on human health. The remaining impurities can be relatively easily extracted.

2.7.5 Slags

Slag is a byproduct of metallurgical smelting processes and is a mixture of metal oxides, silicon dioxide, and various compounds. It is generated during the combustion of raw ore or the extraction of specific minerals from smelting materials. Large quantities of slag are produced globally and improper or unplanned disposal of this slag into the environment leads to severe contamination. Different types of industries around the world produce various types of slag [25]. Three of them were examined in this work, which are the ones described below.

- **Lead Slag**

  Lead slag is produced during the lead recovery process from various wastes, such as dust and slimes generated during flue gas cleaning in copper processing.

- **Granulated Slag**

Granulated slag is generated during a rapid water-cooling process of electric furnace residuum.

- **Shaft Furnace Slag**

Shaft furnace slag is produced in a shaft furnace where it takes place the melting of the ores and the converter slag in the form of briquettes.

3. Initial approach for the estimation of ECF with a Matlab code

This work constitutes the third attempt to improve the estimation of ECF for NORMs. In 2017 the first approach [3] to develop a MATLAB code to compute the ECF for the NORMs of interest with the "Integral Method" was carried out. This effort continued in 2021 [4] to address the deficiencies that emerged during the initial exploration of this topic. Further details are provided below regarding the valuable information obtained from these efforts and the areas identified for improvement.

3.1 First approach

3.1.1 Steps followed for the estimation of ECF

Taking into consideration that gamma-spectroscopy analysis of environmental samples requires the use of ECFs, this work focused on energies ranging from 40 to 400 keV. The reason is mainly because of the various characteristic photons that NORMs emit below 400 keV, such as ^{210}Pb (46.52 keV), ^{241}Am (59.54 keV), ^{234}Th (63.29 keV), ^{212}Pb (238 keV), ^{214}Pb (295 and 352 keV) and ^{228}Ac (338 keV).

Analytical and Monte Carlo simulation techniques were used to estimate the ECFs for the NORMs of interest, such as soil, red mud, fly ash, phosphogypsum, and three different types of slags derived from copper processing.

In particular, the first step was to calculate the mass attenuation coefficients for all the materials. These were utilized in the next step to calculate the linear attenuation coefficients necessary to determine the ECFs with the "Integral Method". For that reason, the code MUPLOT[7] was utilized that is developed by the University of Bologna and is freely available online. Additionally, because of the lack of literature concerning the densities of materials, the following formula was used:

$$\boldsymbol{\rho} = \sum_{\boldsymbol{i}} \boldsymbol{\rho_i w_i} \tag{3-1}$$

Then, a MATLAB code was developed, which computes the ECFs with the "Integral Method". The inputs given were the sample geometry, the photon energy, and the material type. Regarding the geometry, this program provided the option to choose between two different geometries, "Geometry 2" and "Geometry 8", which are two cylindrical geometries used at NEL-NTUA, based on a cylindrical containment with the following dimensions respectively: r = 3,6cm and t = 6,9cm for "Geometry 2", r=3,6cm and t = 1,08cm for "Geometry 8". The program calculated the mass attenuation coefficient for the values that were not already calculated by the code MUPLOT. This was done by using the following empirical equation:

[7] It is available on the website: http://shape.ing.unibo.it/html/muplot.htm

$$ln(\mu) = A\,ln^2(E) + B\,ln(E) + C \Rightarrow \mu = e^{A\ln(E)^2 + Bln(E) + C} \quad (3\text{-}2)$$

The constants A, B, and C were derived by interpolating the natural logarithm of the mass attenuation coefficient over the natural logarithm of the energy. An indicative graph for the calibration source material 4M HCl is shown in Figure 3-1:

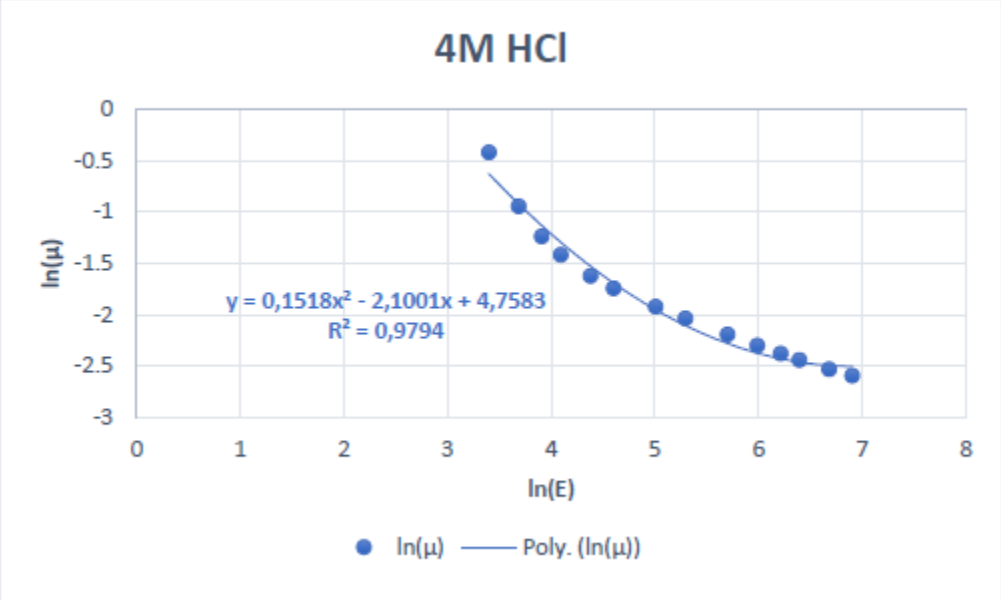

Figure 3-1 The plot of the natural logarithm of the mass attenuation coefficient over the natural logarithm of the energy for the 4M HCl solution[3]

Then the mass attenuation coefficients were multiplied by the densities to obtain the linear attenuation coefficients for both the sample and the calibration source. The code gave as an output the ECF. This first application was focused on the NEL-NTUA LEGe detector, for which the fictitious source-to-detector distance was considered constant for all the energies and equal to 2 cm.

Moreover, Monte Carlo simulations were performed for the NORMs mentioned above, as well as the calibration source 4M HCl, corresponding to the geometry of the LEGe detector and the two sample geometries. The ECFs were obtained as the ratio between the efficiencies of the simulated material and the calibration source. In that way, it was possible to compare the ECF values calculated with the simulations and the ones derived by the "Integral Method".

Lastly, for comparative purposes, the program CALCEFF was also used, which is part of the code SPUNAL that is used at NEL-NTUA for gamma spectroscopic analysis. This in-house developed code was developed in Fortran and runs under UNIX environment. SPUNAL calculates the ECFs using the "Integral Method", various materials, including soil 3% and fly ash, for energies up to 200 keV.

3.1.2 Conclusions and areas for improvement

The last step was to compare and analyze all the results obtained with the different methods. Some of the main points and conclusions are described below. Due to uncertainties, the results derived by MATLAB and PENELOPE did not correspond perfectly as shown in Figure 3.2.

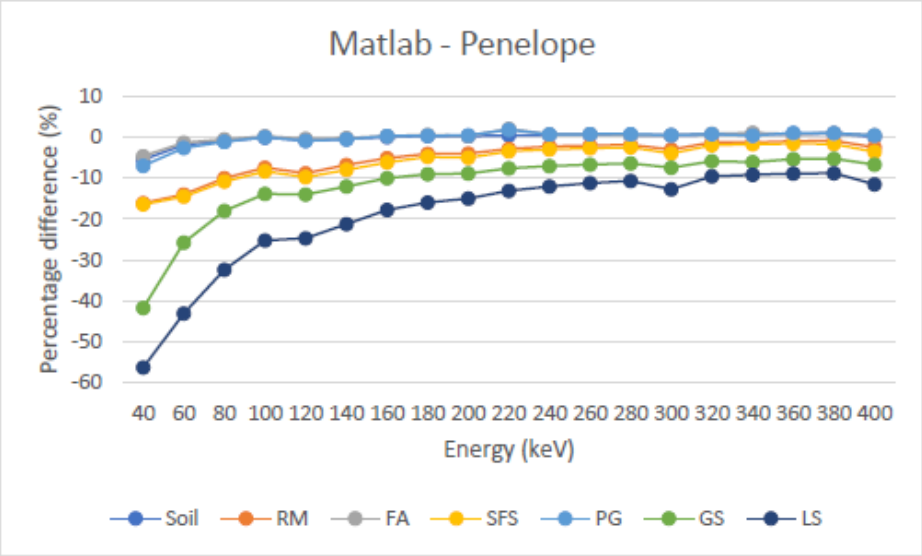

Figure 3-2 Percentage difference between the efficiency correction factor values obtained with MATLAB and PENELOPE [3]

A reason that was considered to contribute significantly to these differences, was the fact that PENELOPE and MATLAB used different data systems and calculation procedures to get the mass attenuation coefficient. Hence, these values led to different results. Consequently, it was deemed of great importance to solve this problem in the future.

Another reason that needed further investigation, was the correlations used to fit the linear attenuation coefficients with energy for various materials. In fact, it was considered that a third-order polynomial, or splitting the energy range into more sub-regions, would be useful.

Overall, the results obtained with the different methods did not deviate greatly for energies above 200 keV. However, for lower energies significant differences were observed which in the case of Lead Slag reached ~60%. In general, it was concluded that there was still room for improvement, to diminish the differences even more, and investigate how every single parameter affects the calculation of the ECF. Also, an important outcome was that an ECF is needed even for energies well above 400 keV, especially for dense materials, contrary to what it was originally believed that corrections up to the energy of 200keV would be sufficient.

3.2 Upgrade of the MATLAB program-Second approach

3.2.1 Steps followed for the estimation of ECF

Subsequently, the work conducted in the initial thesis was extended by a second thesis, which concentrated on upgrading the MATLAB code in various ways. The main goal was to enhance the accuracy of the results, as well as to increase flexibility and ease of use.

Regarding the accuracy of the results, it was mainly improved by the introduction of better fittings to calculate the total mass attenuation coefficient μ_m. Calculating this factor using the same data with the Monte Carlo simulations was deemed very important. Therefore, all the mass attenuation values were calculated from the beginning based on the data obtained from the PENELOPE simulation code, with the program tables.exe. These calculations were now made for 14 energy levels between 30 keV and 2000 keV, while for the densest material Lead Slag, they were made for 27 energy levels. Subsequently, to find the best correlation to fit the data (E, μ_m), the plot of the natural logarithm of the mass attenuation coefficient μ_m over the natural logarithm of the energy was split in the energy region into two sub-regions and two-third-order polynomials were used to cover each part. The result is shown in Figure 3-3 below.

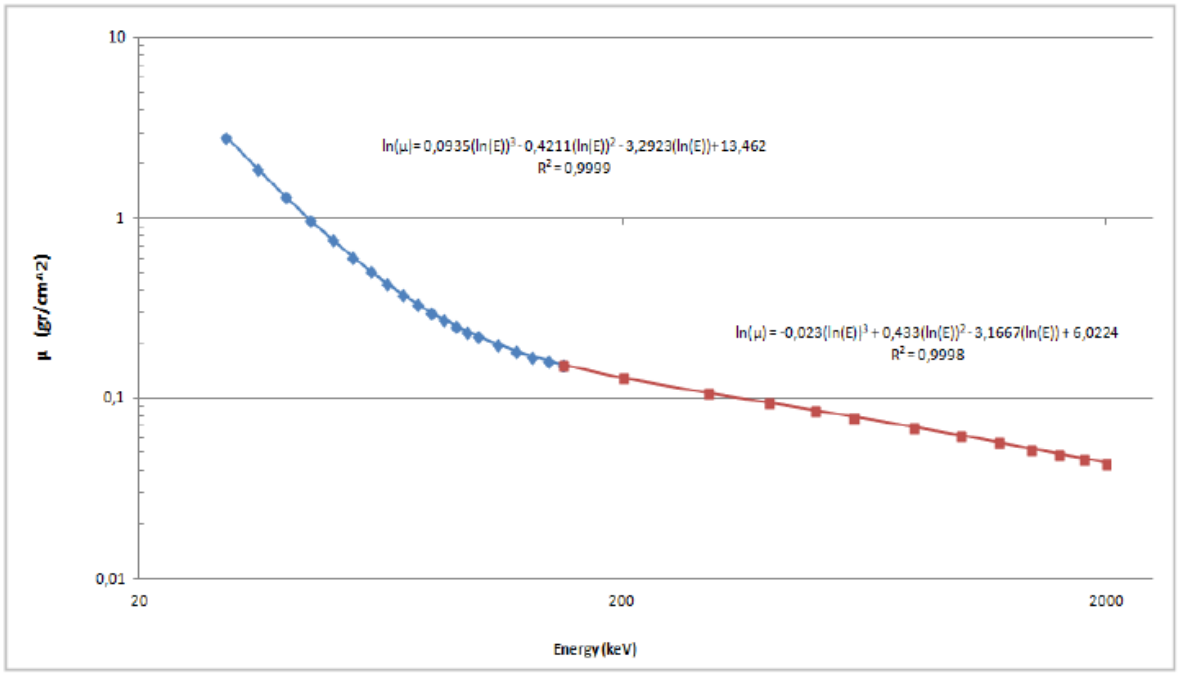

Figure 3-3 The plot of the natural logarithm of the mass attenuation coefficient over the natural logarithm of the energy for the LS presented as an example with two-third-order polynomials[4]

Hence, the equation used by the new MATLAB program to calculate the mass attenuation coefficient for each sub-energy region was:

$$\mu_m = e^{[A\cdot(\ln E)^3+B\cdot(\ln E)^2+C\cdot\ln E+D]} \quad (3\text{-}3)$$

Where, for each material, the values of A, B, C, and D are determined for each energy sub-region.

Thereafter, the thesis focused on the flexibility of the MATLAB program. Consequently, the first modification was to let the user set manually the value of the EID. The program requires, as input, the sum of the distance from the source (bottom of the sample) to the detector and the EID within the detector.

Another change in the program was the possibility for the user to choose manually the desired material density, while typical values were provided on the screen for assistance.

Besides the changes mentioned above, modifications were implemented to allow the user the flexibility to select any cylindrical geometry by specifying its height and radius. However, the user was still able to choose from the default geometries, “Geometry 2” and “Geometry 8”.

Also, the material “Water” was added to the list of materials, which could be considered either as a material to be analyzed or as a calibration source.

The final modification to the program was the extension of the energy range up to 2000 keV. This was deemed important as many isotopes of interest emitted by environmental samples and NORMs, often exceed the energy of 1000 keV, and their ECF is not equal to one.

To make this program more user-friendly and facilitate its use, it was necessary to develop a standalone application, thereby eliminating the requirement for MATLAB software installation. In particular, a standalone desktop application in the form of ”.exe” was created with MATLAB-GUI. The user gives as inputs the geometry of the sample, the source-to-detector distance, the material, the material’s density, the photon energy, and the program calculate the mass attenuation coefficient, and the ECF.

3.2.2 Conclusions and areas for improvement

The standalone application that was created is shown in Figure 3-4. The flexibility that the new code provided allowed for the estimation of ECF for various scenarios of materials, densities, geometries and photon energies The program results and the comparisons made with Monte-Carlo simulation results indicated that the accuracy in ECF calculation was generally sufficient, except in cases involving high-density materials and relatively low-energy photons. Specifically, the results between MATLAB and Monte Carlo simulations had a percentage difference of 20% for the higher-density materials and 5% for low-density materials. The results regarding the percentage difference between MATLAB and Monte Carlo simulations are shown in greater detail in Figure 3-5

Figure 3-4 Running the application with an example [4]

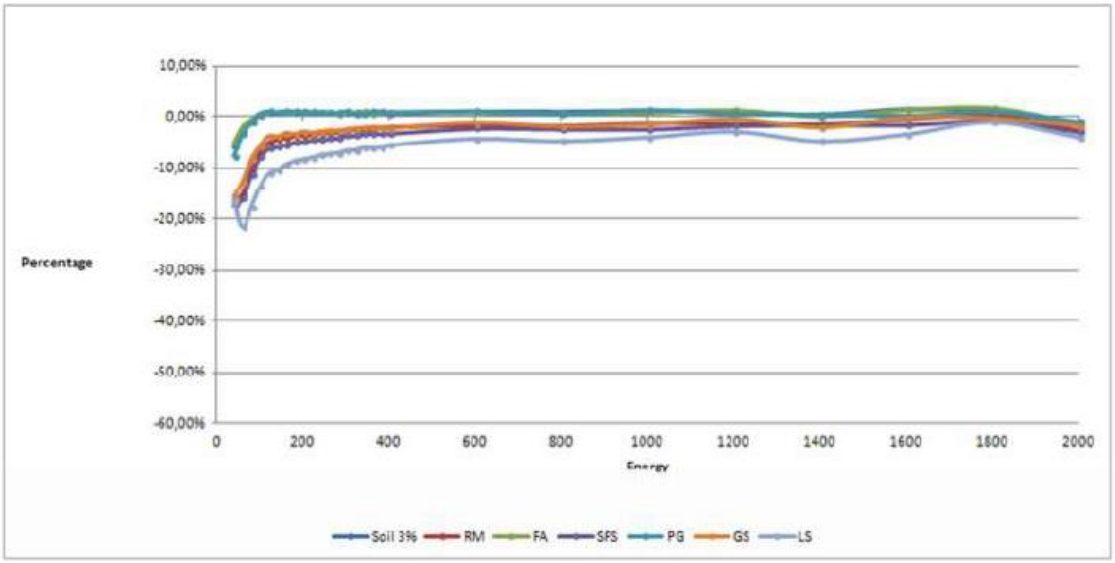

Figure 3-5 Percentage difference between MATLAB and Monte Carlo simulations [4]

With the program being more flexible and user-friendly, it was able to further study the effect of EID . A parametric analysis showed that the EID is energy-dependent and ECF seems to depend on the distance (d). Therefore, a systematic study in this field could potentially fix some inaccuracies in the results.

Overall, despite the significant improvements in enhancing the code's accuracy, there were still areas that require further investigation. Modifications can be made to ameliorate the results in low energies for dense materials where the differences are maximum. The areas that should be examined are the influence of the EID, as well as other phenomena that were not taken into consideration so far, such as the near elastic scattering which affects the photopeak shape at low energies especially for higher densities.

4. The calculation of the Effective Interaction Depth (EID)

As mentioned in the previous paragraph, a significant conclusion drawn from the previous thesis [4], was the great influence of the EID on the estimation of the ECF. Consequently, it was deemed important to investigate this parameter further. This work focused on the detector XtRa, which is in operation the NEL-NTUA. To calculate the EID, Monte-Carlo simulations were conducted. Furthermore, the EID was also estimated experimentally to ensure completeness and enable cross-referencing with the simulations. Both methods are described in detail below. Moreover, the results derived from these methods are thoroughly discussed.

4.1 Monte-Carlo simulations for the calculation of the EID

4.1.1 PENELOPE code

The Monte-Carlo code used to perform the simulations is PENELOPE (**PEN**etration and **E**nergy **LO**ss of **P**ositrons and **E**lectrons). It is a computer code system that performs Monte-Carlo simulations of coupled electron-photon transport in various materials across a wide energy range, from a few hundred electron volts (eV) to approximately 1 gigaelectron volt (GeV) [26]. The interaction processes on which the code is based, are the dominant ones for the energy range mentioned previously, which are the photoelectric effect, coherent (Rayleigh) scattering, incoherent (Compton) scattering, and electron-positron pair production. The distribution package of PENELOPE includes three main programs, PENSLAB, PENCYL, and PENMAIN. According to the geometry and the nature of the problem, the appropriate program is used.

4.1.2 The procedure of the simulations

For the simulations conducted in this work, the main program PENMAIN was used, because it is suitable for simulations with complicated geometries. Moreover, it was considered important to run the simulations for the energy range of 40-1000 keV, because, as mentioned in previous paragraphs, the radionuclides of interest for detecting NORMs, emit photons within this range. Additionally, the EID varies more significantly within this region. The prerequisite to run the simulations is the preparation of the geometry file, the material files, and the input file. All of them are built in a text editor, but further details about these files are given below.

4.1.3 Geometry file

The geometry file of the XtRa detector (.geo file) was used for the simulations. It includes all the information regarding the bodies and modules constituting the detector system. These files are structured in three distinct sections. In the first part, the quadric surfaces limiting the bodies are defined. After this part follows the definition of the bodies, including information about their materials and the surfaces that define their borders. The third

section defines the modules of the geometry that contain the bodies. An example of the structure of these files is shown in Figure 4-1.

```
0000000000000000000000000000000000000000000000000000000000000000
SURFACE (   2)   PLANE Z2=-16.65
INDICES=( 0, 0, 0, 1, 1)
Z-SCALE=( 1.665000000000000E+01,   0)
0000000000000000000000000000000000000000000000000000000000000000
0000000000000000000000000000000000000000000000000000000000000000
BODY    (  32)   Ge Dead Layer peripheral
MATERIAL(   4)
SURFACE (  23), SIDE POINTER=(+1)
SURFACE (  22), SIDE POINTER=(-1)
SURFACE (   3), SIDE POINTER=(-1)
SURFACE (  47), SIDE POINTER=(+1)
0000000000000000000000000000000000000000000000000000000000000000
0000000000000000000000000000000000000000000000000000000000000000
MODULE  (  90)   Whole XtRa
MATERIAL(  10)
SURFACE ( 110), SIDE POINTER=(-1)
BODY    (   1)
BODY    (   2)
BODY    (   3)
BODY    (   4)
BODY    (   5)
BODY    (   6)
BODY    (   7)
BODY    (   8)
BODY    (   9)
BODY    (  10)
BODY    (  11)
BODY    (  12)
BODY    (  13)
BODY    (  14)
BODY    (  15)
BODY    (  16)
BODY    (  17)
BODY    (  18)
BODY    (  19)
BODY    (  20)
```

Figure 4-1 The structure of the geometry file

To ensure the simulations are as realistic as possible, the entire detector system was modeled within an encompassing air sphere. This configuration accounts for interactions occurring in the air before particles reach the detector. Furthermore, because the file is built in a text editor, it is not possible to have a direct visualization of the geometry, therefore the application gview2d was used for that purpose. These visualizations are shown in Figure 4-2. The right figure illustrates the materials of the geometry system, while the left figure shows the bodies that comprise it. Each material and body is depicted in a different color.

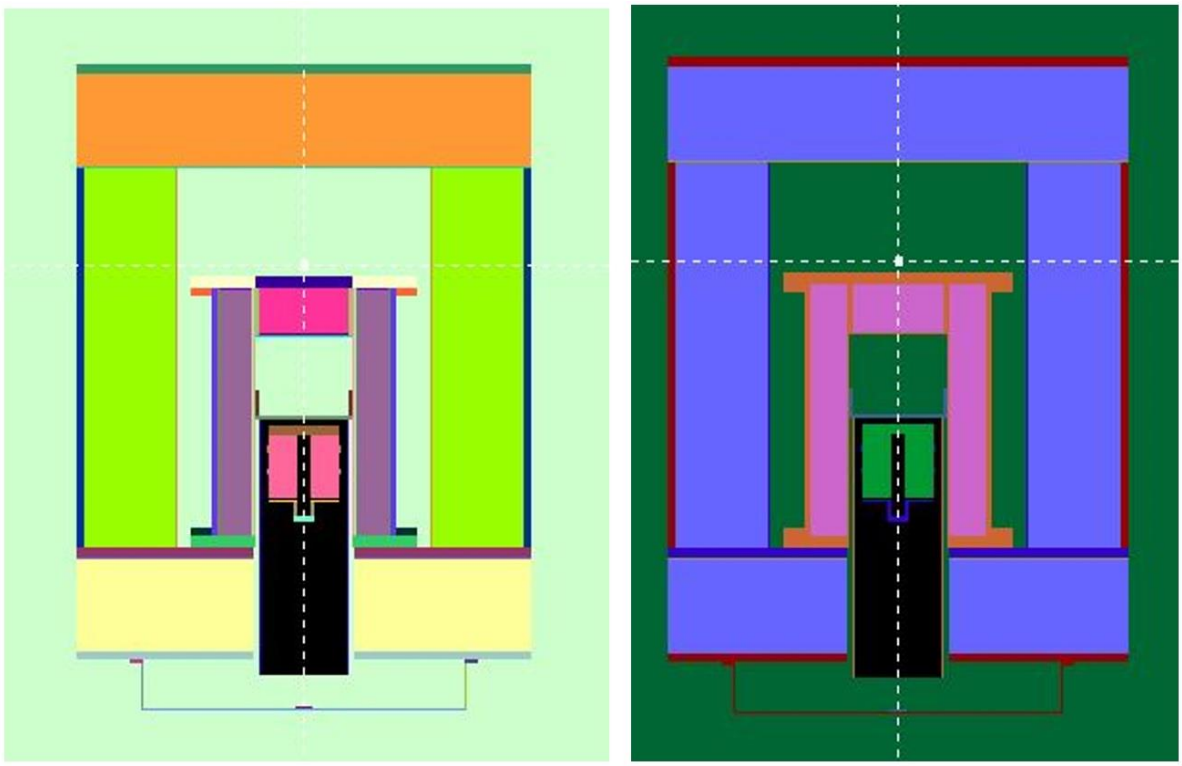

Figure 4-2 The geometry illustrations of the XtRa detector (left picture in bodies, right picture in materials)

4.1.4 Material files

The material files (.mat files) required to run the simulations were generated by the program material.exe, using the list of materials already existing in PENELOPE's database. The process followed is thoroughly described in [27]. Each file contains information about the physical properties of a material, such as the interaction cross-sections.

4.1.5 Input file

The input file (.in file) is built by the user in a text editor, and it has all the necessary information for the simulation. This includes the type of primary particles to be simulated, their energy, the desired number of simulated showers, and a list of material files, among other parameters. Additionally, the file specifies the position of the point source for each simulation, which is assumed to be isotropic. One important parameter that must be defined in the .in file is the number and types of detectors that will be used during the simulation. In this work one Energy Deposition Detector named "spc-enddet-01" was used to record the energy spectrum of the photons which deliver their energy to the actual detector used. This detector comprises of two bodies of the whole system geometry (body 15 and body 16). An example of the structure of the input file is given below.

```
TITLE  XtRa @ 40keV air Z=-8.32
       >>>>>>>> Source definition.
SKPAR  2        [Primary particles: 1=electron, 2=photon, 3=positron]
SENERG 4.000E4          [Initial energy (monoenergetic sources only)]
SPOSIT 0.0 0.0 -8.32                      [Coordinates of the source]
SCONE  0 0 180                          [Conical beam; angles in deg]
       >>>>>>>> Material data and simulation parameters.
MFNAME Carbon.mat                      [Material file, up to 20 chars]
MSIMPA 1E3 1E3 1E4 0.1 0.1 1E4 1E3           [EABS(1:3),C1,C2,WCC,WCR]
MFNAME Aluminum.mat                    [Material file, up to 20 chars]
MSIMPA 1E3 1E3 1E4 0.1 0.1 1E4 1E3           [EABS(1:3),C1,C2,WCC,WCR]
MFNAME Copper.mat                      [Material file, up to 20 chars]
MSIMPA 1E3 1E3 1E4 0.1 0.1 1E4 1E3           [EABS(1:3),C1,C2,WCC,WCR]
MFNAME Germanium.mat                   [Material file, up to 20 chars]
MSIMPA 1E3 1E3 1E4 0.1 0.1 1E4 1E3           [EABS(1:3),C1,C2,WCC,WCR]
MFNAME Iron.mat                        [Material file, up to 20 chars]
MSIMPA 1E3 1E3 1E4 0.1 0.1 1E4 1E3           [EABS(1:3),C1,C2,WCC,WCR]
MFNAME Lead.mat                        [Material file, up to 20 chars]
MSIMPA 1E3 1E3 1E4 0.1 0.1 1E4 1E3           [EABS(1:3),C1,C2,WCC,WCR]
MFNAME Tin.mat                         [Material file, up to 20 chars]
MSIMPA 1E3 1E3 1E4 0.1 0.1 1E4 1E3           [EABS(1:3),C1,C2,WCC,WCR]
MFNAME Polypropylene.mat               [Material file, up to 20 chars]
MSIMPA 1E3 1E3 1E4 0.1 0.1 1E4 1E3           [EABS(1:3),C1,C2,WCC,WCR]
MFNAME NaI.mat                         [Material file, up to 20 chars]
MSIMPA 1E3 1E3 1E4 0.1 0.1 1E4 1E3           [EABS(1:3),C1,C2,WCC,WCR]
MFNAME Air.mat                         [Material file, up to 20 chars]
MSIMPA 1E3 1E3 1E4 0.1 0.1 1E4 1E3           [EABS(1:3),C1,C2,WCC,WCR]
       >>>>>>>> Geometry and local simulation parameters.
GEOMFN XtRa_air.geo                    [Geometry file, up to 20 chars]
       >>>>>>>> Emerging particles. Energy and angular distributions.
NBE    0 4.1E4 200                     [Energy window and no. of bins]
NBANGL 10 10              [No. of bins for the angles THETA and PHI]
       >>>>>>>> Energy-deposition detectors (up to 25).
ENDETC 0 4.1E4 1000                    [Energy window and no. of bins]
EDBODY 15                                                [Active body]
EDBODY 16                                                [Active body]
       >>>>>>>> Job properties.
RESUME dump.dmp               [Resume from this dump file, 20 chars]
DUMPTO dump.dmp                  [Generate this dump file, 20 chars]
DUMPP  3.6E3                                [Dumping period, in sec]
NSIMSH 1E7                    [Desired number of simulated showers]
TIME   5E5                       [Allotted simulation time, in sec]
END                                [Ends the reading of input data]
```

Figure 4-3 The structure of the input file

4.1.6 Output file

After the simulation has finished, various files are generated. One of the output files, which contains all the important information about the deposited energy spectrum in the energy deposition detector. This file can be opened with a text editor, and its data can be processed using Microsoft Excel. It consists of three columns, with the number of rows depending on the number of bins defined in the input file to divide the energy range. In this case, the energy was divided into 1000 bins. The first column contains the values of the deposited energy in eV. The second column contains the values of the probability density in 1/(eV*particle), and the third column contains the statistical uncertainty, defined as 3 σ. An example of this file's structure is shown below.

```
#  Results from PENMAIN. Output from energy-deposition detector #  1
#  Deposited energy spectrum.
#  WARNING: May be strongly biased if interaction forcing is used!
#  1st column: deposited energy (eV).
#  2nd column: probability density (1/(eV*particle)).
#  3rd column: statistical uncertainty (3 sigma).

  2.050000E+01  2.439024E-09  7.317073E-09
  6.150000E+01  7.317073E-09  1.267354E-08
  1.025000E+02  4.878049E-09  1.034790E-08
  1.435000E+02  1.000000E-35  1.000000E-35
  1.845000E+02  4.878049E-09  1.034790E-08
  2.255000E+02  4.878049E-09  1.034790E-08
  2.665000E+02  7.317073E-09  1.267354E-08
  3.075000E+02  2.439024E-09  7.317073E-09
  3.485000E+02  4.878049E-09  1.034790E-08
  3.895000E+02  1.463415E-08  1.792309E-08
  4.305000E+02  9.756098E-09  1.463414E-08
  4.715000E+02  4.878049E-09  1.034790E-08
  5.125000E+02  1.463415E-08  1.792309E-08
```

Figure 4-4 The structure of the output file

4.1.7 The procedure for the calculation of the EID for the XtRa detector with Monte-Carlo simulations

One of the main goals of this work was to estimate the EID for the XtRa detector at various energies, so that it will be incorporated in the Matlab code. As mentioned in the previous paragraph, this investigation was crucial to determine whether this factor improves the calculation of the ECF using the "Integral Method", thereby ensuring that the results closely approximate the ECF obtained through simulations.

The procedure followed to calculate the EID is described in [5]. According to this method, the first step is to position a point source at various distances on the symmetry axis of the

detector and measure its peak count rates n(d). The values of the peak count rates change according to the inverse square law as follows:

$$\boldsymbol{n(d) \propto \frac{1}{d^2}} \tag{4-1}$$

This leads to the following formula:

$$\boldsymbol{\frac{1}{\sqrt{n(d)}} \propto d} \tag{4-2}$$

The next step is to plot the inverse of the square root of the count rate $\frac{1}{\sqrt{n(d)}}$, against the distance between the point source and the detector endcap. This should result in a straight line as shown in the following graph.

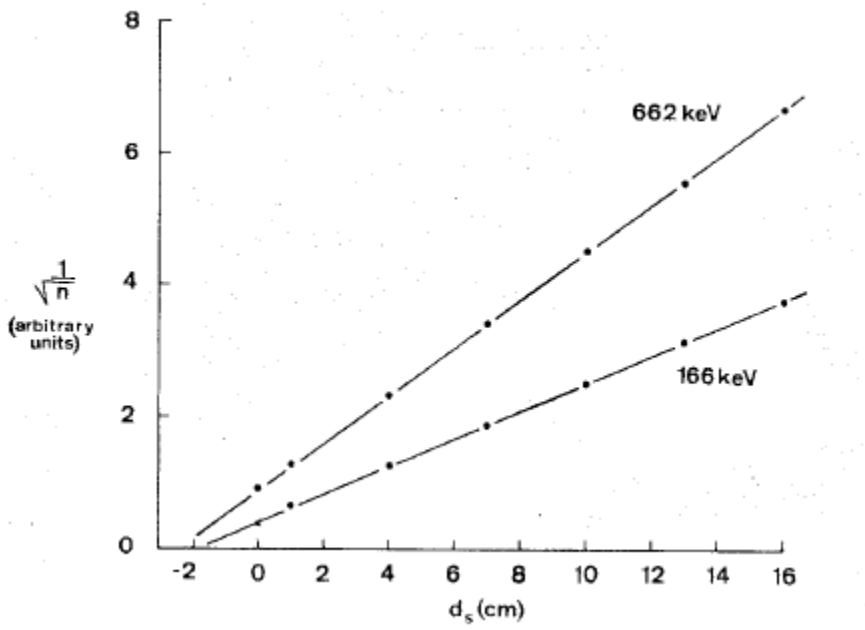

Figure 4-5 The plot to calculate the EID [5]

The final step to estimate the EID for each energy level is to extrapolate the line to the infinity count rate, corresponding to distance 0 and find the value of the fictitious point-detector position. This distance is referenced from point 0, which is the top of the Polypropylene cap. Nevertheless, to calculate the distance of the EID inside the detector, with the reference point being the top of the detector's dead layer, it is necessary to subtract the distance d_s (from the source to the detector endcap) and the distance d_c (from the endcap to the detector surface) from the value obtained from the graph.

In this work, the EID was calculated for ten distinct energy levels, specifically for 40 keV, 50 keV, 100 keV, 150 keV, 200 keV, 250 keV, 300 keV, 350 keV, 500 keV, and 1000 keV. Following

the procedure mentioned above, nine simulations were conducted for each energy level. For each of them, the isotropic point source was positioned at a different distance from the detector. In particular, the reference point was the polypropylene cap, which is situated on top of the vacuum area containing the Germanium detector body. Thus, along the symmetry axis of the detector, the point source was simulated, firstly, located on top of the Polypropylene cap (considered distance of 0 cm), to 8 cm from it, in 1 cm increments.

It is noteworthy that a point source was used to estimate the EID instead of a volume source, which would allow for the consideration of the phenomenon of self-absorption within the source. There are a couple of reasons for this choice. Firstly, with a volume source, self-absorption would prevent a linear relationship in the plot of the inverse square root of the count rate against the distance. Consequently, it would be impossible to extrapolate the curve to determine a fictitious point-detector position. Furthermore, when calculating the double integral to estimate the ECF, the phenomenon of self-absorption is already considered. Hence, using a volume source would result in considering this phenomenon twice.

4.1.8 Output files processing

To ensure the accuracy of all simulations, statistical uncertainties were calculated for the bins corresponding to the photopeak. As explained in [27], the percentage error was determined by dividing the statistical uncertainty, 3 σ (third column of the output file "spc-enddet-01.dat") by the probability density (second column of the output file "spc-enddet-01.dat") and multiplying this quotient by 100. For all conducted simulations, this error was found to be lower than 1%. Consequently, the results are deemed to be highly accurate.

To calculate the value of the inverse square root of the count rate $\frac{1}{\sqrt{n(d)}}$, for creating plots for the estimation of the EID for each energy, the following calculation was done.

$$\boldsymbol{n(d) = p_d \cdot dE \cdot Nt} \tag{4-3}$$

Where:

- p_d is the probability density 1/(eV*particle)
- dE is the bin width
- N_t is the total number of simulated photons

This multiplication gives us the number of photons recorded in the bin. The number of bins that need to be added is given by the following formula [28]:

$$\boldsymbol{n = \frac{1.5 \cdot FWHM}{dE}} \tag{4-4}$$

Where:

- FWHM is the Full Width at Half Maximum
- dE is the bin width

This formula is used because a full energy peak in the real spectrum, is delimited in the region [centroid ± 1.5·FWHM], thus including more bins than just the photopeak to include all the photons that would deposit their energy in the detector is crucial. To experimentally determine the full energy peak efficiency for photons with energy E, the net area of the full energy peak in the spectrum is assumed to represent the number of photons depositing energy E in the detector. However, a small number of photons with slightly reduced energy, due to prior scattering may also be recorded in the full energy peak. This results in a minor asymmetry in the peak, which is more evident for low-energy photons and photon sources with significant self-absorption. Despite this, the asymmetry is often so small that the photopeak can still be treated as a singlet. Therefore, when determining a full energy peak efficiency through simulation, all photons that might be recorded in the photopeak, including those with slightly reduced energy, should be considered [29]. Consequently, for the correct determination of the number of photons recorded under the photopeak, it is suggested to use the bins that include the photon energy region [E-n÷E], where n was defined in equation (4-4).

4.2 Results

4.2.1 Spectrum graphs

In this paragraph, spectrum graphs are displayed for all the respective energies used in the Monte-Carlo simulations for the calculation of the EID. These spectra provided valuable insights into the detected photo peaks, leading to several interesting conclusions. In general, as will be discussed in more detail below each graph, the identified photo peaks have four different origins.

- The full energy peak of the monoenergetic point source for each energy
- Photo peak created by the characteristic X-ray photon due to the photoelectric effect with the materials of the detector
- Photo peak created by X-ray escape peaks due to photons that interacted with the germanium, but the characteristic X-ray escaped, and therefore it creates a peak in the spectrum at an energy lower than the incident X-ray energy
- Photo peak created by characteristic X-ray photons due to the photoelectric effect with the materials of the detector, which subsequently interacted with the germanium, and the characteristic X-ray escaped.

The table 4.1 that follows shows the different K and L characteristics of X-ray photons of the materials that comprise the detector [30] and may be recorded in the simulated spectrum. It is worth noting that many of these peaks are not detected in the experimental spectrum as they are obscured by background fluctuations.

Table 4-1 The K and L characteristics of X-ray photons of the materials that comprise the detector

Material	$K_{\alpha 1}$(keV)	$K_{\alpha 2}$(keV)	K_{β}(keV)	$L_{\alpha 1}$(keV)	$L_{\alpha 2}$(keV)	$L_{\beta 1}$(keV)	$L_{\beta 2}$(keV)	L_{γ}(keV)
Aluminum	1.48	1.49	1.56					
Copper	8.05	8.03	8.91	0.93	0.93			
Germanium	9.89	9.86	10.98	1.19	1.19	1.22		
Lead	74.97	72.8	84.94	10.55	10.45	12.61	12.62	14.76
Tin	25.27	25.04	28.49	3.44	3.44	3.66	3.9	4.13
Sodium	28.61	28.32	32.29	3.94	3.93	4.22	4.51	4.8
Natrium	1.04	1.04	1.07					

Below each spectrum, a table is provided that lists the energies of most of the detected photo peaks along with their respective origins. It is important to note that not all photo peaks from the same origin have identical energies. This variation arises because the simulations at different energies were conducted using different energy bin-widths.

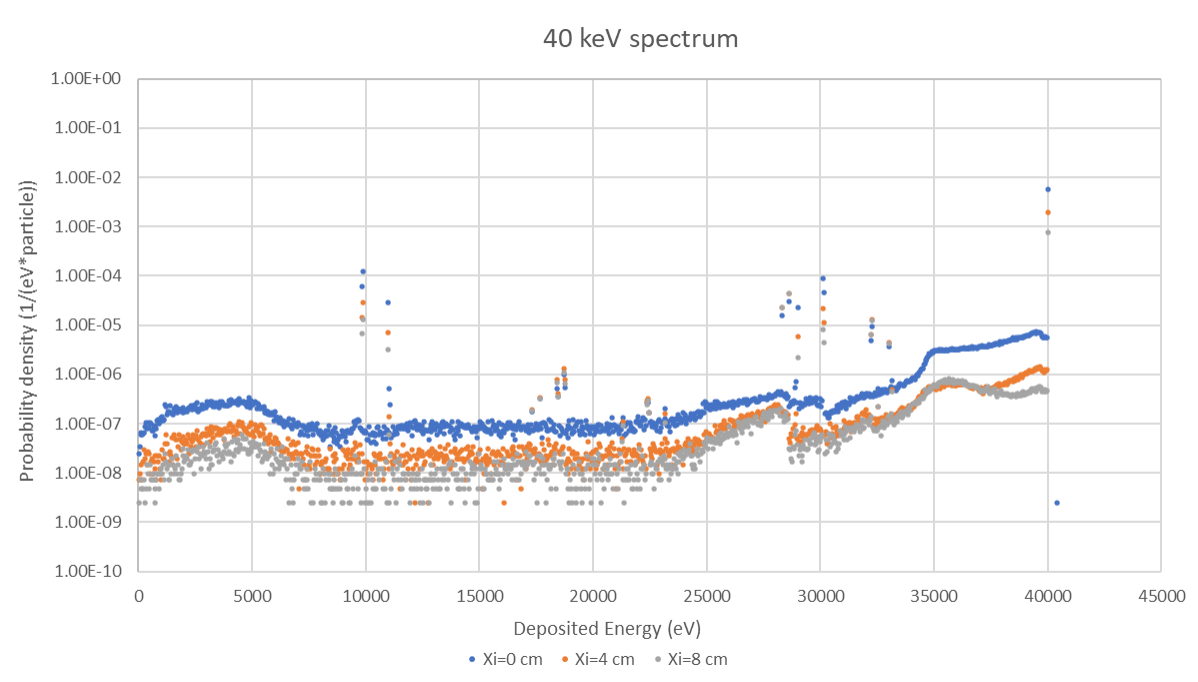

Figure 4-6 The spectrum for 40 keV

Table 4-2 The origin of the photo peaks for the spectrum of 40 keV

The energy of the photo peak (keV)	Origin of the photo peak
39.9	The full energy peak of the monoenergetic point source
30.1	The escape peak of the $K_{\alpha 1}$ X-ray emission line of Germanium
29.0	The escape peak of the K_{β} X-ray emission line of Germanium
10.9	The characteristic K_{β} X-ray of Germanium, which was detected because the photon interacted with the dead layer of the detector
9.9	The characteristic $K_{\alpha 1}$ X-ray of Germanium, which was detected because the photon interacted with the dead layer of the detector

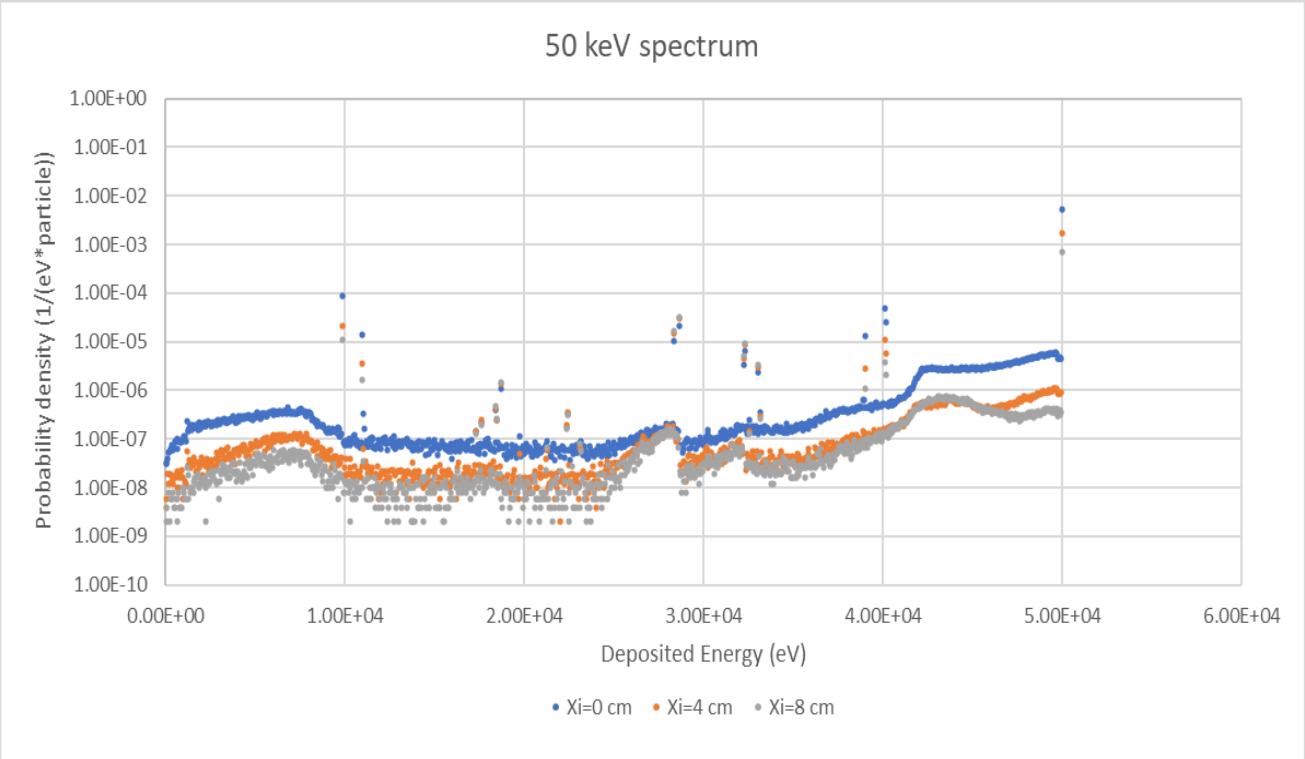

Figure 4-7 The spectrum for 50 keV

Table 4-3 The origin of the photo peaks for the spectrum of 50 keV

The energy of the photo peak (keV)	Origin of the photo peak
50.0	The full energy peak of the monoenergetic point source
40.1	The escape peak of the Kα1 X-ray emission line of Germanium
39.0	The escape peak of the Kβ X-ray emission line of Germanium
32.3	The characteristic Kβ X-ray of Sodium
28.6	The characteristic Kα1 X-ray of Sodium
28.3	The characteristic Kα2 X-ray of Sodium
11.0	The characteristic Kβ X-ray of Germanium, which was detected because the photon interacted with the dead layer of the detector
9.9	The characteristic Kα1 X-ray of Germanium, which was detected because the photon interacted with the dead layer of the detector

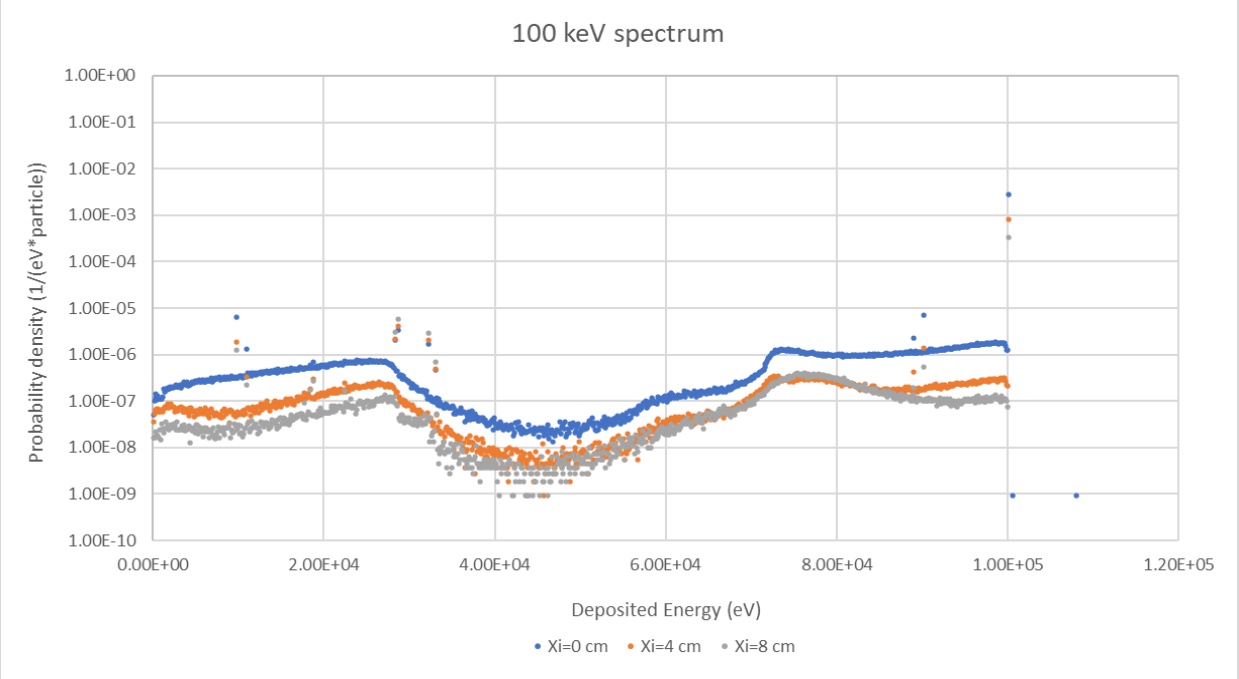

Figure 4-8 The spectrum for 100 keV

Table 4-4 The origin of the photo peaks for the spectrum of 100 keV

The energy of the photo peak (keV)	Origin of the photo peak
100.0	The full energy peak of the monoenergetic point source
90.1	The escape peak of the Kα1 X-ray emission line of Germanium
89.0	The escape peak of the Kβ X-ray emission line of Germanium
32.3	The characteristic Kβ X-ray of Sodium
28.7	The characteristic Kα1 X-ray of Sodium
10.9	The characteristic Kβ X-ray of Germanium, which was detected because the photon interacted with the dead layer of the detector
9.8	The characteristic Kα1 X-ray of Germanium, which was detected because the photon interacted with the dead layer of the detector

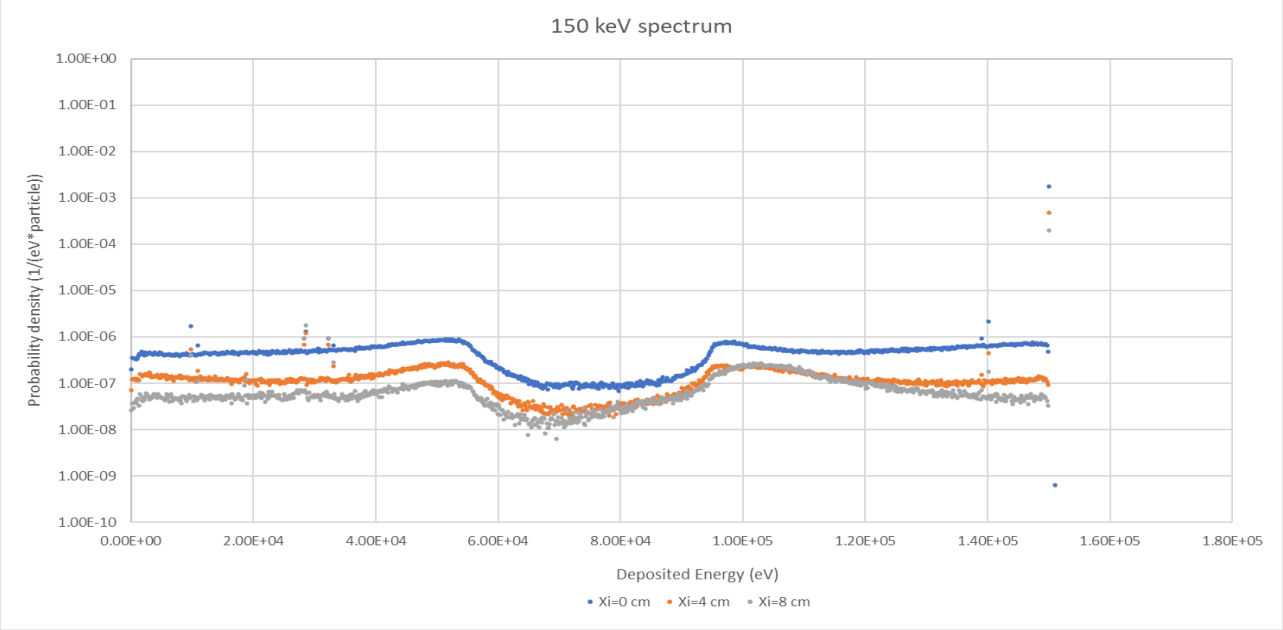

Figure 4-9 The spectrum for 150 keV

Table 4-5 The origin of the photo peaks for the spectrum of 150 keV

The energy of the photo peak (keV)	Origin of the photo peak
150.0	The full energy peak of the monoenergetic point source
140.0	The escape peak of the Kα1 X-ray emission line of Germanium
32.2	The characteristic Kβ X-ray of Sodium
28.6	The characteristic Kα1 X-ray of Sodium
9.8	The characteristic Kα1 X-ray of Germanium, which was detected because the photon interacted with the dead layer of the detector

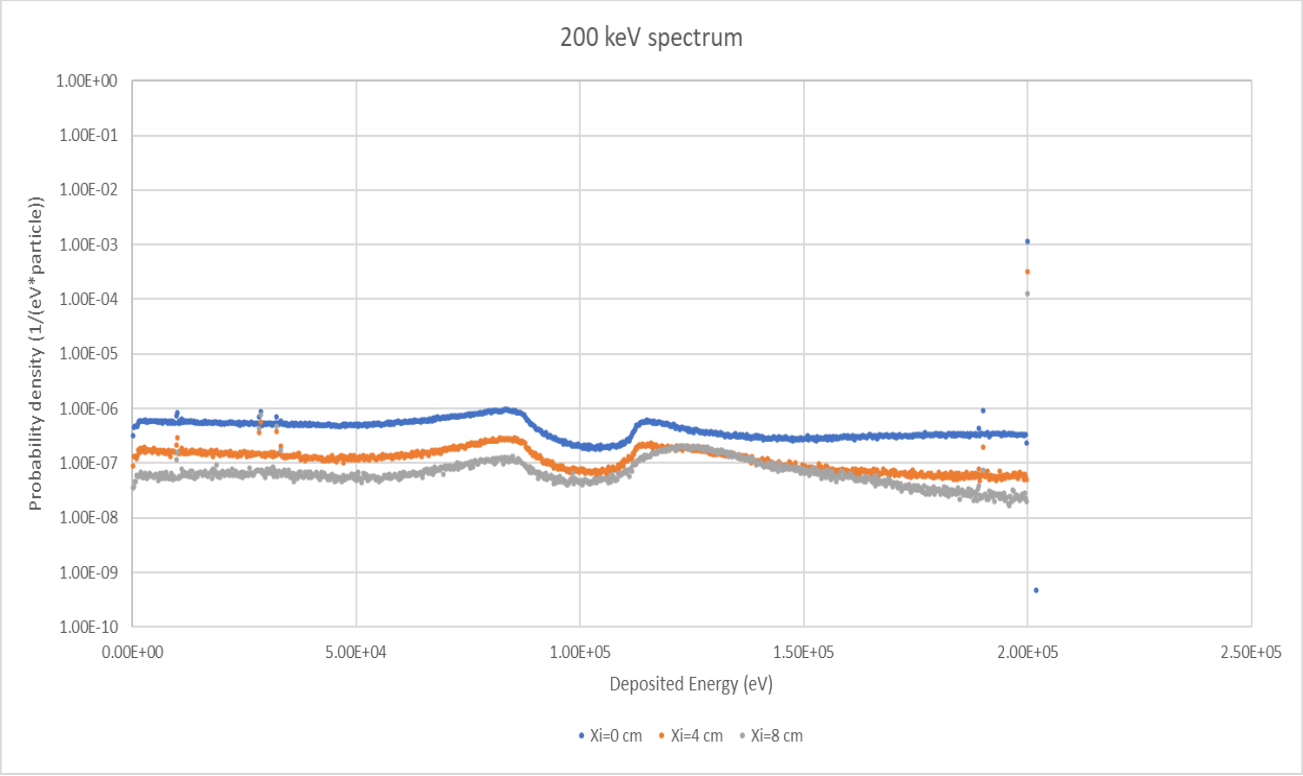

Figure 4-10 The spectrum for 200 keV

Table 4-6 The origin of the photo peaks for the spectrum of 200 keV

The energy of the photo peak (keV)	Origin of the photo peak
200.0	The full energy peak of the monoenergetic point source
190.0	The escape peak of the Kα1 X-ray emission line of Germanium
28.7	The characteristic Kα1 X-ray of Sodium
9.9	The characteristic Kα1 X-ray of Germanium, which was detected because the photon interacted with the dead layer of the detector

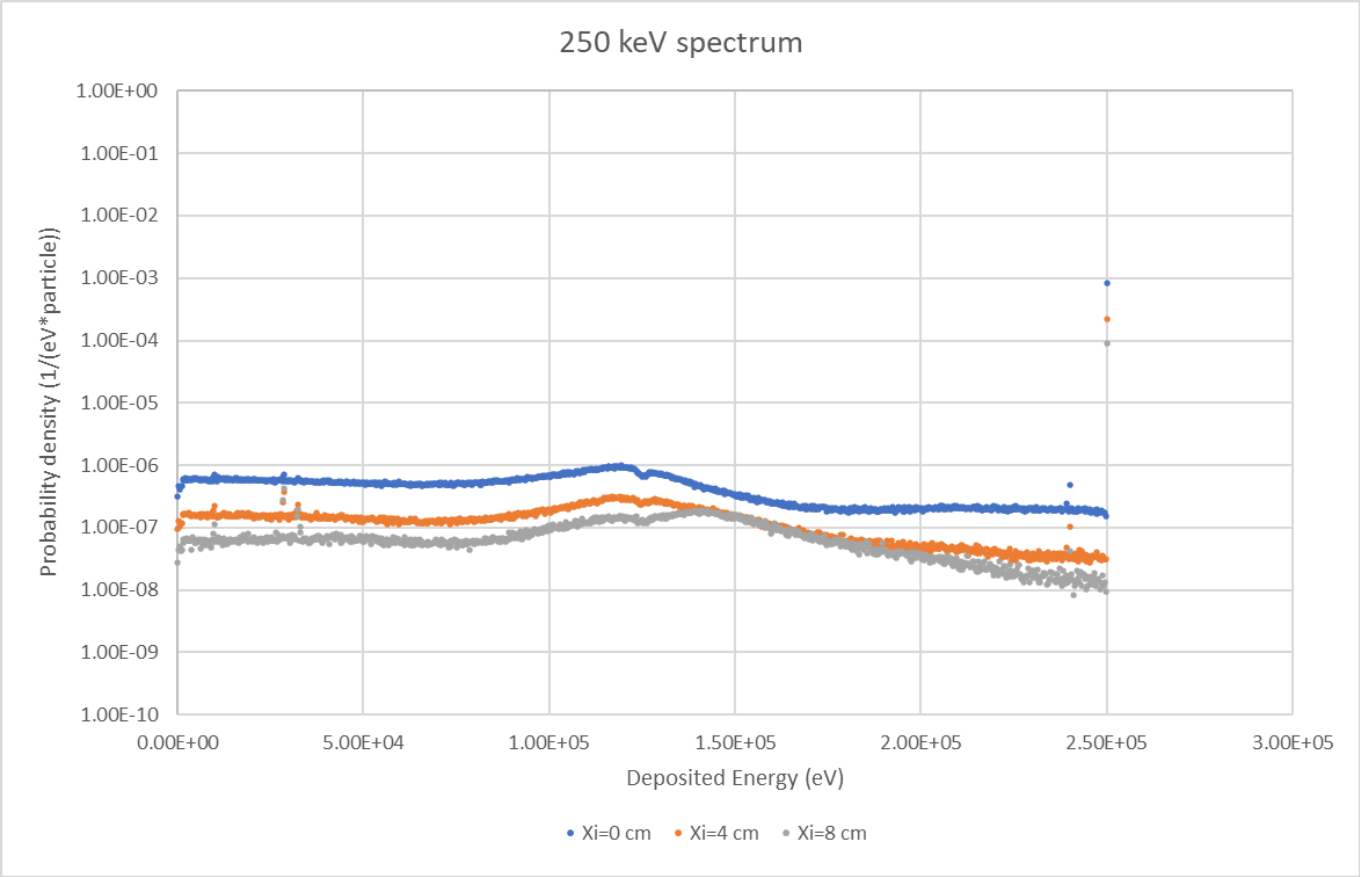

Figure 4-11 The spectrum for 250 keV

Table 4-7 The origin of the photo peaks for the spectrum of 250 keV

The energy of the photo peak (keV)	Origin of the photo peak
250.0	The full energy peak of the monoenergetic point source
240.0	The escape peak of the Kα1 X-ray emission line of Germanium
28.7	The characteristic Kα1 X-ray of Sodium

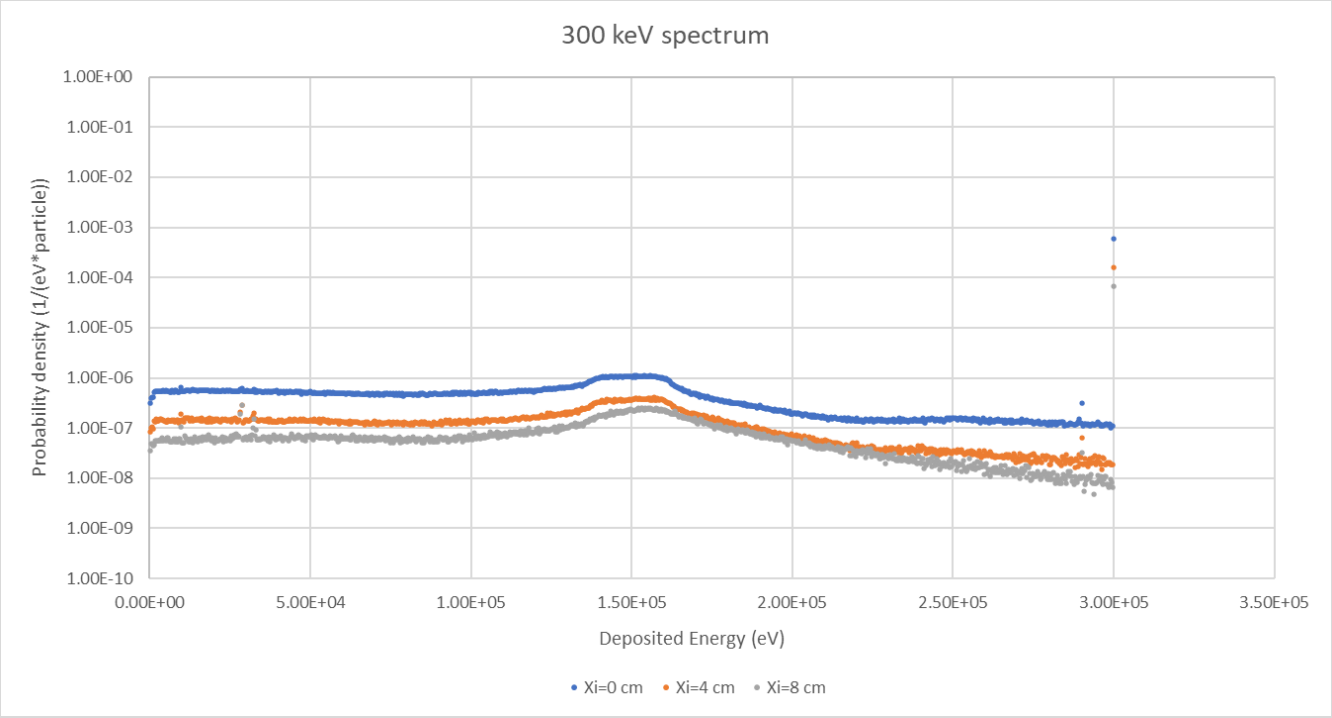

Figure 4-12 The spectrum for 300 keV

Table 4-8 The origin of the photo peaks for the spectrum of 300 keV

The energy of the photo peak (keV)	Origin of the photo peak
300.0	The full energy peak of the monoenergetic point source
290.0	The escape peak of the Kα1 X-ray emission line of Germanium

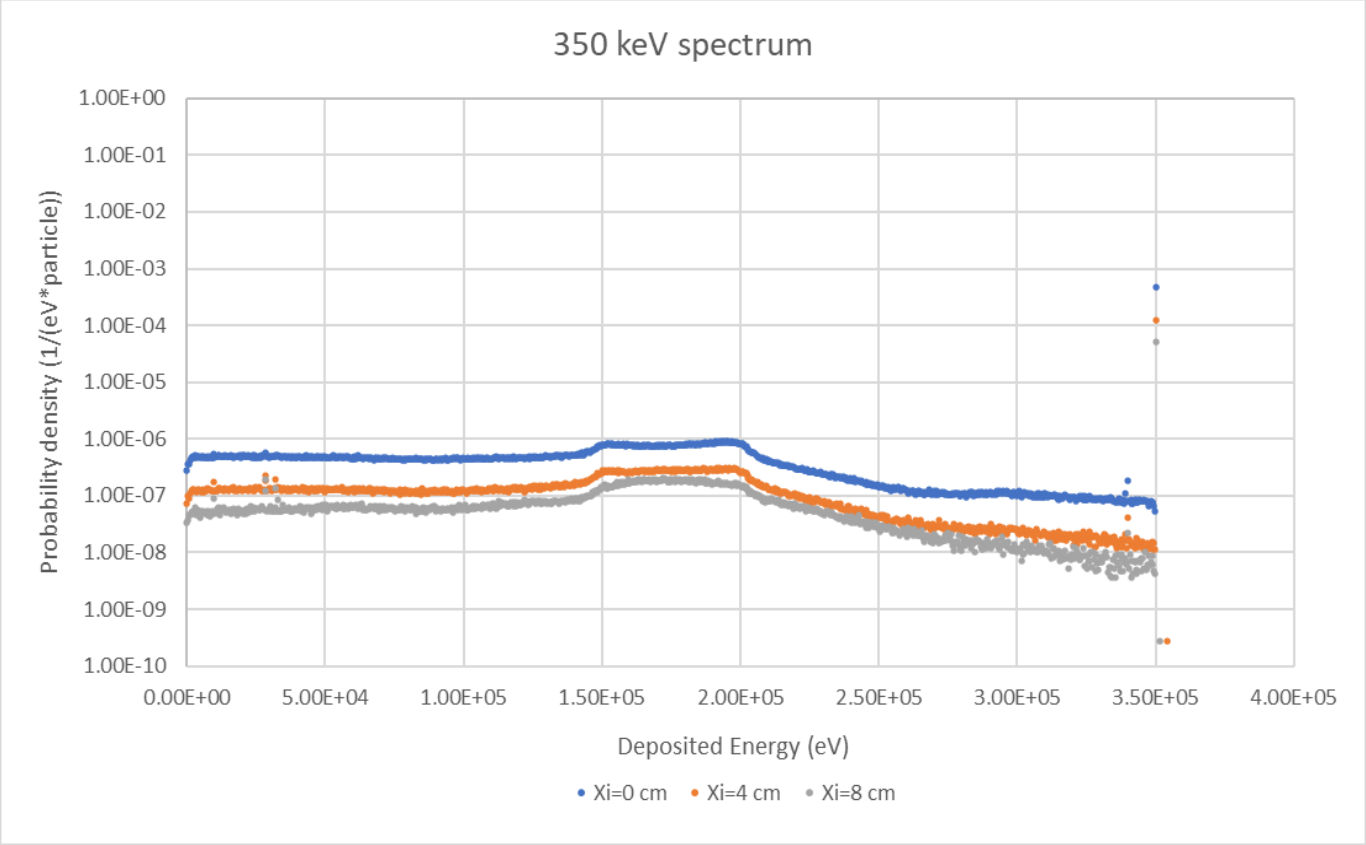

Figure 4-13 The spectrum for 350 keV

Table 4-9 The origin of the photo peaks for the spectrum of 350 keV

The energy of the photo peak (keV)	**Origin of the photo peak**
350.0	The full energy peak of the monoenergetic point source
340.0	The escape peak of the Kα1 X-ray emission line of Germanium

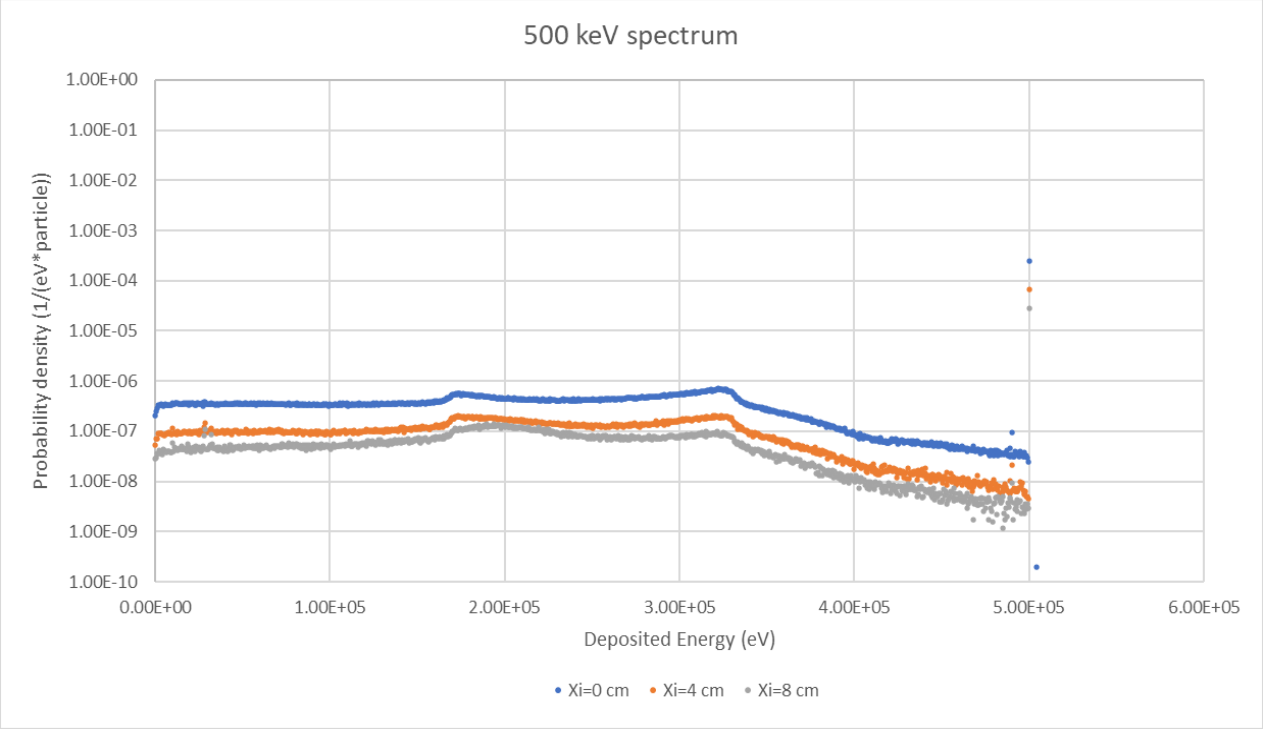

Figure 4-14 The spectrum for 500 keV

Table 4-10 The origin of the photo peaks for the spectrum of 500 keV

The energy of the photo peak (keV)	**Origin of the photo peak**
500.0	The full energy peak of the monoenergetic point source
490.0	The escape peak of the Kα1 X-ray emission line of Germanium

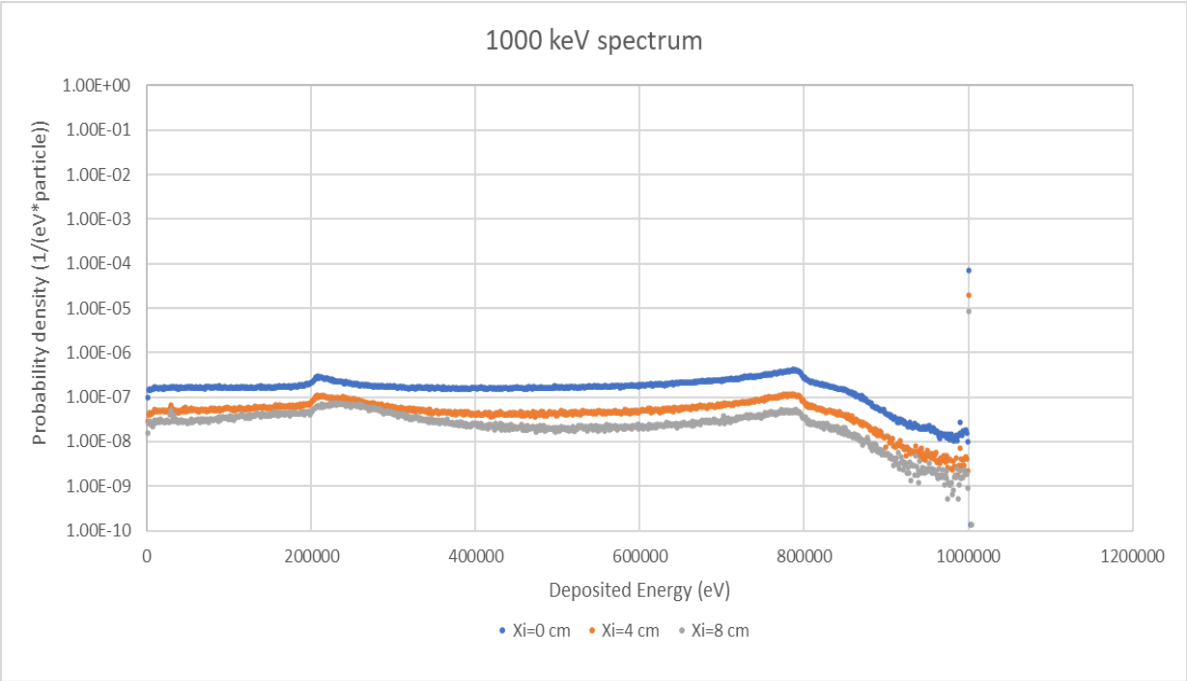

Figure 4-15 The spectrum for 1000 keV

Table 4-11 The origin of the photo peaks for the spectrum of 1000 keV

The energy of the photo peak (keV)	Origin of the photo peak
1000.0	The full energy peak of the monoenergetic point source

4.2.2 Effective Interaction Depth Graphs

In this paragraph are displayed the graphs that led to the calculation of the EID for the XtRa detector for all the distinct energies, following the procedure described in 4.1.7. Firstly, the graphs derived for distances of the point source 0 to 8 cm are presented. Below each graph, there is a table displaying the calculated EID with the reference point at the polypropylene cap and the associated error for each calculation. Additionally, the table includes the EID with the reference point at the top of the dead layer of the detector, which is determined by deducting the following distance from the calculated value.

$$d_s + d_c = 0.93\ cm$$

Where:

- d_s is the distance from the source to the detector endcap
- d_c is the distance from the endcap to the detector surface

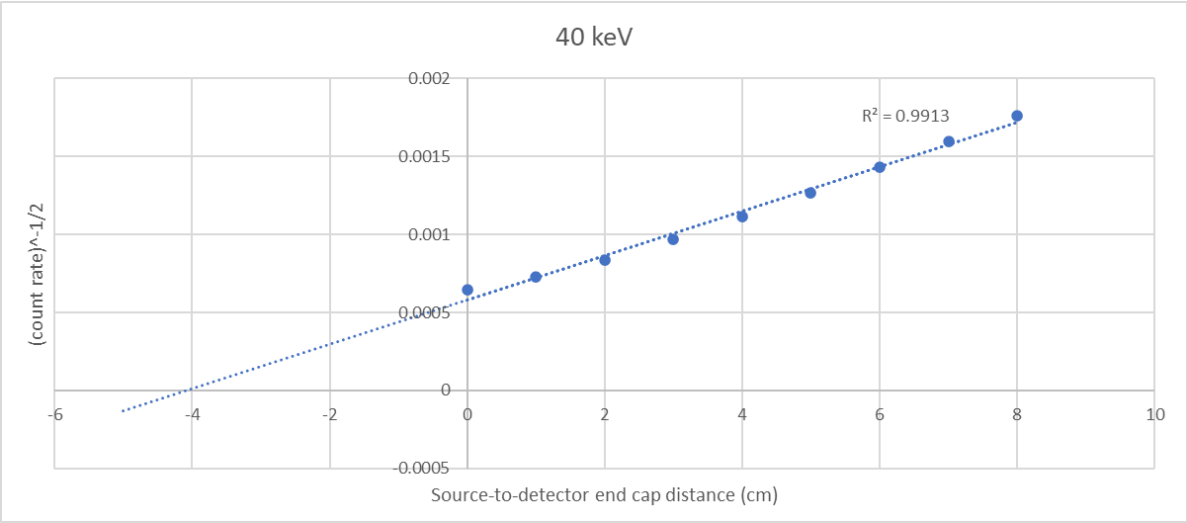

Figure 4-16 The plot to calculate the EID at 40 keV

Table 4-12 The EID values at 40 keV

EID with the reference point at the top of the Polypropylene cap (cm)	Uncertainty (cm)	EID with the reference point at the top of the detector (cm)
4.09	0.22	3.16

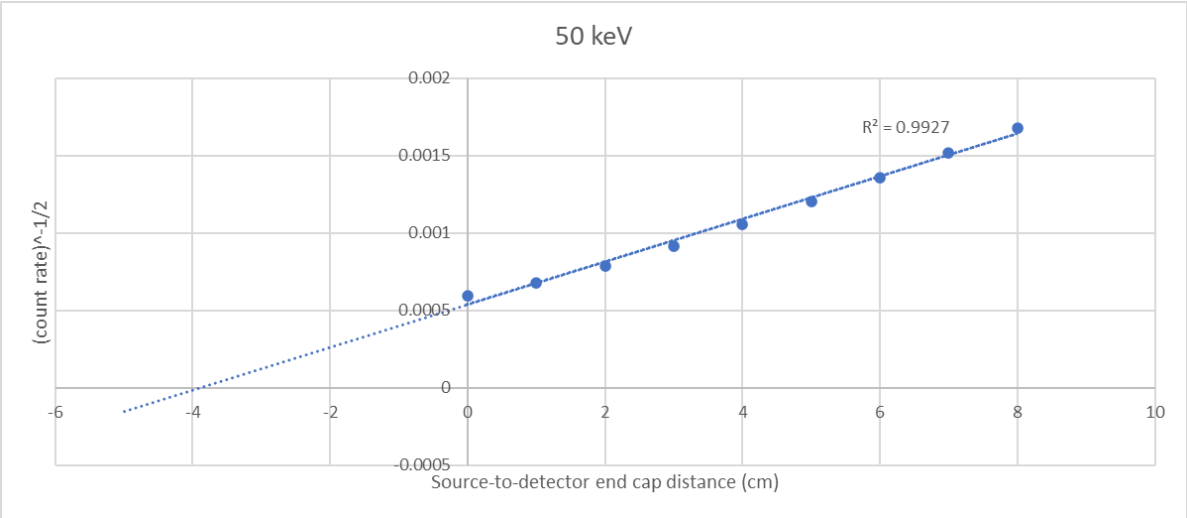

Figure 4-17 The plot to calculate the EID at 50 keV

Table 4-13 The EID values at 50 keV

EID with the reference point at the top of the Polypropylene cap (cm)	Uncertainty (cm)	EID with the reference point at the top of the detector (cm)
3.90	0.19	2.97

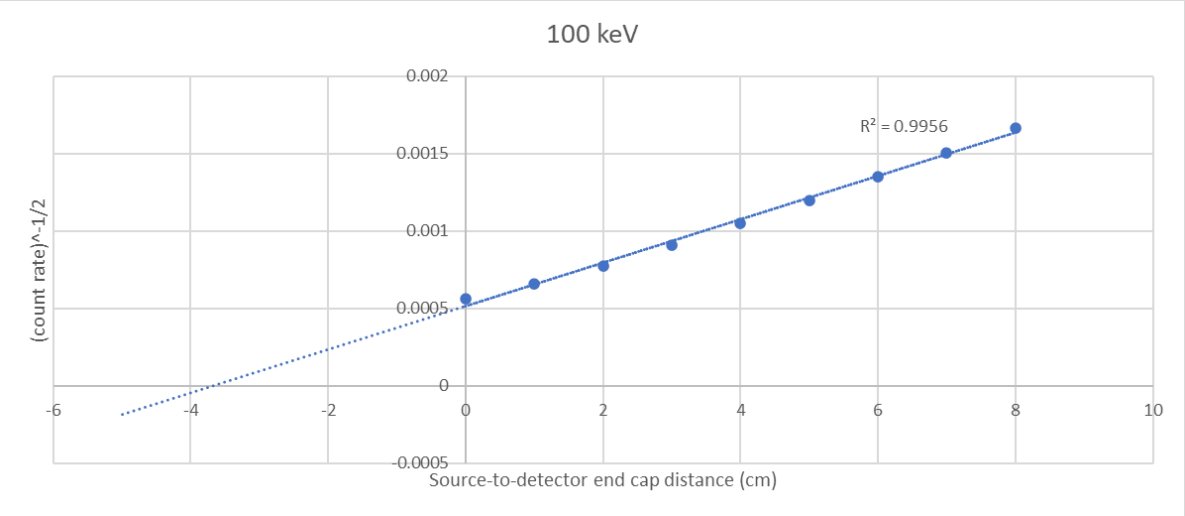

Figure 4-18 The plot to calculate the EID at 100 keV

Table 4-14 The EID values at 100 keV

EID with the reference point at the top of the Polypropylene cap (cm)	Uncertainty (cm)	EID with the reference point at the top of the detector (cm)
3.70	0.15	2.77

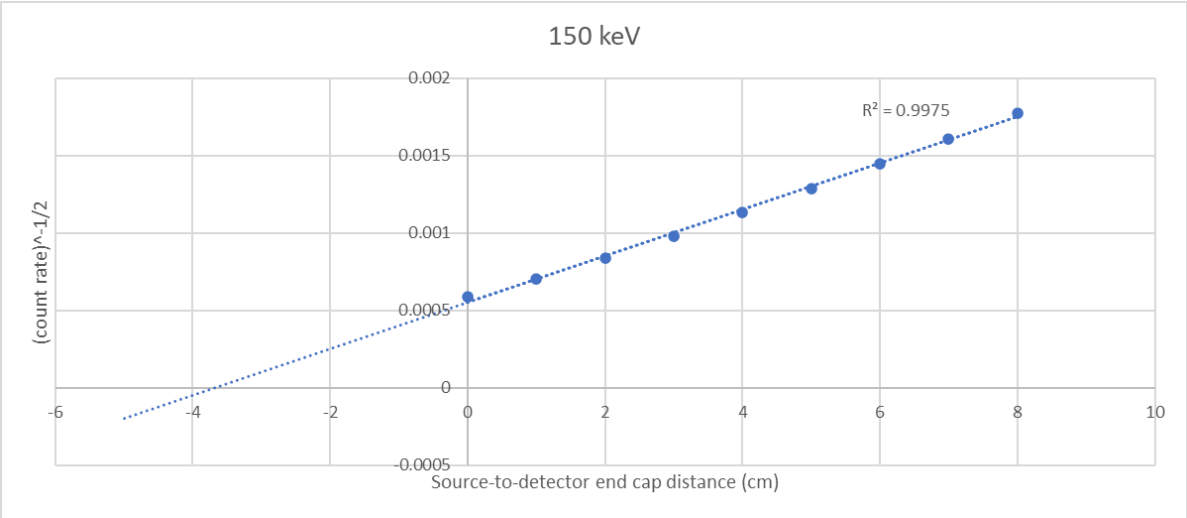

Figure 4-19 The plot to calculate the EID at 150 keV

Table 4-15 The EID values at 150 keV

EID with the reference point at the top of the Polypropylene cap (cm)	Uncertainty (cm)	EID with the reference point at the top of the detector (cm)
3.69	0.11	2.77

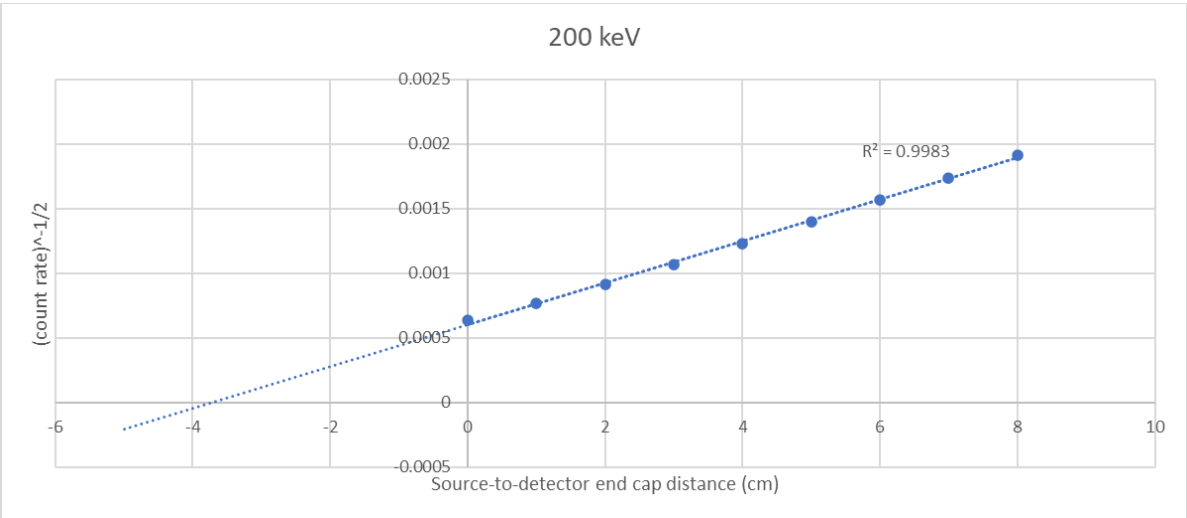

Figure 4-20 The plot to calculate the EID at 200 keV

Table 4-16 The EID values at 200 keV

EID with the reference point at the top of the Polypropylene cap (cm)	Uncertainty (cm)	EID with the reference point at the top of the detector (cm)
3.74	0.09	2.82

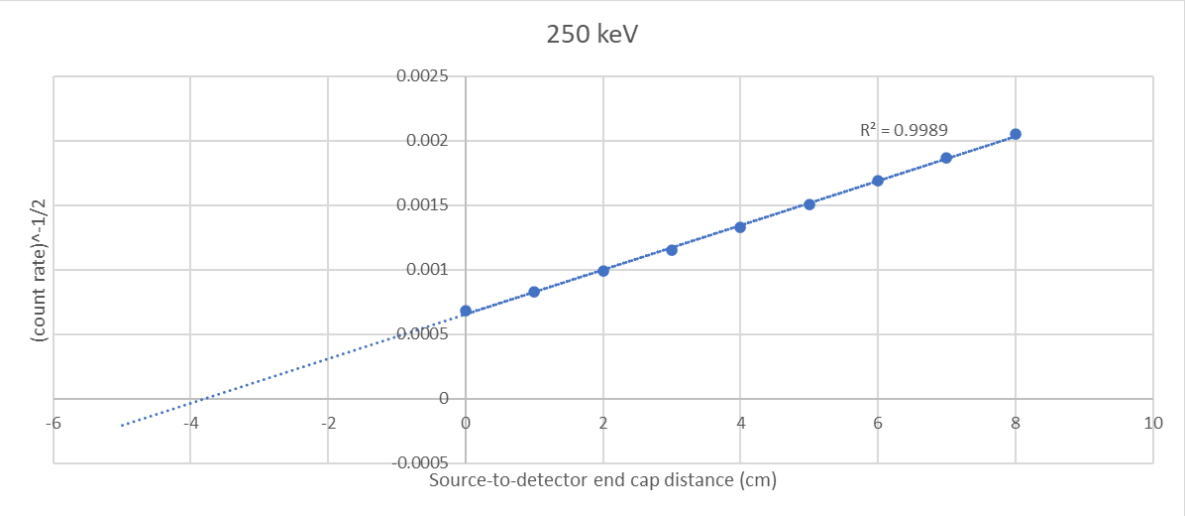

Figure 4-21 The plot to calculate the EID at 250 keV

Table 4-17 The EID values at 250 keV

EID with the reference point at the top of the Polypropylene cap (cm)	Uncertainty (cm)	EID with the reference point at the top of the detector (cm)
3.8	0.08	2.88

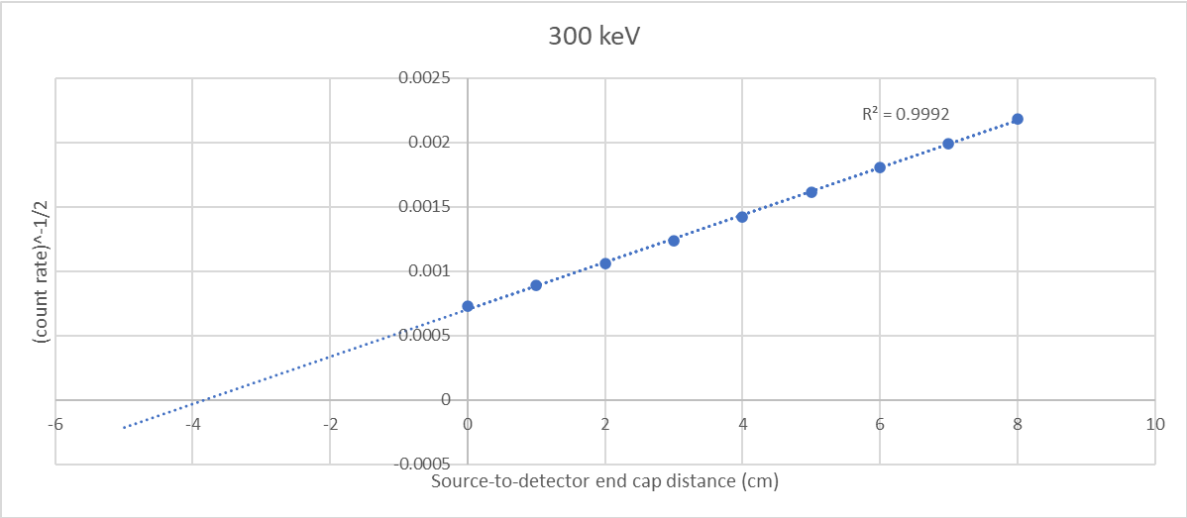

Figure 4-22 The plot to calculate the EID at 300 keV

Table 4-18 The EID values at 300 keV

EID with the reference point at the top of the Polypropylene cap (cm)	Uncertainty (cm)	EID with the reference point at the top of the detector (cm)
3.85	0.06	2.92

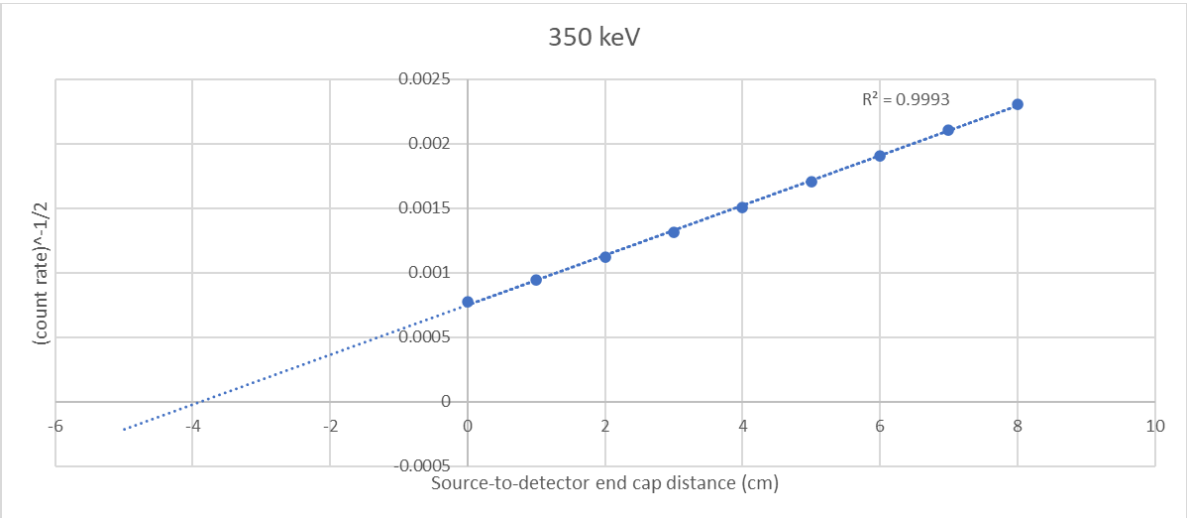

Figure 4-23 The plot to calculate the EID at 350 keV

Table 4-19 The EID values at 350 keV

EID with the reference point at the top of the Polypropylene cap (cm)	Uncertainty (cm)	EID with the reference point at the top of the detector (cm)
3.89	0.06	2.96

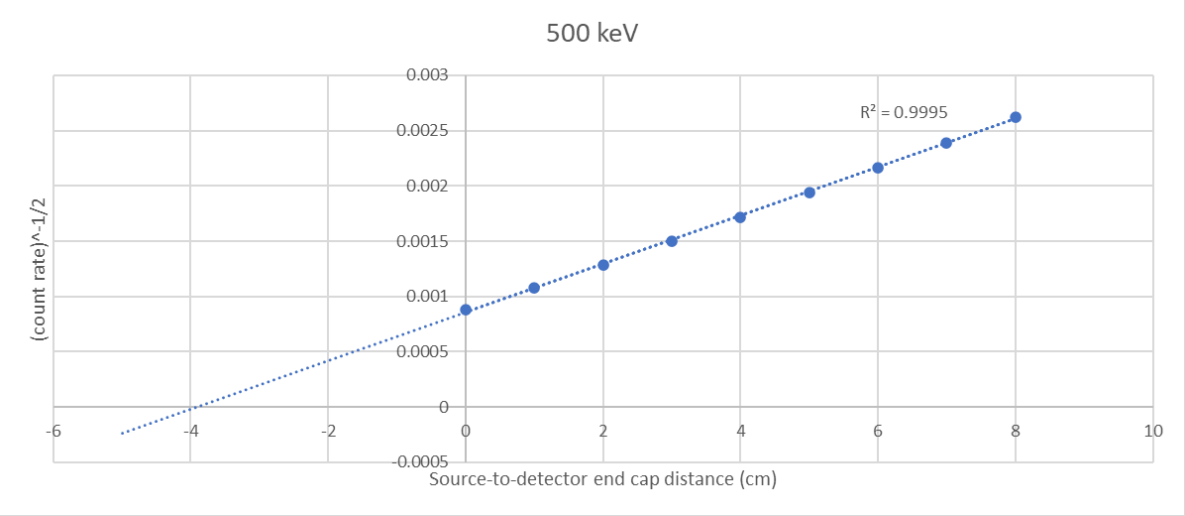

Figure 4-24 The plot to calculate the EID at 500 keV

Table 4-20 The EID values at 500 keV

EID with the reference point at the top of the Polypropylene cap (cm)	Uncertainty (cm)	EID with the reference point at the top of the detector (cm)
3.93	0.05	3.00

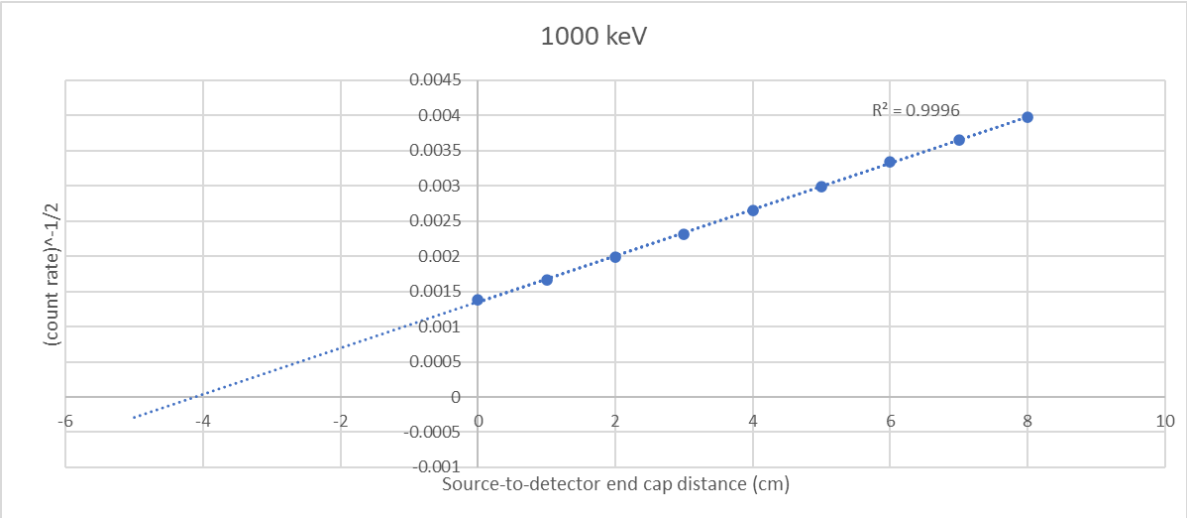

Figure 4-25 The plot to calculate the EID at 1000 keV

Table 4-21 The EID values at 1000 keV

EID with the reference point at the top of the Polypropylene cap (cm)	Uncertainty (cm)	EID with the reference point at the top of the detector (cm)
4.12	0.05	3.19

It is noteworthy that the fit of the linear regression is slightly worse for the lower energies (<150 keV) compared to the higher energies. Eventually, the graph that provides the EID related to the energy, with a reference point at the top of the detector calculated from the graphs above, is shown below.

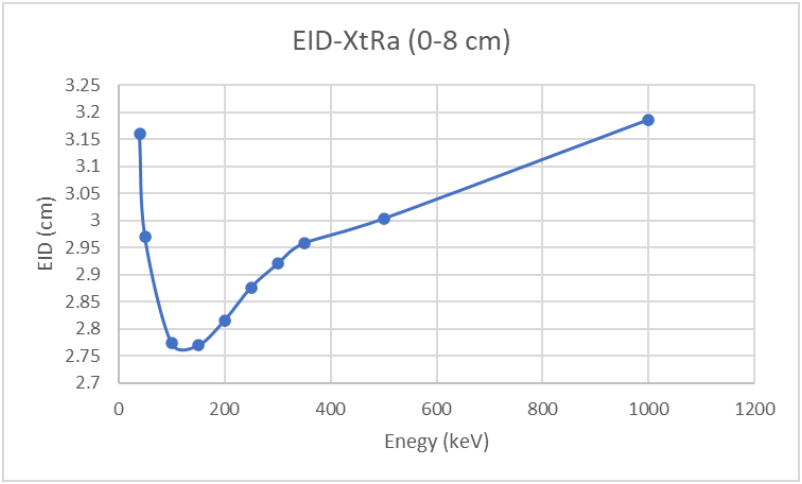

Figure 4-26 The EID-Energy plot for the detector XtRa

The shape of the EID-Energy plot is not as one would expect, presenting a slight increase with energy. In the low energy there appears to be a minimum at about 120 keV. In the literature, the concept of the EID as a function of photon energy, has been investigated mostly experimentally and for energies higher than 59.5 keV and it presents the expected behavior. However, according to [6], the EID value shows different behavior for the energy ranges 26.6-59.5 keV and 59.5-1332 keV. More specifically, the EID decreases with increasing energy up to 37.3 keV and then it increases until it reaches a plateau. This behavior was attributed in [6] to the dead layer thickness of the Germanium crystal that was used during simulation. This conclusion was derived after conducting Monte-Carlo simulations with various dead-layer thicknesses. In the figure below, the graph created by [6], shows the relationship between the EID and the photon energy. Comparing the Figure 4-26 with Figure 4-27, it is obvious that they both show the same behavior. Therefore, it is very probable that the graph created shows this unexpected behavior because of the dead layer thickness of the Germanium used in the simulations. It is worth mentioning that a detector characterization prior to M-C simulation results to a set of the detector geometrical characteristics that will give consistent results between simulation and experiment, provided that the geometry simulated is not radically different from the one used for the detector characterization.

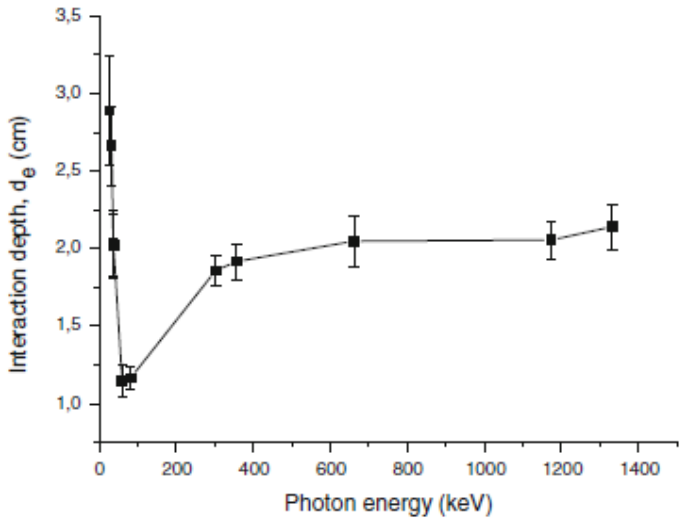

Figure 4-27 Dependence of the EID on the photon energies for 26.6-1332 keV[6]

4.3 Experimental determination of the EID and comparison with the simulation results

For the determination of the EID for the XtRa detector, an experiment was also conducted with a ^{241}Am point source emitting photons at 59.54 keV. To this end, a special setup was utilized that allows the point source to be positioned at different distances along the axis of

the detector. The count rate of the source was measured at 8 distinct distances, ranging from 16.7 cm up to 23.7 cm, away from the detector, with an increment of 1 cm. The graph below was created based on the experimental measurements, enabling the calculation of the EID.

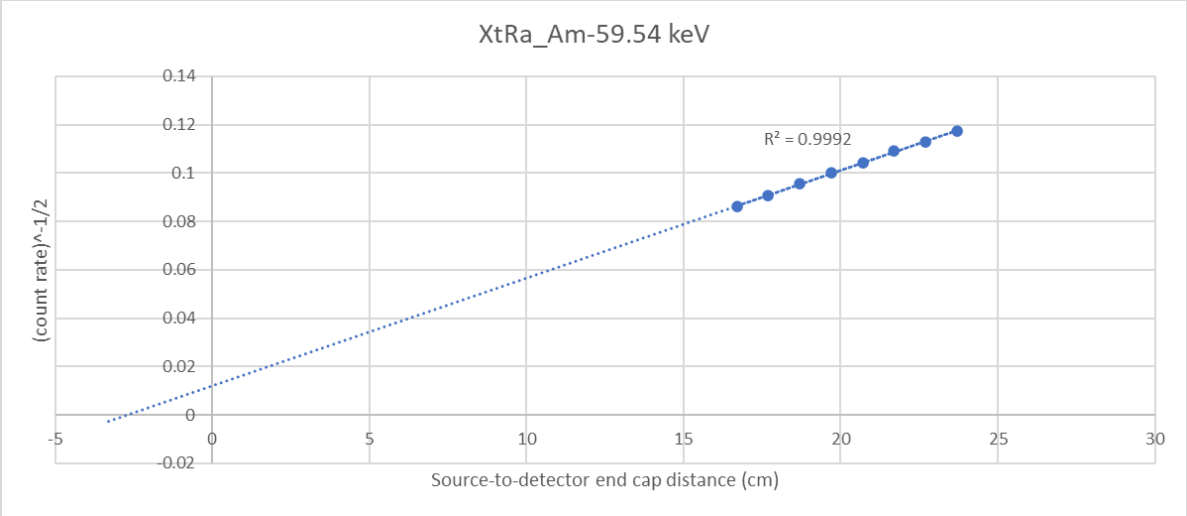

Figure 4-28 The plot created experimentally to calculate the EID

Table 4-22 The experimental values of EID

EID with the reference point at the top of the Polypropylene cap (cm)	Uncertainty (cm)	EID with the reference point at the top of the detector (cm)
2.73	0.23	1.80

As shown in the table above, the value of the EID with the reference point at the top of the detector is 1.8 cm, which differs significantly from the value found with Monte-Carlo simulations for the energy of 50 keV, which is 2.9 cm. At this point it should be mentioned that the fitting presented in Figures 4.17 and 4.18 appears to slightly deviate from linearity as it is indicated the R^2. This deviation should be attributed to the dead layer problem mentioned previously. Therefore, it was deemed important to use only part of the data derived from the simulations to approach as much as possible the experimental value. For that reason, instead of calculating the EID as shown in 4.2.2, new graphs were created with the values referring to the point source at distances 4-8 cm. These graphs which give much better R^2 values are presented below.

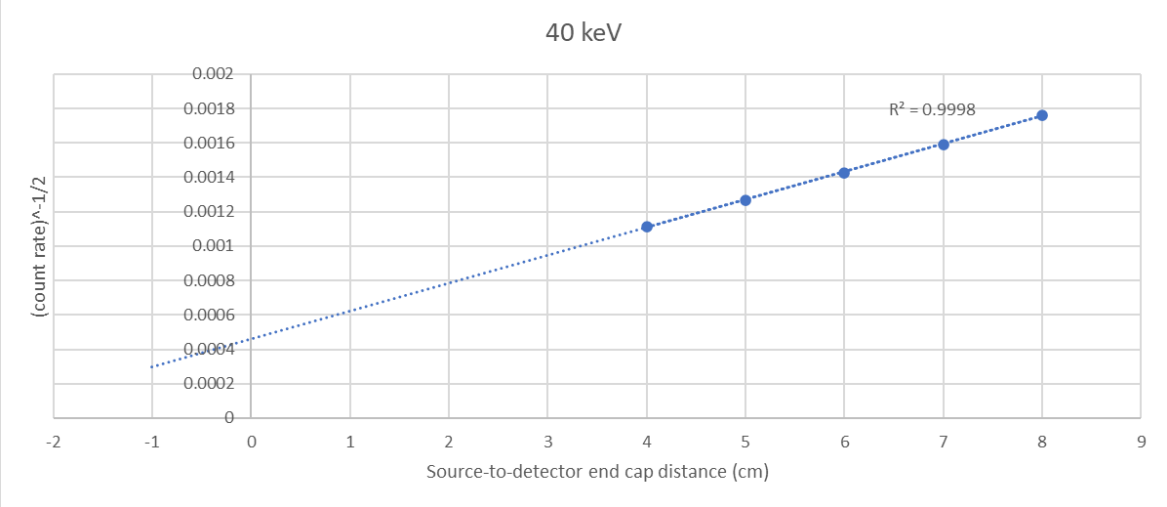

Figure 4-29 The new plot to calculate the EID at 40 keV

Table 4-23 The new EID values at 40 keV

EID with the reference point at the top of the Polypropylene cap (cm)	Uncertainty (cm)	EID with the reference point at the top of the detector (cm)
2.86	0.06	1.93

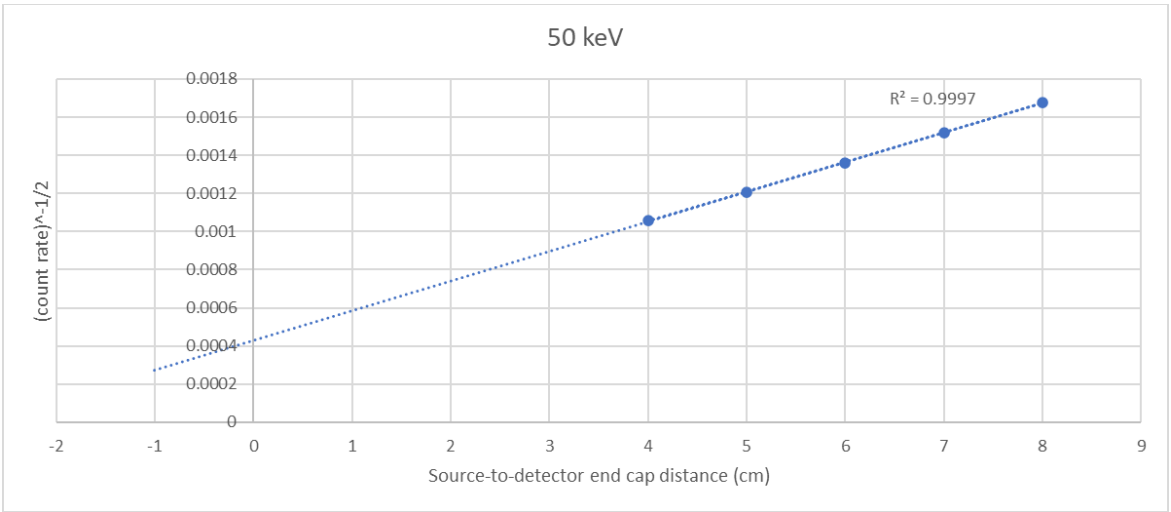

Figure 4-30 The new plot to calculate the EID at 50 keV

Table 4-24 The new EID values at 50 keV

EID with the reference point at the top of the Polypropylene cap (cm)	Uncertainty (cm)	EID with the reference point at the top of the detector (cm)
2.77	0.06	1.84

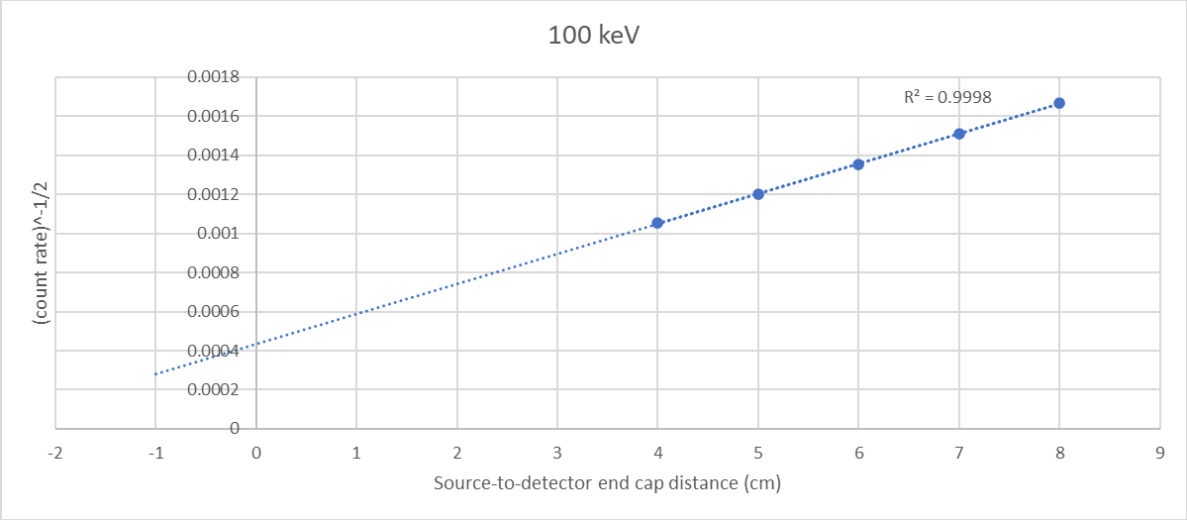

Figure 4-31 The new plot to calculate the EID at 100 keV

Table 4-25 The new EID values at 100 keV

EID with the reference point at the top of the Polypropylene cap (cm)	Uncertainty (cm)	EID with the reference point at the top of the detector (cm)
2.84	0.05	1.91

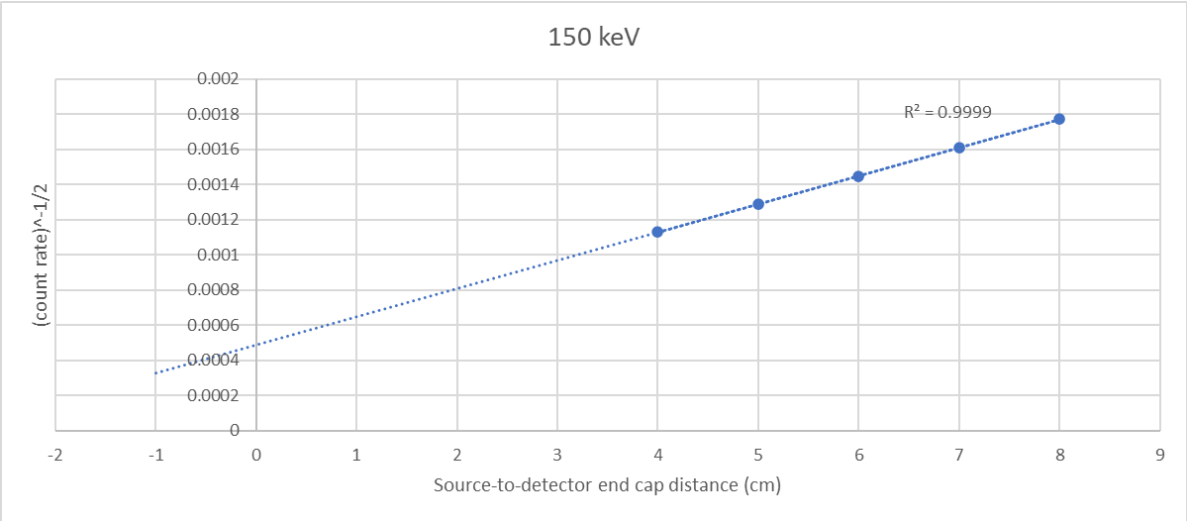

Figure 4-32 The new plot to calculate the EID at 150 keV

Table 4-26 The new EID values at 150 keV

EID with the reference point at the top of the Polypropylene cap (cm)	Uncertainty (cm)	EID with the reference point at the top of the detector (cm)
3.03	0.03	2.10

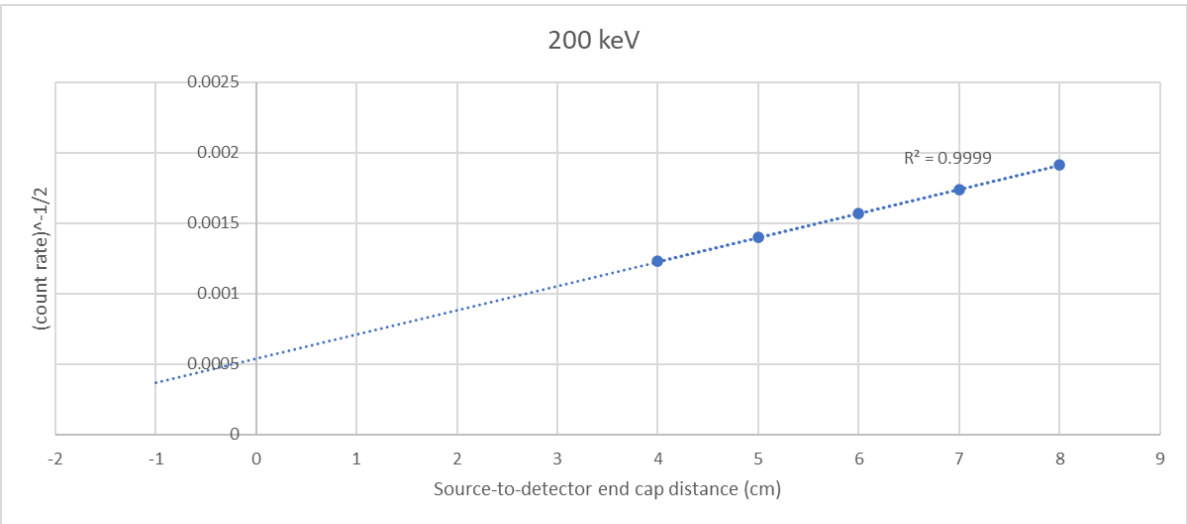

Figure 4-33 The new plot to calculate the EID at 200 keV

Table 4-27 The new EID values at 200 keV

EID with the reference point at the top of the Polypropylene cap (cm)	Uncertainty (cm)	EID with the reference point at the top of the detector (cm)
3.18	0.04	2.25

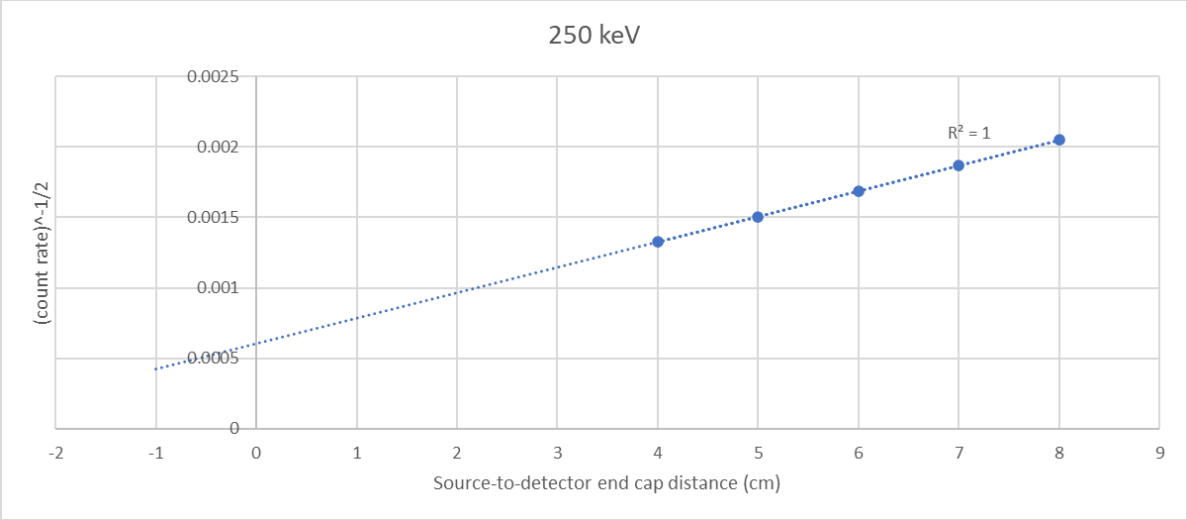

Figure 4-34 The new plot to calculate the EID at 250 keV

Table 4-28 The new EID values at 250 keV

EID with the reference point at the top of the Polypropylene cap (cm)	Uncertainty (cm)	EID with the reference point at the top of the detector (cm)
3.34	0.03	2.41

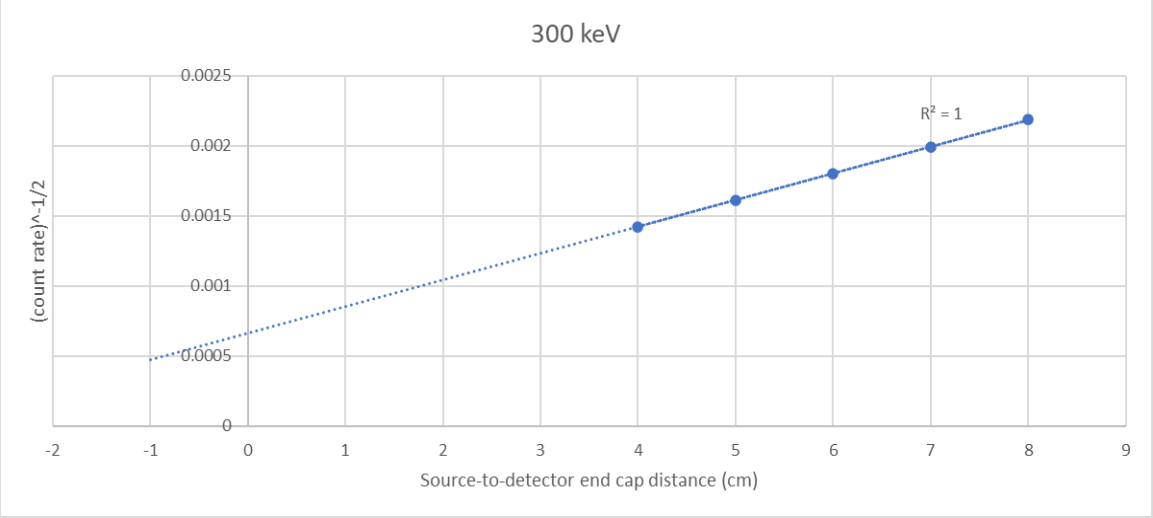

Figure 4-35 The new plot to calculate the EID at 300 keV

Table 4-29 The new EID values at 300 keV

EID with the reference point at the top of the Polypropylene cap (cm)	Uncertainty (cm)	EID with the reference point at the top of the detector (cm)
3.48	0.01	2.55

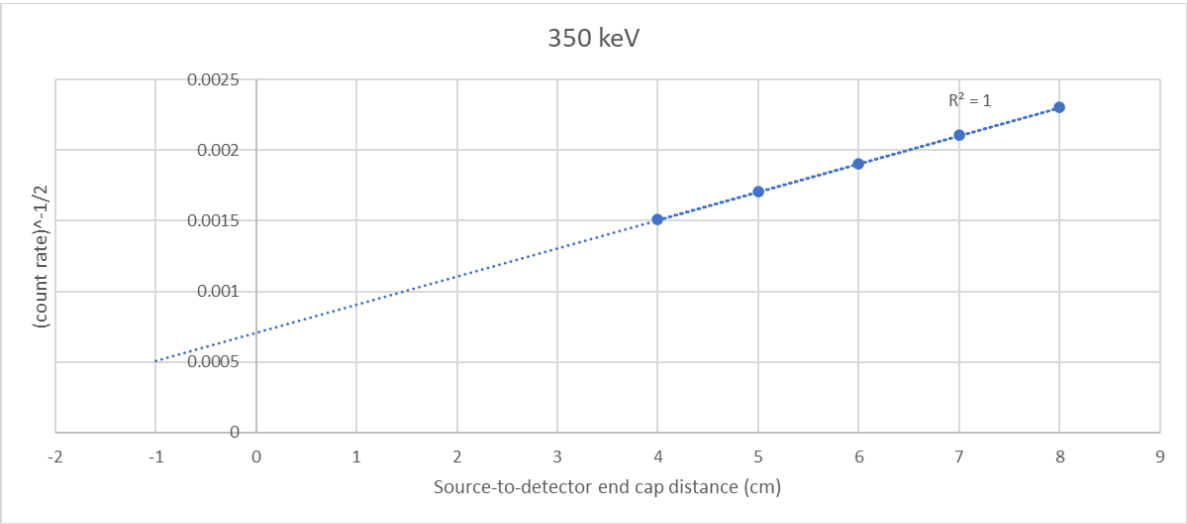

Figure 4-36 The new plot to calculate the EID at 350 keV

Table 4-30 The new EID values at 350 keV

EID with the reference point at the top of the Polypropylene cap (cm)	Uncertainty (cm)	EID with the reference point at the top of the detector (cm)
3.55	0.02	2.62

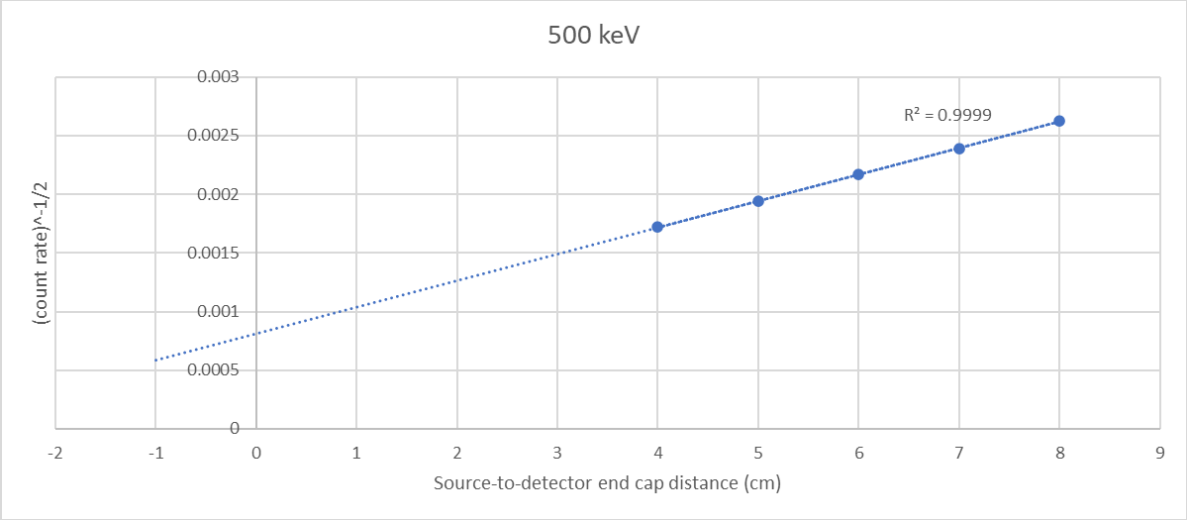

Figure 4-37 The new plot to calculate the EID at 500 keV

Table 4-31 The new EID values at 500 keV

EID with the reference point at the top of the Polypropylene cap (cm)	Uncertainty (cm)	EID with the reference point at the top of the detector (cm)
3.60	0.03	2.67

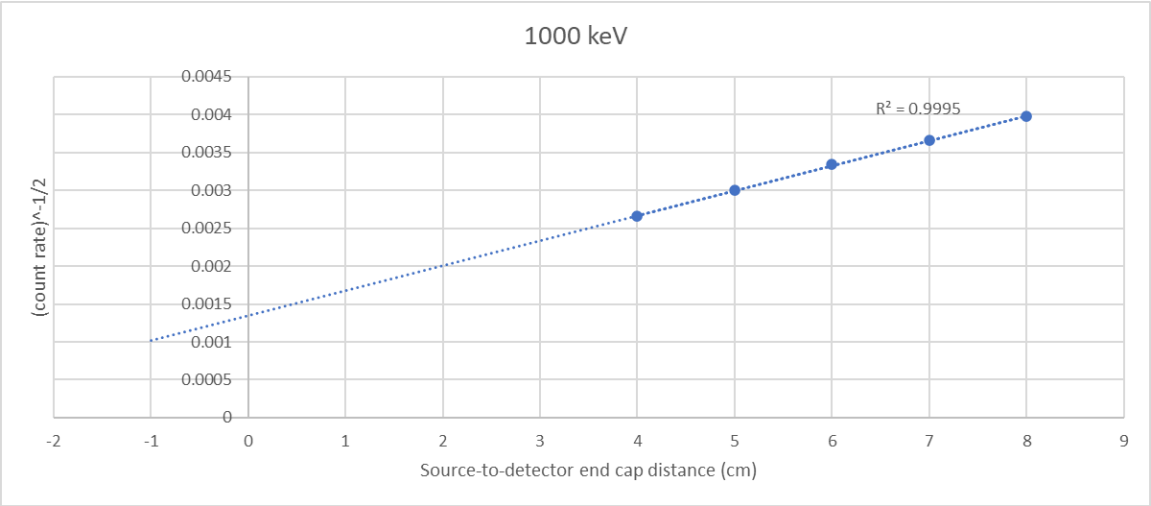

Figure 4-38 The new plot to calculate the EID at 1000 keV

Table 4-32 The new EID values at 1000 keV

EID with the reference point at the top of the Polypropylene cap (cm)	Uncertainty (cm)	EID with the reference point at the top of the detector (cm)
4.07	0.09	3.14

The graph that provides the EID calculated from the graphs above, and its dependence on photon energy is shown below.

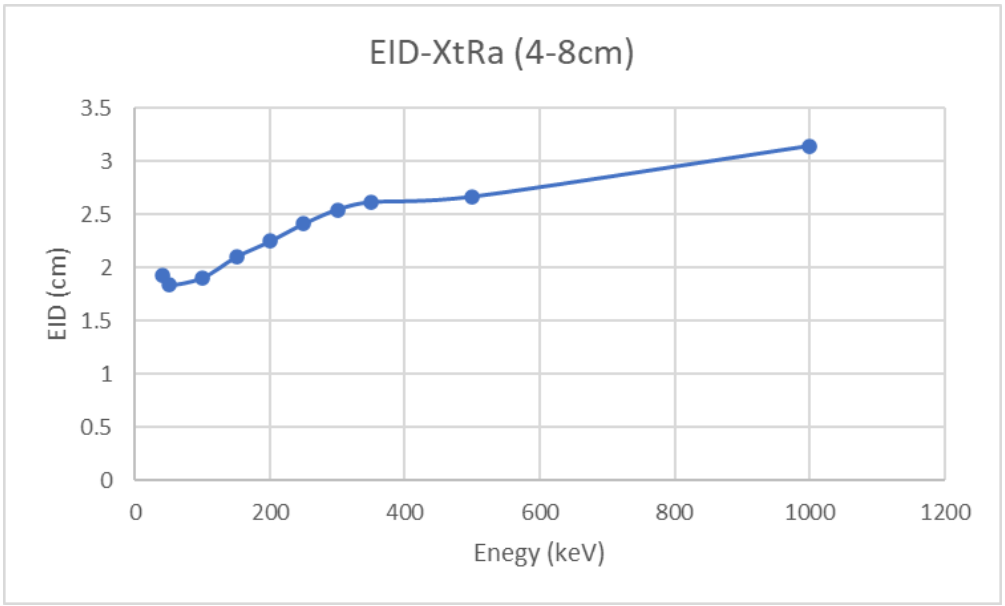

Figure 4-39 The new EID-Energy plot for the detector XtRa

It is of great importance that in this case the value of the EID for the energy 59.54 keV, is 1.85 cm, which is significantly closer to the experimental value. Moreover, the behavior of the EID-Energy graph seems to rule out the impedance of choosing the appropriate dead layer thickness for the simulations. That is probably because, for distances closer to the detector, the importance of the dead layer thickness becomes greater than for distances that are more distant from the detector. For these reasons, the Figure 4-39 was deemed more appropriate to be incorporated into the Matlab code for the calculation of the ECF. More details about the Matlab code created are given in the next chapter.

5. The upgrade of the Matlab code for the calculation of the Efficiency Correction Factors

In this chapter are presented all the modifications and upgrades made in the present work to make the Matlab standalone application for the calculation of ECF for NORM created in [4], more flexible and user-friendly. The two main pillars of improvement were the enhancement of the application's GUI to increase user convenience and the introduction of an EID-Energy function to incorporate this value in the calculation of the ECF. More details about these changes in the code are given in the next paragraph. Moreover, the procedure for creating the new standalone application is explained in this chapter, as the tool deployed is different from the one used for the first standalone application. Finally, the results obtained with the Matlab code are shown and compared with the results derived from PENELOPE simulations.

5.1 Matlab code modifications

As mentioned above, the first modification was the upgrade of the GUI of the standalone application. The feature of having an intuitive standalone application is very crucial because it ensures easy operation for any user without additional dependencies and programming knowledge. Also, it facilitates the parametric study of various parameters and their effect on ECF. Hence, attention to detail was given so that the interface environment is as self-explanatory as possible. The figure below shows the updated interface, while the exact procedure for creating it is described in the next paragraph.

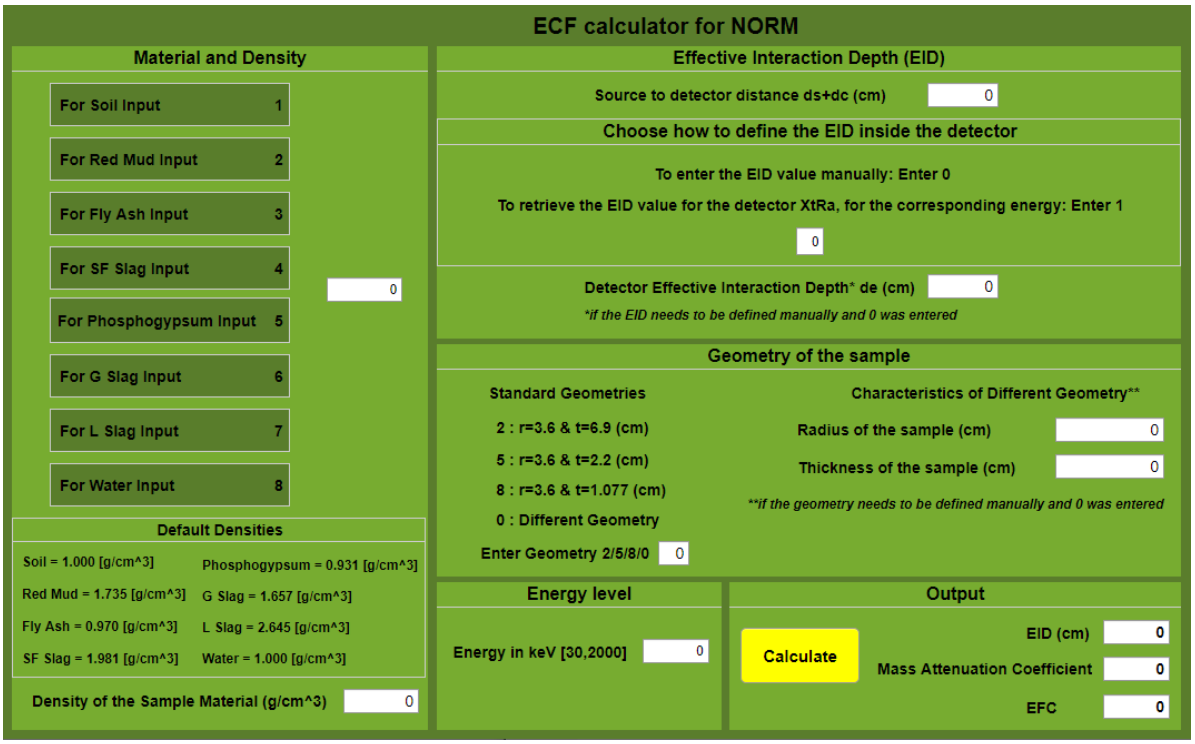

Figure 5-1 The GUI of the new standalone application

However, the most significant modification was the introduction of the function that defines the EID based on the energy level for a specific detector (in our case the XtRa detector), as illustrated in Figure 4-39. Specifically, in the previous version of the Matlab code the user was able to give as an input the sum of the distance from the source to the detector and the EID inside the detector. Nevertheless, for a specific detector, the source-to-detector distance remains constant, while the EID inside the detector varies with energy. On the other hand, the user might decide to put the sample far from the detector (e.g. in hot samples). Hence, in the updated version of the code, this distance was divided into two distinct parts. These are the following:

- The constant distance for a determined detector, from the source to the top of the detector (d_s+d_c)
- The EID inside the detector, defined as the distance from the top of the detector to a fictitious interaction point inside the detector (d_e)

The first distance, which is the distance from the source to the detector, can be specified by the user in the standalone application. For the second distance, which is the EID within the detector, the user has the option to either manually set this value or retrieve it from the function provided in the code for the XtRa detector. Specifically, due to the functional behavior of the graph, a 3rd-degree polynomial function was used to fit the graph as shown in the graph below.

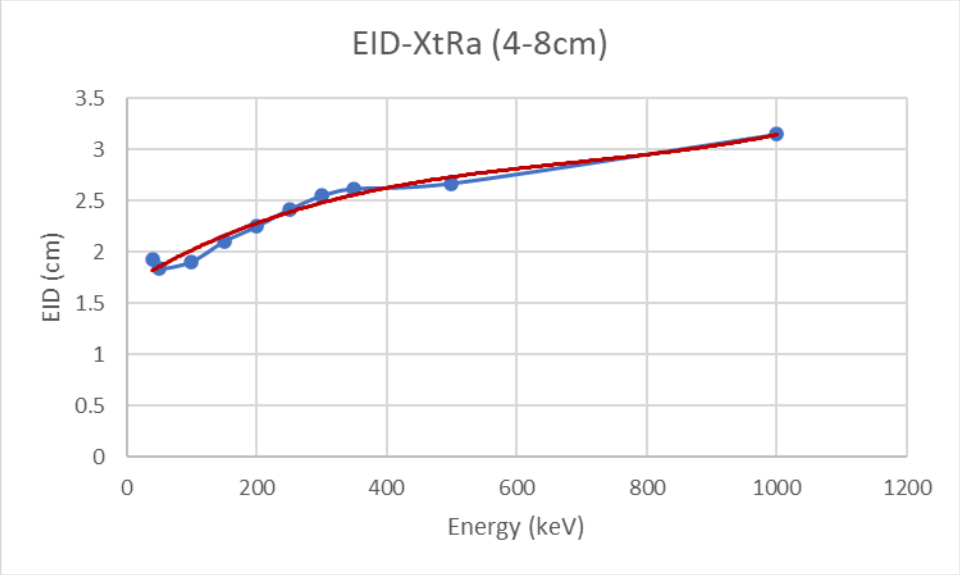

Figure 5-2 The 3rd-degree polynomial fit

$$y = 2.21034E-09 * x^3 - 4.60668E-06 * x^2 + 3.86501E-03 * x + 1.67236E+00 \quad (5\text{-}1)$$

The above polynomial function (5-1) has been integrated into the MATLAB code, allowing the user to retrieve the corresponding EID value for any desired energy level. For energies above 1000 keV, the EID value remains the same as that for 1000 keV, because for higher energies the EID doesn't change considerably, to affect the calculations.

5.2 Matlab standalone application

5.2.1 Modifications in the Matlab code

The main modifications made in the code were regarding the parameter of the distance between the source and the "fictitious" detector point. More specifically, this distance was previously set as a single value, while in this work it is split into two parts. The first part is the source-to-detector distance (d_s+d_c), which is fixed for each sample-to-detector setup and is a known value. The second part is the detector EID (d_e), which is energy-dependent and can be determined through simulations or experimentally. As described in the previous paragraph, the EID value was determined through simulations for the XtRa detector, and a polynomial function that fit accurately the EID-Energy graph was integrated into the code. Consequently, when the user defines the energy level, the respective EID value is automatically retrieved to calculate the ECF. However, in case the user wants to calculate

the ECF for another detector than the XtRa, there is the possibility to define this value manually.

5.2.2 Modifications in the GUI of the standalone application

The updated standalone application was created in the App Designer of Matlab. MATLAB App Designer is a powerful tool for creating interactive applications. It offers a comprehensive environment for designing app layouts and programming their behavior. Furthermore, it is very easy for developers to integrate a variety of UI components into their applications and finally package them into standalone executables, allowing users to run them without needing MATLAB installed.

The first step to launch the App Designer is to type “appdesigner” in the Command Window. Then a drag-and-drop interface appears that allows the user to construct the interface of the application in the desired way. The creation and design of the app layout take place in the design view, as shown in the figure below.

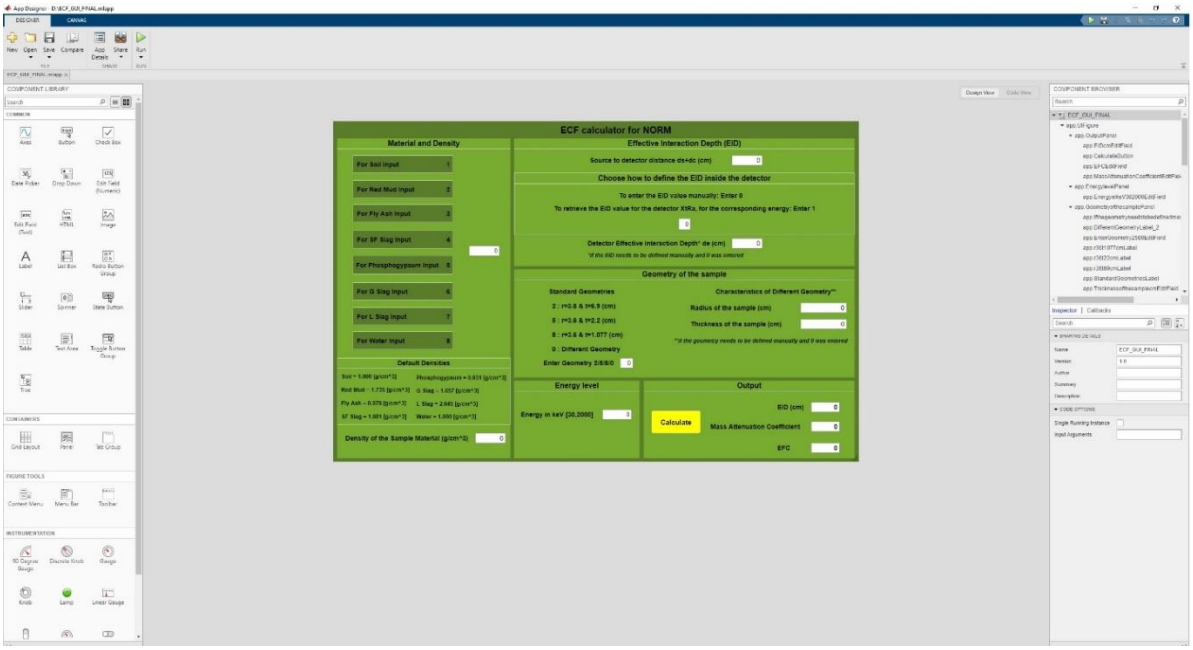

Figure 5-3 The appdesigner interface

By switching to the code view the user can write callback functions and the necessary script. Callback functions execute specific actions in response to events caused by the user, such as clicking a button or entering a value in corresponding fields. Therefore, each value entered by the user triggers a callback function.

After completing the design of the GUI, and the code running in the background, the next step is to package the app as a standalone application. This is a straightforward procedure using the Application Compiler. By navigating to the “Designer” tab in App Designer and selecting “Share”, followed by “Standalone Desktop App”, the Application Compiler opens. Then the developer configures settings such as the application information, icon, and installation options. After that, by clicking “Package” Matlab will compile the application into a standalone executable (.exe file), which is ready to be distributed and installed.

5.2.3 The final version of the standalone application

The updated standalone application is shown in Figure 5-4. To calculate the ECF the user first selects the material by choosing the corresponding number. Next, the user enters the density of the sample material, which can either be the default density provided in the layout or a custom value. Following this, the user defines the distance between the sample and the detector. The source-to-detector distance is entered in the first field. The user then decides whether to manually input the EID value or retrieve the pre-calculated value for the XtRa detector, by entering 0 or 1, respectively. If manually entered, the user then fills the next field with the desired value. Subsequently, the sample's geometry is defined. The user can select one of the standard geometries ("2", "5", or "8"), with dimensions provided in the layout, or enter 0 to define a custom geometry. Finally, the user specifies the energy level within the range of 30 to 2000 keV. After completing these fields, the code calculates the ECF and the mass attenuation coefficient of the material by clicking the calculate button. If the user opts to retrieve the EID, its value is displayed after clicking the button.

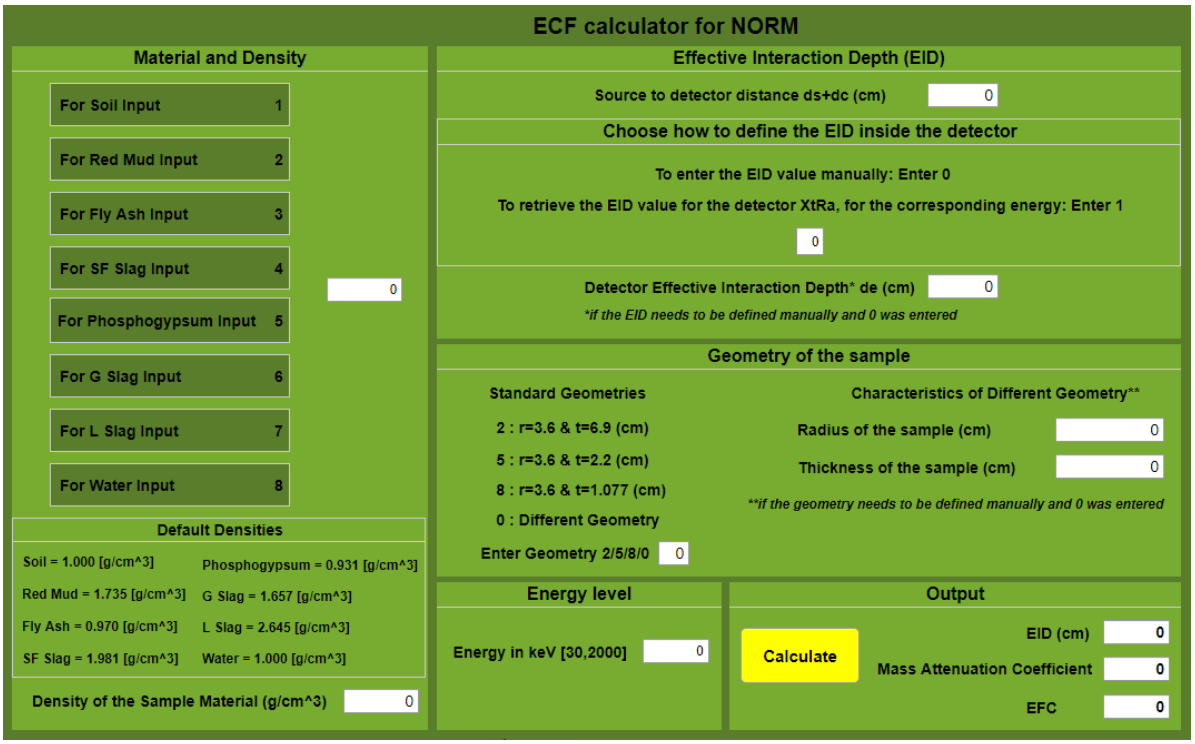

Figure 5-4 The GUI of the new standalone application

5.3 Results derived from the Matlab code

The main goal of this work is to calculate the ECF for seven typical NORMs. This was achieved by using the Matlab code. In this work it was considered important to calculate and present the ECF values for the worst-case scenario of the self-absorption phenomenon. This scenario corresponds to the sample geometry with the largest volume (and higher thickness), referred to as "Geometry 2" (r=3.6 cm & t=6.9 cm) among the default sample geometries used at NEL-NTUA. Therefore, the ECF value was calculated for all the materials and their default densities used in the code, for an energy range of 40-1000 keV. The results are shown in the table 5.1 and figure 5.7 below.

Table 5-1 The results derived from the Matlab code for "Geometry 2"

ECF-Matlab code							
keV	**Soil 3%**	**RM**	**FA**	**SFS**	**PG**	**GS**	**LS**
40	0.6909	0.2954	0.7314	0.2906	0.6238	0.3547	0.1749
60	0.8613	0.4605	0.8951	0.4427	0.8267	0.5228	0.2971
80	0.9606	0.5882	0.9884	0.557	0.9534	0.6432	0.4033
100	1.017	0.6745	1.0406	0.6329	1.0279	0.7207	0.4806
150	1.0531	0.7494	1.0742	0.6974	1.0784	0.7803	0.5621
200	1.0637	0.775	1.0839	0.7184	1.0931	0.8015	0.5916
300	1.0713	0.7964	1.0905	0.7372	1.1038	0.8192	0.6163
400	1.0723	0.8085	1.0905	0.7491	1.1048	0.8295	0.6317
500	1.0713	0.8158	1.0888	0.7568	1.1032	0.8359	0.6420
1000	1.0653	0.8277	1.0812	0.7707	1.094	0.8467	0.6600

Some very useful conclusions can be drawn from the graph presented at Figure 5.7. Firstly, the graph clearly shows that the ECF values increase inversely with the material's density. In fact, lead slag which has the highest density, has the lowest ECF values, while phosphogypsum which has the lowest density, has the greater ECF values. Specifically, the lowest the density the more the ECF value tends to the value 1, meaning that there is a greater need for the highest density materials to have a self-attenuation correction.

Another useful conclusion drawn is that for low energies, the need for a self-attenuation correction is more significant than for higher energies, for all the materials regardless of their density, since the ECF values are lower at lower energies.

Moreover, the functional behavior of the graphs for all the materials is very similar. As seen from Figure 5-5, while the energy increases the ECF factor tends asymptotically to a value. However, the slope of the graphs for the lower-density materials tends to become horizontal starting from lower energy levels compared to the higher-density materials. This leads to the conclusion that especially for higher-density materials, a self-attenuation correction is needed for energies as high as 1000 keV.

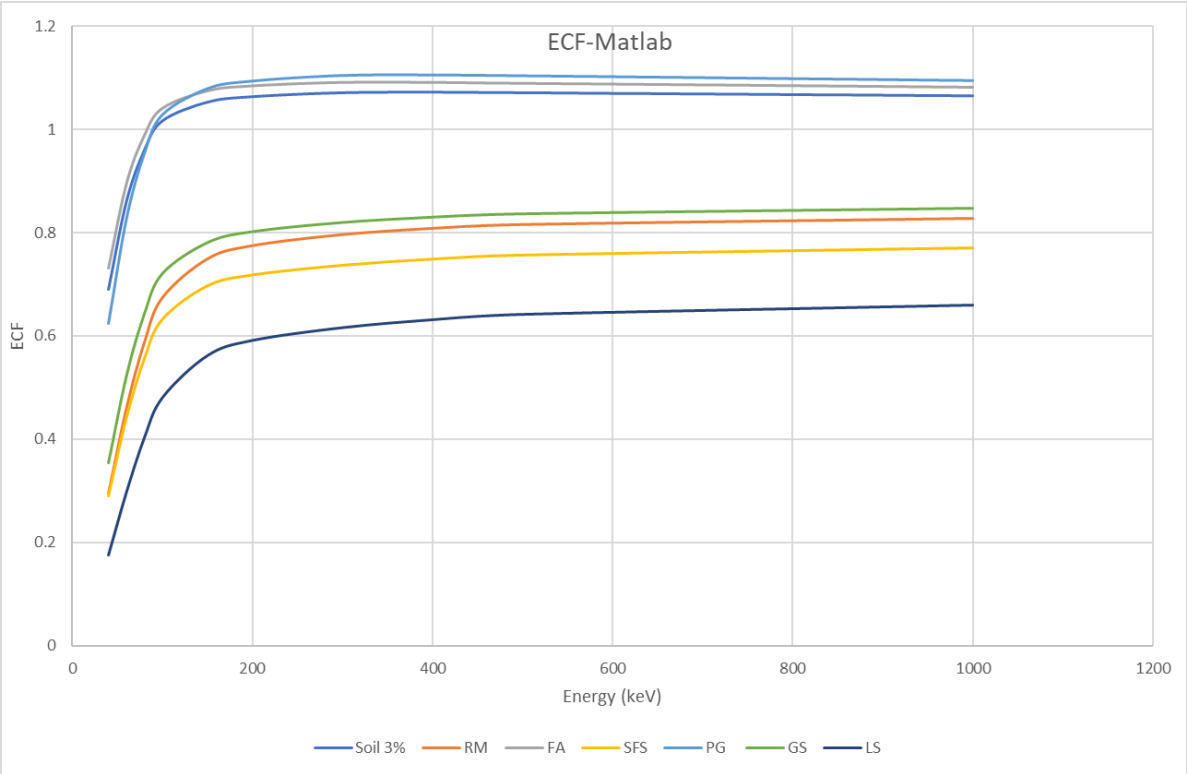

Figure 5-5 The ECF-Energy plot for all the materials

It is very important to notice that in all cases the ECF value is significantly different to 1. The reason for this should be thoroughly investigated. In conclusion, the ECF value is highly dependent on both the energy and the density of the material, hence when calculating it, one should be mindful of the desired material density.

5.4 Comparison between ECF results derived from the Matlab code and PENELOPE simulations

The upgrades and modifications made in this work aimed to minimize the difference between the ECF values calculated with the Matlab code and PENELOPE simulations. Therefore, several PENELOPE simulations were conducted to calculate the ECF values for the seven NORMs investigated in this work, for their default densities in the energy range of 40-1000 keV. Particularly, it was considered important to run the simulations for the worst-case scenario in terms of the self-absorption phenomenon, as mentioned in the previous paragraph. Consequently, the sample geometry used for all the materials was "Geometry 2" (r=3.6 cm & t=6.9 cm).

To examine whether the introduction of the EID distance in the code ameliorates the results, it was considered necessary to check the results from the Matlab code when the EID value

remains constant. Thus, an average value of the EID was considered at 2 cm, and the results are shown in Table 5-2.

This paragraph presents the results from the M-C simulations and compares them with the results from the Matlab code, both for a constant EID and the values integrated into the code. Each graph shown below corresponds to a different material. Moreover, for each material, a graph showing the percentage differences between the results is displayed, to facilitate a straightforward evaluation of the outcomes.

Table 5-2 The results derived from PENELOPE simulations for "Geometry 2"

ECF-PENELOPE							
keV	**Soil 3%**	**RM**	**FA**	**SFS**	**PG**	**GS**	**LS**
40	0.6802	0.2676	0.7238	0.2656	0.6064	0.3275	0.1537
60	0.8934	0.4752	0.9243	0.4569	0.8592	0.5427	0.2949
80	0.9830	0.6383	1.0048	0.6025	0.9812	0.6911	0.4325
100	1.0171	0.7262	1.0366	0.6818	1.0275	0.7679	0.5243
150	1.0427	0.8157	1.0561	0.7649	1.0602	0.8396	0.6323
200	1.0430	0.8437	1.0540	0.7934	1.0613	0.8619	0.6750
300	1.0379	0.8680	1.0463	0.8218	1.0555	0.8826	0.7120
400	1.0366	0.8805	1.0448	0.8381	1.0487	0.8974	0.7367
500	1.0380	0.8936	1.0503	0.8536	1.0530	0.9057	0.7555
1000	1.0294	0.9143	1.0333	0.8848	1.0347	0.9252	0.8020

As is made clear from the results presented in Table 5.2 there is a need for efficiency corrections even for energies as high as 1000 keV. However, the correction factors determined by M-C simulation are lower than those determined by the Matlab code. As we consider the M-C simulation as the reference method, it appears that the Matlab code overestimated the self-attenuation correction required.

Table 5-3 The results derived from the Matlab code for "Geometry 2" for EID=2 cm (constant)

ECF-Matlab code for EID=2 cm (constant)							
keV	**Soil 3%**	**RM**	**FA**	**SFS**	**PG**	**GS**	**LS**
40	0.6897	0.2941	0.7303	0.2894	0.6225	0.3533	0.1740
60	0.8598	0.4571	0.8939	0.4393	0.8250	0.5194	0.2940
80	0.9602	0.5853	0.9883	0.5539	0.9529	0.6404	0.3999
100	1.0172	0.6724	1.0409	0.6306	1.0282	0.7188	0.4780
150	1.0525	0.7514	1.0734	0.6996	1.0775	0.7821	0.5648
200	1.0620	0.7795	1.0817	0.7237	1.0906	0.8056	0.5981
300	1.0672	0.8057	1.0852	0.7485	1.0976	0.8277	0.6307
400	1.0674	0.8188	1.0843	0.7619	1.0975	0.8389	0.6483
500	1.0660	0.8268	1.0821	0.7706	1.0953	0.8459	0.6598
1000	1.0568	0.8462	1.0705	0.7941	1.0815	0.8635	0.6908

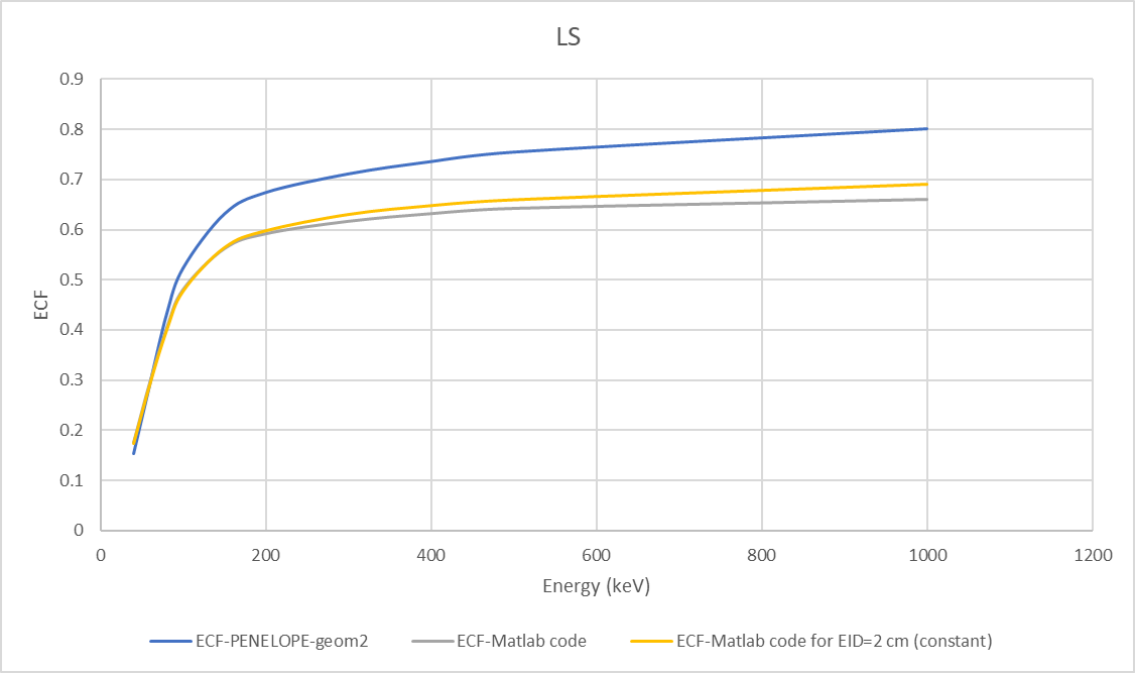

Figure 5-6 The ECF-Energy plots for Lead Slag

As can be seen in Figure 5.8 where the ECF results for Lead Slag are presented, for low energy photons, up to ~80keV simulation results and Matlab code results are almost the same which is of great importance since this indicates that the code provides good quality results for the very important low energy region. For higher energies the results gradually deviate. However, it appears that the EID selection does not play such an important role. The percentage difference between the Matlab code results for constant EID and M-C simulation results are presented in Figure 5.9. Similar results are presented for the other materials in Figures 5.9 – 5.21.

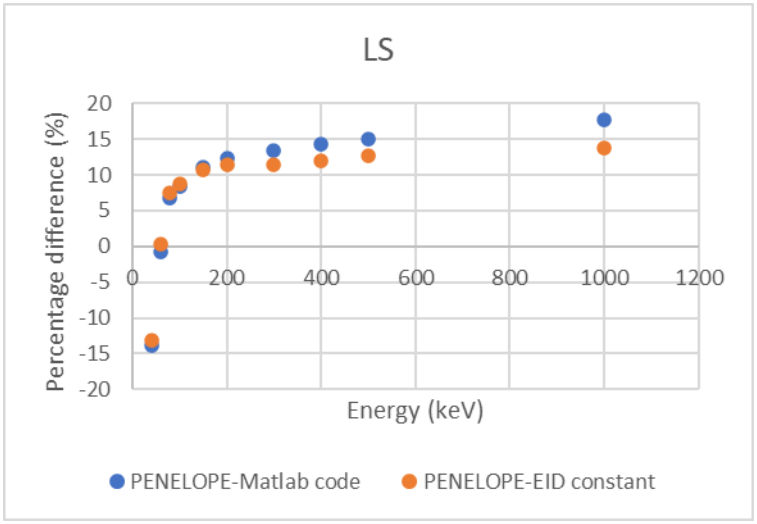

Figure 5-7 The percentage differences between Matlab and PENELOPE for Lead Slag

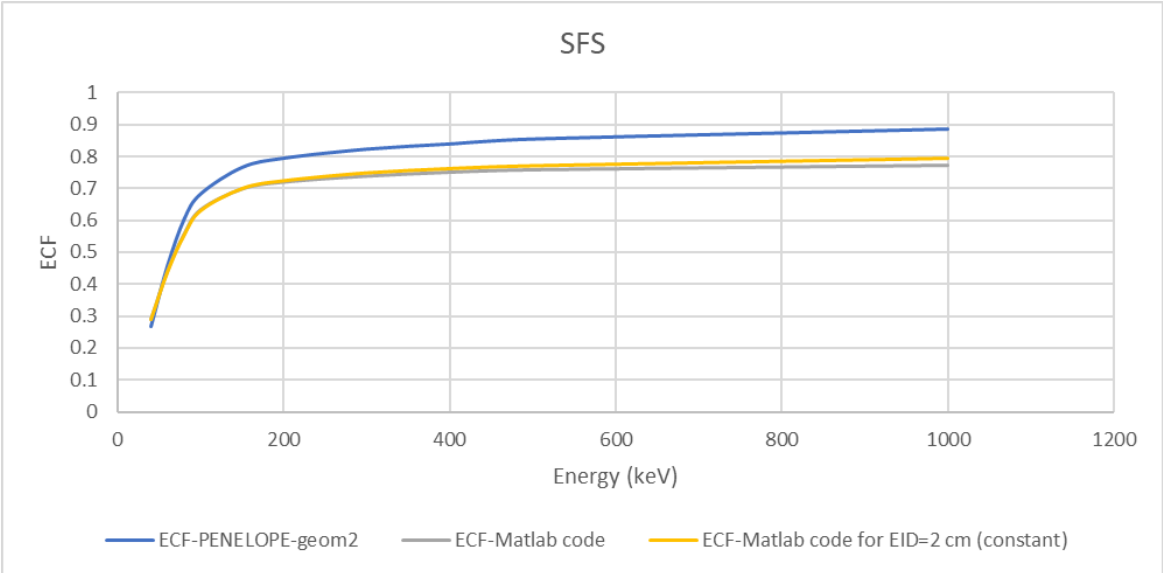

Figure 5-8 The ECF-Energy plots for Shaft Furnace Slag

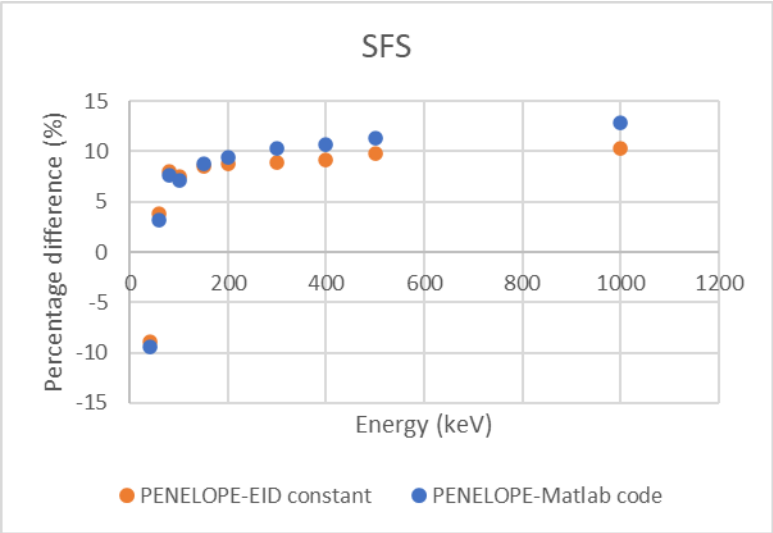

Figure 5-9 The percentage differences between Matlab and PENELOPE for Shaft Furnace Slag

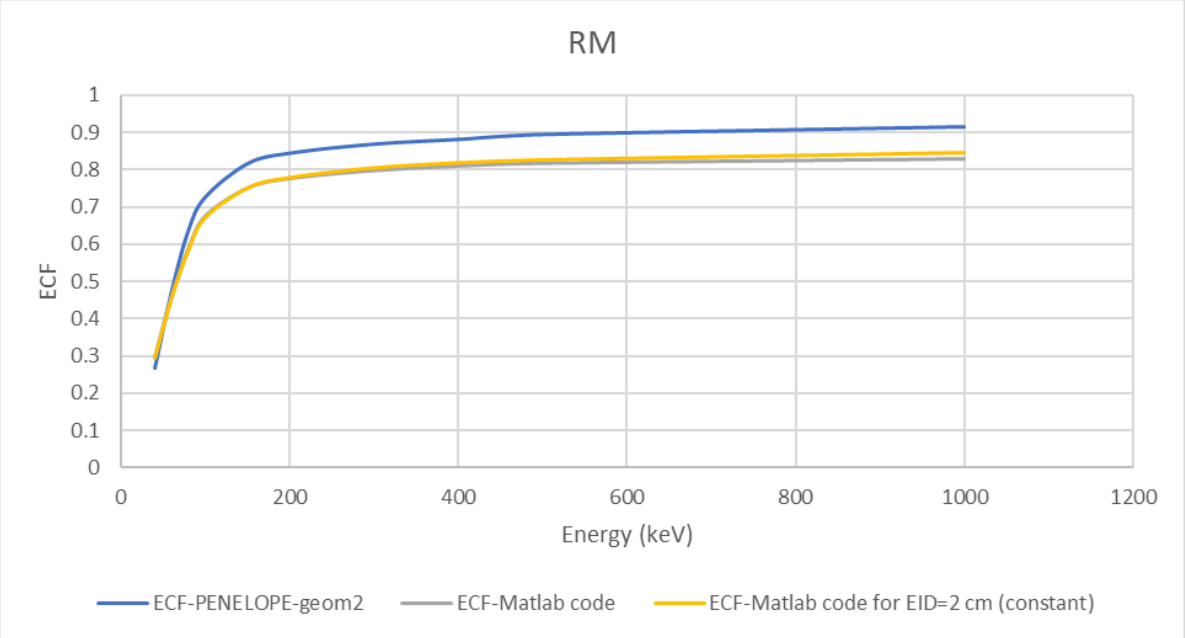

Figure 5-10 The ECF-Energy plots for Red Mud

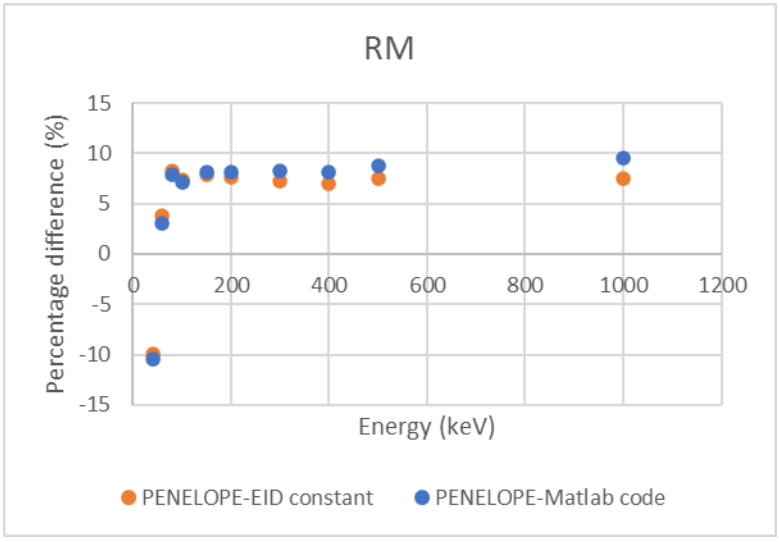

Figure 5-11 The percentage differences between Matlab and PENELOPE for Red Mud

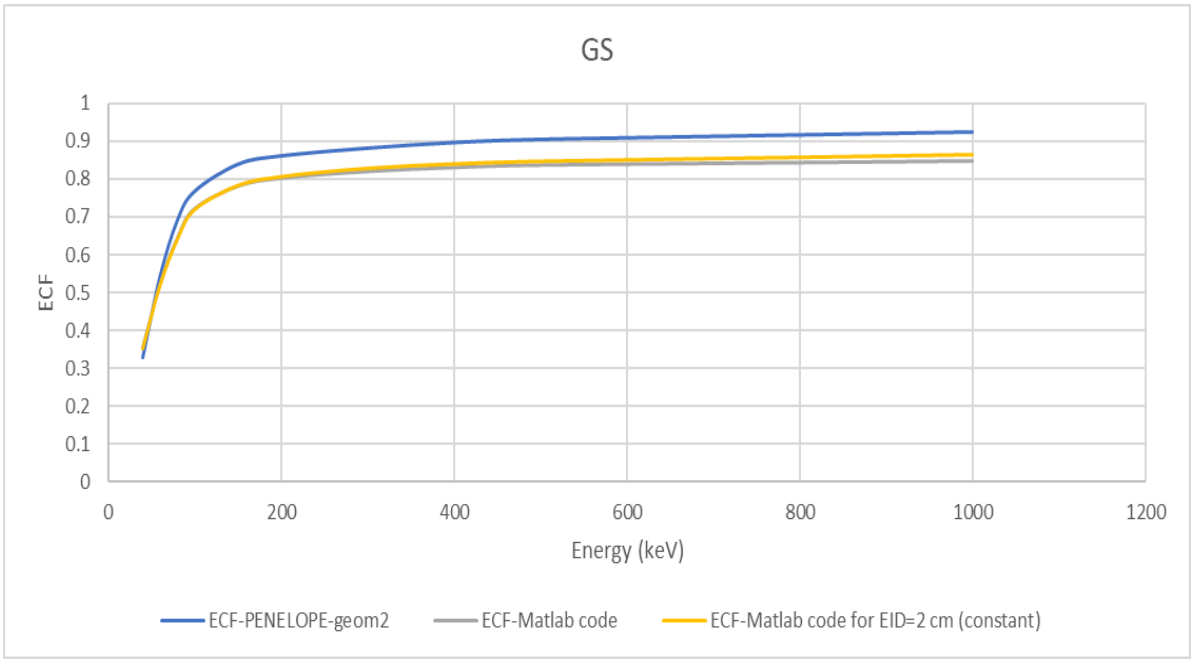

Figure 5-12 The ECF-Energy plots for Granulated Slag

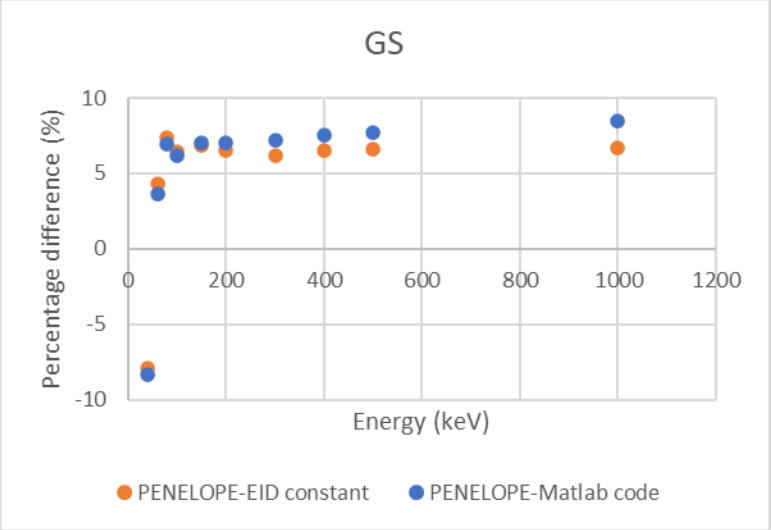

Figure 5-13 The percentage differences between Matlab and PENELOPE for Granulated Slag

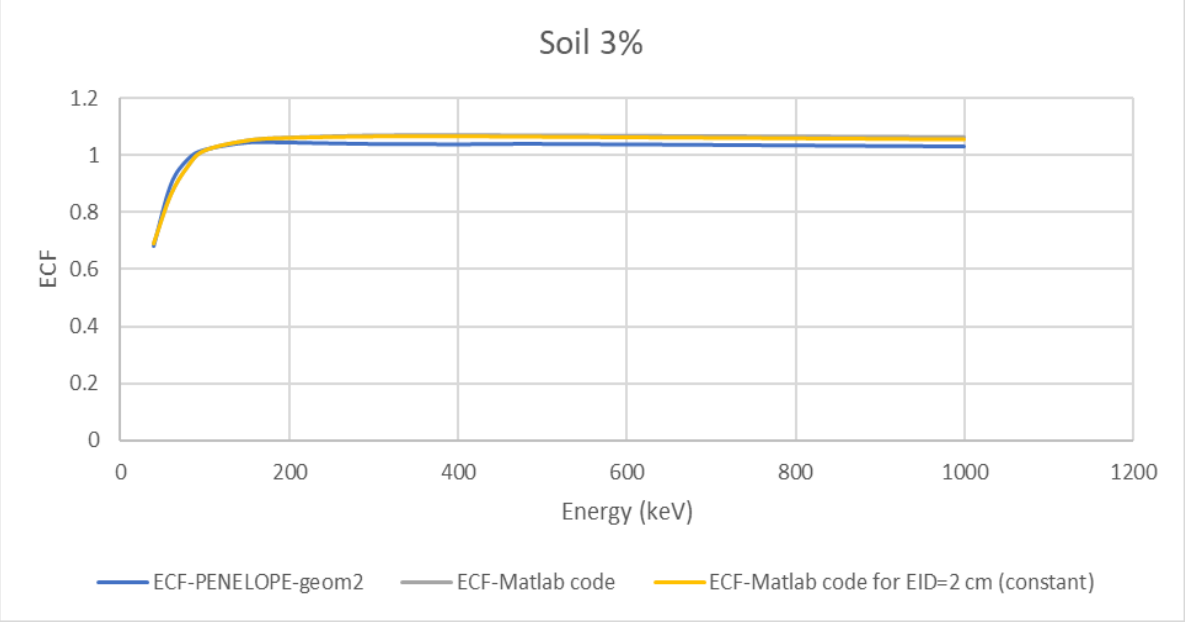

Figure 5-14 The ECF-Energy plots for Soil 3%

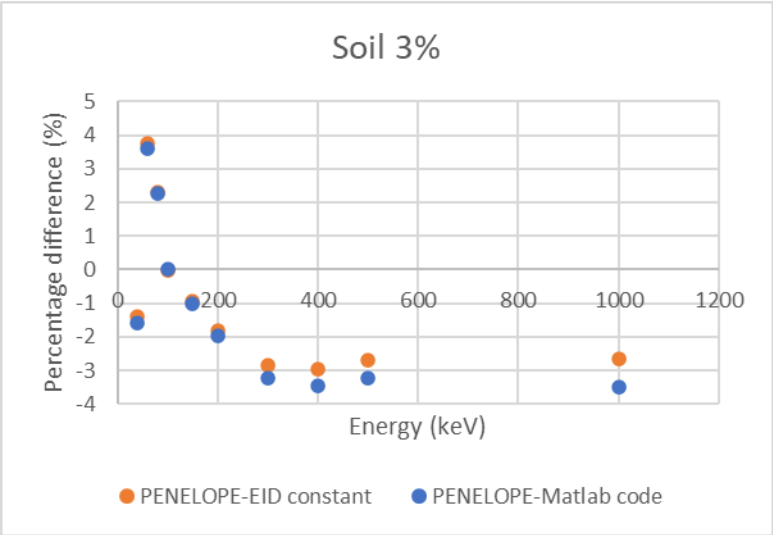

Figure 5-15 The percentage differences between Matlab and PENELOPE for Soil 3%

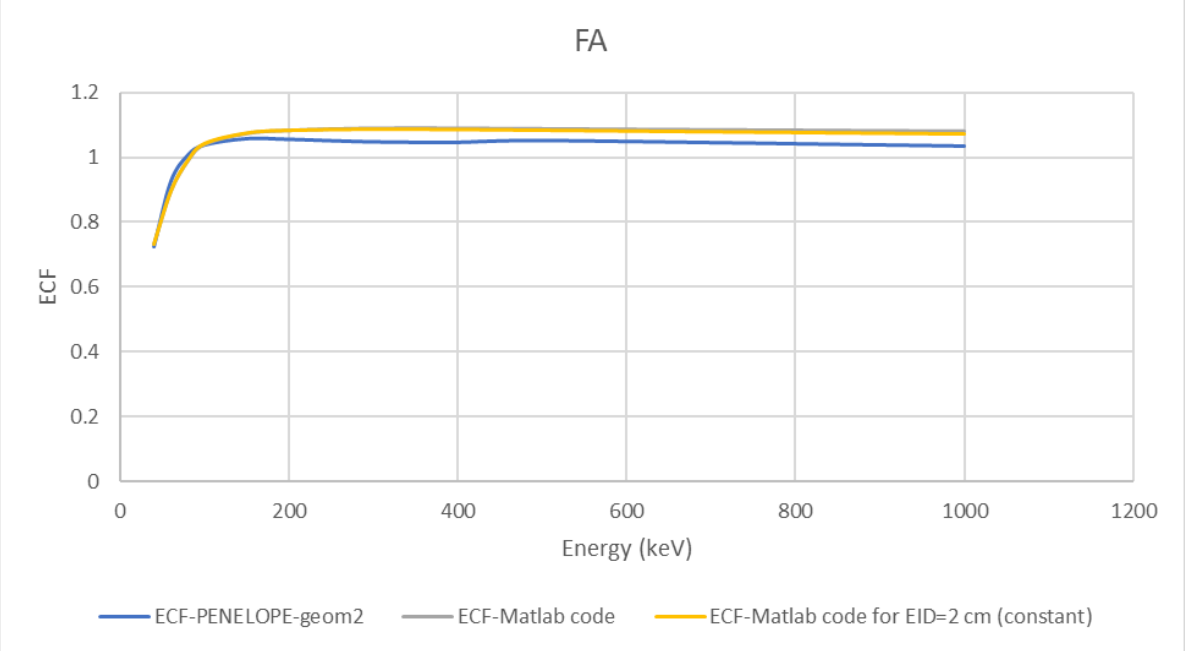

Figure 5-16 The ECF-Energy plots for Fly Ash

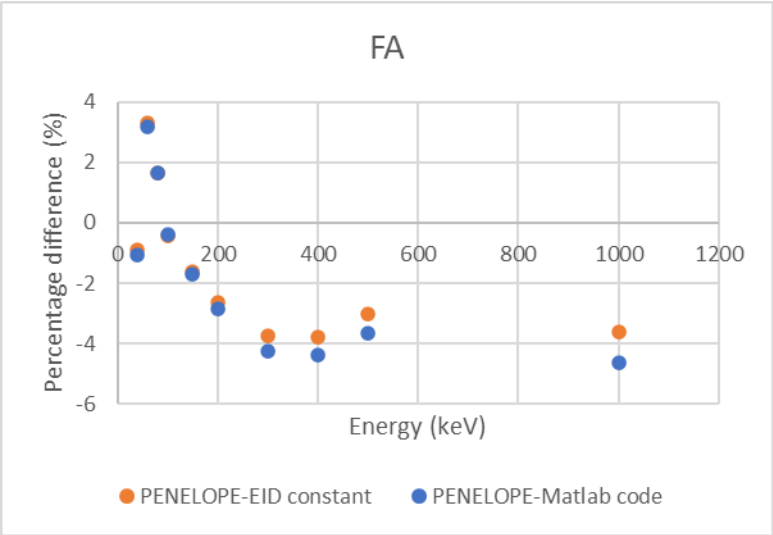

Figure 5-17 The percentage differences between Matlab and PENELOPE for Fly Ash

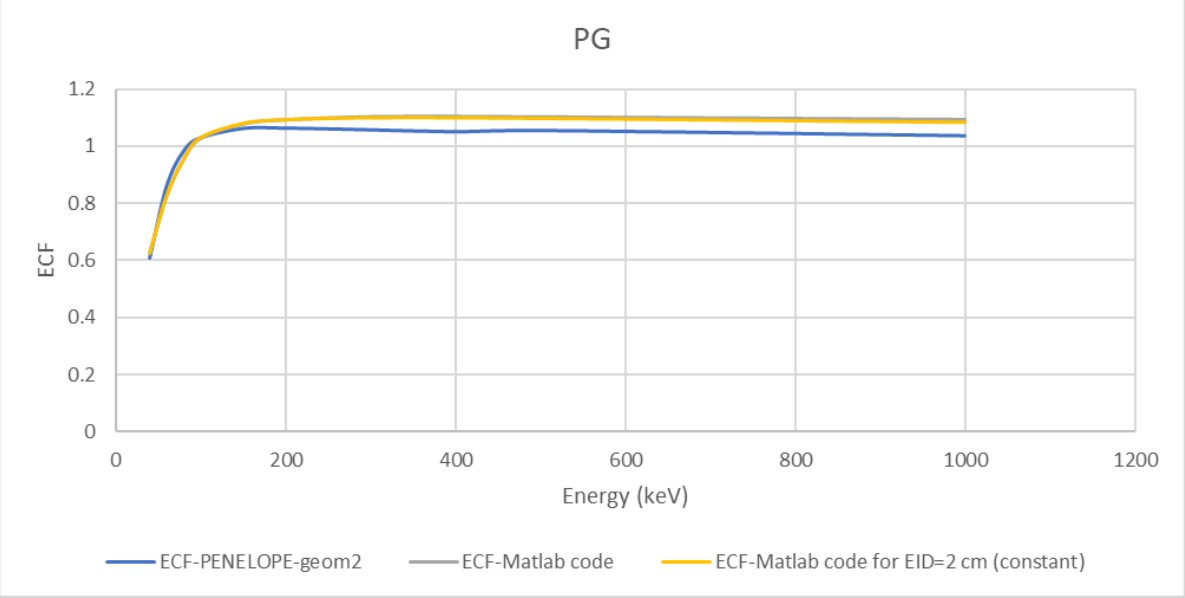

Figure 5-18 The ECF-Energy plots for Phosphogypsum

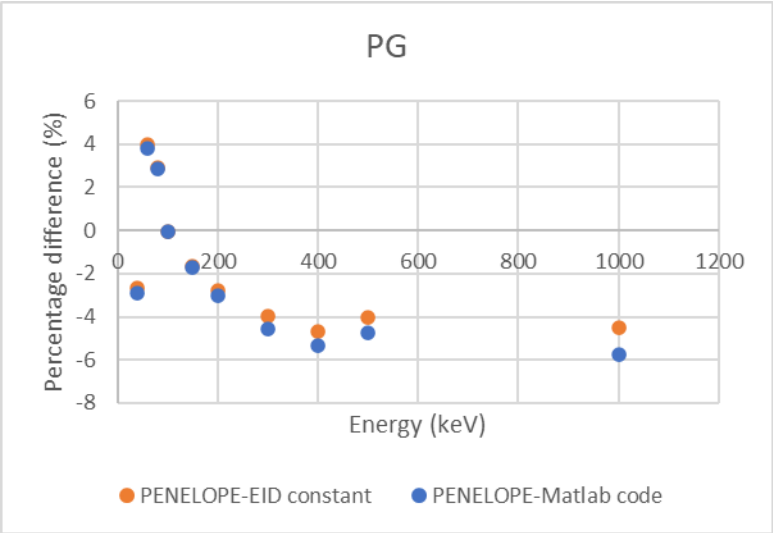

Figure 5-19 The percentage differences between Matlab and PENELOPE for Phosphogypsum

From the graphs shown above, it is feasible to verify the accuracy of the Matlab code, as well as the contribution of the EID as a parameter that can improve the results and minimize the difference with the results derived from the PENELOPE simulations. Generally, the results presented above have great consistency and satisfactory accuracy for most of the materials and in a wide energy range.

More specifically, one of the conclusions drawn is that for materials with a density above 1 g/cm^3, such as Lead Slag, Shaft Furnace Slag, Red Mud, and Granulated Slag, the ECF values calculated using the Matlab code are lower than those calculated with the PENELOPE simulations. On the other hand, for materials with a density lower than 1 g/cm^3, such as Soil 3%, Fly Ash, and Phosphogypsum the results from the Matlab code are slightly higher than the PENELOPE simulation results. This indicates a strong dependency between density and ECF calculation, highlighting the need for further investigation in this area.

It is important to note the highest percentage differences observed for each material. A clear relationship exists between the density of the materials and the magnitude of these differences. In general, these differences refer to the highest energy level calculated, which is 1000 keV, whereas at lower energy levels, the differences significantly drop. In particular, the highest differences detected are for Lead Slag, approximately 15% at 1000 keV. Shaft Furnace Slag shows the highest difference of approximately 12% at 1000 keV, followed by Red Mud with a decrease to approximately 10%, and Granulated Slag with the highest difference dropping further to approximately 8%. The lowest values of the highest differences are observed for materials with densities lower than 1 g/cm^3. Specifically, Soil shows approximately 3% as the highest difference, while Fly Ash and Phosphogypsum differences are approximately 4% and 5%, respectively. For energies below 100 keV, the ECF

values achieve their highest accuracy. It is evident that there is still room for improvement in the code, especially for the higher density materials, and for the higher energy levels. However, considering that this represents the first attempt to calculate ECF for the XtRa detector, the entire endeavor is considered successful.

It should be noted at this point that the XtRa detector is a very large detector with a diameter of 3'', much higher than the cylindrical sample diameter. This means that there are photons emitted from the top of the sample which reach the detector after exiting from the side of the sample and not from the sample bottom. This means that the distance z calculated and used in the integral formula may not be the appropriate one to be used for the attenuation of these photons. This might be a good explanation for the deviations between Matlab code and M-C simulation results.

Another notable conclusion drawn is the impact of the EID value, particularly how the results are influenced by whether this value remains constant or varies with energy. In fact, the difference between the two results is very slight with some of the values derived being almost identical. This might be due to the selection of a constant distance of 2 cm, which represents an average EID value across all energies. Consequently, it does not vary significantly compared to the EID values at distinct energy levels, which typically show small differences among them. The energy region where the introduction of the EID functions improves the results is the lower range.

5.5 The effect of the material density on the calculation

As mentioned in the previous paragraph the ECF seems to be highly dependent on the density of the sample. Subsequently, this parameter was investigated further for three materials of different "default" densities, for four different energy levels. Specifically, the ECF values were calculated with the Matlab code, for Lead Slag, whose default density is 2.645 g/cm^3, Red Mud, whose default density is 1.735 g/cm^3, and Soil, whose default density is 1 g/cm^3. For each material, the calculations were made for different densities around the default values, to compare the results. The graphs presented in Figures 5.22, 5.23 and 5.24 show how the ECF changes with the different densities for each energy level. This investigation of great importance since it is very unlikely that in real life applications the densities of the materials that will have to be analyzed will be the default densities. Furthermore, it should be taken into consideration that even for the very same material the packing density when preparing a sample is not standard but depends – among other things – on the effort put by the analyst when preparing the sample. Needless to say, how important is the effect of the material's exact composition, which in most cases is not known by the analyst.

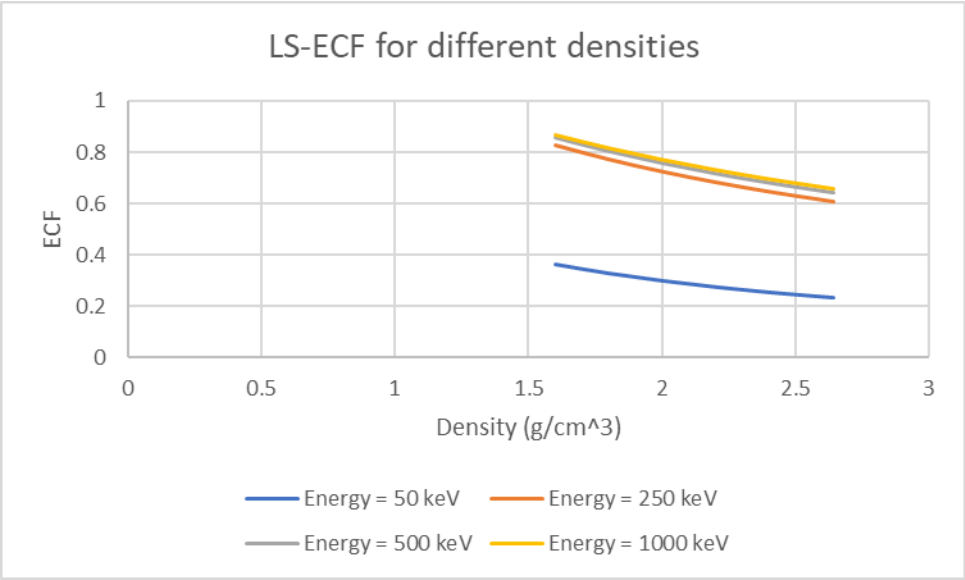

Figure 5-20 The ECF for different densities of Lead Slag

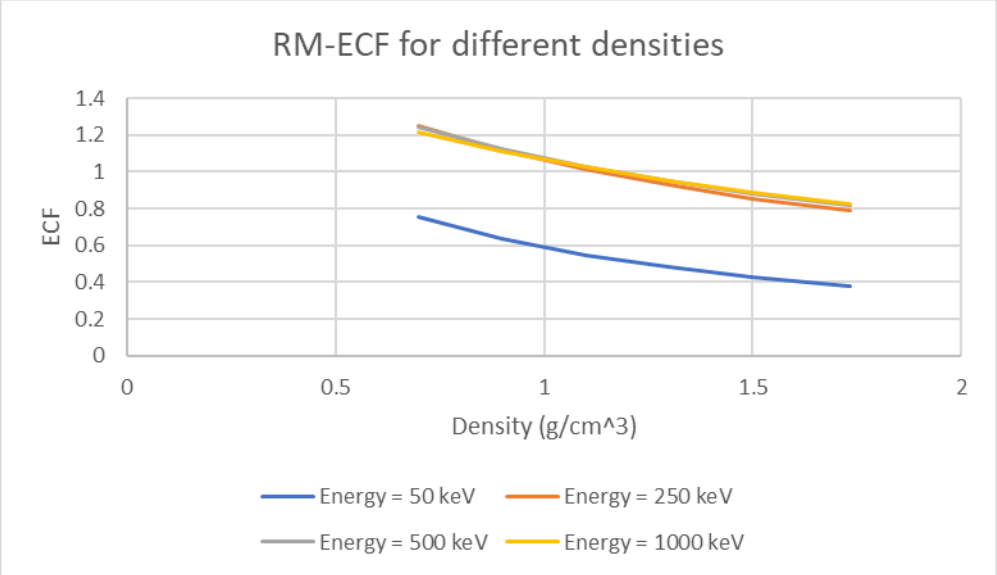

Figure 5-21 The ECF for different densities of Red Mud

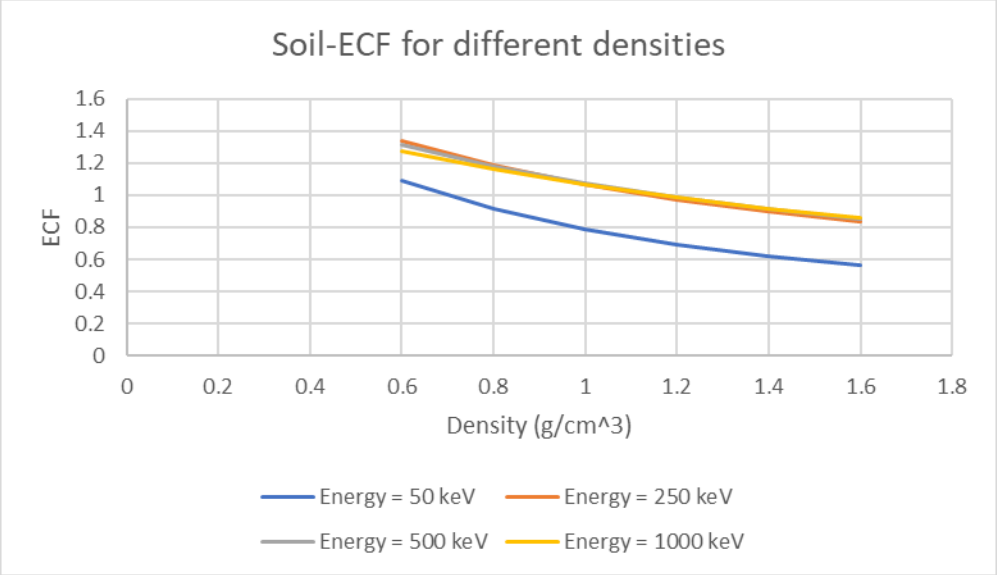

Figure 5-22 The ECF for different densities of Red Mud

The graphs above clearly show that material density significantly influences the calculation of the ECF value. It is also evident that the lower the energy level, the higher the influence. Additionally, it is worth mentioning that the ECF values decrease as the density increases. In fact, for Lead Slag, the percentage difference between the lowest and highest ECF values is approximately 50% at 50 keV, whereas this difference decreases to approximately 30% at 1000 keV. For Red Mud, the percentage difference starts at approximately 98% at 50 keV and drops to approximately 47% at 1000 keV. For Soil, the corresponding percentage differences are approximately 48% and 32%, respectively.

6. Conclusions

The primary aim of this research was to expand the capabilities of the Matlab code developed in previous works for the calculation of the efficiency correction factor (ECF) required in gamma spectroscopic analysis. This work mainly focused on germanium detector XtRa, operating at the NEL-NTUA, which is used to measure the radioactivity of various samples, including those containing Naturally Occurring Radioactive Materials (NORMs). However it can be used for other detectors and any cylindrical sample configuration.

To this day, the analysis of environmental radioactivity samples, such as soil, slags, red mud, and others, remains a complicated topic due to the various parameters that affect the procedure. These parameters include the sample composition, which directly influences its linear attenuation coefficient, the sample's density, and volume, the sample-to-detector setup, as well as the differences between the reference source used for the efficiency calibration of the detector, and the sample being analyzed. Moreover, a major barrier to the accurate calculation of the radioactivity of various samples, particularly NORMs, is the phenomenon of self-absorption.

This work focused on the upgrade and extension of a Matlab code initially developed in the thesis [3], and continued in [4]. The code calculates an Efficiency Correction Factor (ECF) with the "Integral Method" for seven different NORMs (Soil, Fly Ash, Red Mud, Phosphogypsum, and three different slags) using a standard calibration source of 4M HCl. Additionally, several Monte Carlo simulations were conducted to calculate the ECF values and compare them with the results obtained from the Matlab code.

The initial Matlab code created by [3], focused on calculating the ECF for NORMs with the "Integral Method", and the results were compared with Monte-Carlo simulations conducted for the germanium detector LEGe, located in NEL-NTUA. The outcome of that research was very promising but left room for improvement. Specifically, the largest deviations were found in low energies, below 250 keV, for the dense materials, such as the slags. The differences between the Monte-Carlo simulations and the Matlab code in this energy range were found approximately 60%. This divergence was attributed to the significant differences between the linear attenuation coefficients of the materials used in the Matlab code and those used in the PENELOPE code database. Moreover, the energy range for the calculation of the ECF was limited, from 30 to 400 keV, even though correction factors for the self-attenuation are needed for much higher energies as well, as shown in the next thesis, and in this work. Another drawback of the original code was that the user should have Matlab installed, as well as basic programming knowledge.

In the thesis that followed [4], many improvements and upgrades were made to the Matlab code. The focus was on the germanium detector LEGe. Firstly, the linear attenuation coefficients were adjusted to match those used in the PENELOPE database. This change converged the results between the PENELOPE simulations and the Matlab code and dropped

their percentage difference to 20% for the higher density materials and 5% for the low-density materials. Furthermore, the energy range for the ECF calculation was extended to 2000 keV. An important investigation, which also led to the research conducted in this work, was the influence of the Effective Interaction Depth (EID) on the calculation of the ECF. In the first place, this parameter was considered constant, even though it is energy-dependent. Finally, the Matlab code was turned into a standalone application which made it very user-friendly and accessible to everyone. Despite the positive results, there were still areas for improvement, such as studying other detectors, examining the EID value, and extending the capabilities of the Matlab code.

The work presented in this thesis took the research that preceded a step further. To begin with, a thorough investigation was conducted to determine the EID value and its variation with energy for the germanium detector XtRa. To achieve this, several Monte Carlo simulations were run, and the results were plotted in a graph. Besides the simulations, an experiment was also performed, with an Americium point source at 59.54 keV, and the outcomes were crosschecked. A radical change made to the Matlab code was to split the source-to-fictitious point detector distance into two parts. Previously, this parameter was considered constant for the LEGe detector. However, in this work focusing on the XtRa detector, the distance was divided into the source-to-detector distance and the EID within the detector. The source-to-detector distance remains fixed for each sample-detector setup, while for the EID within the detector, a polynomial function was incorporated into the code to retrieve the value based on the desired energy level. This polynomial function fits very accurately the plot created for the EID. Based on this change the ECF values were calculated for different energy levels from the Matlab code, and they were compared to the respective values derived from Monte-Carlo simulations. The entire endeavor is considered successful according to the derived results. More specifically, the percentage differences between the outcomes of the Matlab code and the PENELOPE simulations decreased even further compared to the previous thesis, indicating that the EID indeed plays a significant role in the calculation of the ECF. Moreover, it is noteworthy that the highest differences were found for the higher energies, specifically at 1000 keV, whereas for the energies below 200 keV, the differences were negligible. For the densest material, Lead Slag, the percentage difference was 15% at 1000 keV, while for Soil the respective difference was only 3%.

At this point it should be mentioned that the size of the XtRa detector is much higher than the sample size and this introduces problems with the use of the integral formula as described in paragraph 5.4. The investigation presented in this work should be repeated for other detectors operating at NRL-NTUA, like the LEGe detector or a conventional HPGe.

Another point worth mentioning is the great influence that the material density has on the calculation of the ECF. By changing only this parameter, the ECF can even double. Therefore, the user should accurately know the composition and density of the sample to be analyzed.

Lastly, the GUI of the standalone application was upgraded to make it more user-friendly, and easy to use.

Although many necessary changes and improvements were made in this work, there are still areas for further investigation. First, it would be very useful to include more detectors in the code. In this thesis, a thorough study was conducted on the EID of the detector XtRa. Consequently, it is important to follow up this study with additional detectors and possibly different sample-to-detector setups. Moreover, an investigation of the influence that the dead layer thickness has on determining the EID would be very important. Another improvement would be to extend the materials list. Additionally, it would be interesting to examine in more detail how each parameter affects the calculation of the ECF, such as the volume and density of the sample, and possibly determine their correlation. Lastly, enhancements could be made to the "Integral Method" to minimize the differences between the various methods of calculating the ECF, or to define the cases where this method is sufficient.

Finally, it would be of great interest to investigate what is the ECF for different materials having the same density. This will provide very useful information as to which is the most important parameter affecting self-absorption: material density or material composition.

7. List of Figures

8. List of Tables

9. BIBLIOGRAPHY

[1] Anagnostakis M.J., "Gamma-spectroscopic analysis of low radioactivity samples, in the low energy region," PhD Thesis, NTUA, Athens, 1998.

[2] "Naturally-Occurring Radioactive Materials (NORM) - World Nuclear Association." Accessed: May 21, 2024. [Online]. Available: https://world-nuclear.org/information-library/safety-and-security/radiation-and-health/naturally-occurring-radioactive-materials-norm

[3] F. Tugnoli Ing Domiziano Mostacci, "DETERMINATION OF SELF ABSORPTION CORRECTION FACTORS OF LOW ENERGY PHOTONS USING EXPERIMENTAL, ANALYTICAL AND M-C SIMULATION TECHNIQUES."

[4] I. Alafogiannis, "Development of a computer code for the calculation of self-absorption correction factors in γ-spectrometry application," NTUA-Mechanical Engineering, 2021.

[5] Debertin K. and Helmer RG., *Gamma and X-ray spectrometry with semiconductor detectors*. Amsterdam: Elsevier Science Publisher B.V., 1988.

[6] N. Çelik, U. Çevik, and B. Küçükömeroğlu, "Virtual point detector for HPGe detectors for 26.6-1332 keV photon energies by experiment and Monte Carlo simulation," *J Radioanal Nucl Chem*, vol. 292, no. 3, pp. 1229–1235, 2012, doi: 10.1007/s10967-012-1665-6.

[7] M. J. Anagnostakis and S. E. Simopoulos, "AN EXPERIMENTAL/NUMERICAL METHOD FOR THE EFFICIENCY CALIBRATION OF LOW-ENERGY GERMANIUM DETECTORS," 1996.

[8] Δ. ΛΕΩΝΙΔΟΥ, *ΑΛΛΗΛΕΠΙΔΡΑΣΕΙΣ ΑΚΤΙΝΟΒΟΛΙΩΝ & ΥΛΗΣ-ΔΟΣΙΜΕΤΡΙΑ-ΘΩΡΑΚΙΣΗ*. 1984.

[9] G. Stark, "'gamma ray.' Encyclopedia Britannica, April 22, 2024.," *https://www.britannica.com/science/gamma-ray.*

[10] M. Maqbool, "Interaction of Gamma Rays and X-Rays with Matter," in *An Introduction to Medical Physics*, M. Maqbool, Ed., Cham: Springer International Publishing, 2017, pp. 43–61. doi: 10.1007/978-3-319-61540-0_3.

[11] E. M. Holmbeck, T. M. Sprouse, and M. R. Mumpower, "Nucleosynthesis and observation of the heaviest elements," Feb. 01, 2023, *Springer Science and Business Media Deutschland GmbH*. doi: 10.1140/epja/s10050-023-00927-7.

[12] F. Fang, “Radon Plate-out and the Effects of Airflow and Electric Charge for Dark Matter Experiments,” *SMU Journal of Undergraduate Research*, vol. 8, no. 1, 2024, Jan. 2024, doi: 10.25172/jour.8.1.1.

[13] A. J. B. John R. Lamarsh, *Εισαγωγή στην Πυρηνική Τεχνολογία*, 4th ed. TZIOLA.

[14] Nuclear Power, “Interaction of Gamma Radiation with Matter.” Accessed: May 10, 2024. [Online]. Available: https://www.nuclear-power.com/nuclear-power/reactor-physics/interaction-radiation-matter/interaction-gamma-radiation-matter/

[15] S. Tavernier, “Interactions of Particles in Matter,” in *Experimental Techniques in Nuclear and Particle Physics*, S. Tavernier, Ed., Berlin, Heidelberg: Springer Berlin Heidelberg, 2010, pp. 23–53. doi: 10.1007/978-3-642-00829-0_2.

[16] J. E. Parks, “The Compton Effect-Compton Scattering and Gamma Ray Spectroscopy.” Accessed: May 10, 2024. [Online]. Available: http://www.phys.utk.edu/labs/modphys/Compton%20Scattering%20Experiment.pdf

[17] J. T. Bushberg and J. M. Boone, *The essential physics of medical imaging.* 2011.

[18] Rita Joana da Cruz Roque, “X-ray imaging using 100 µm thick Gas Electron Multipliers operating in Kr-CO2 mixtures,” 2018. doi: 10.13140/RG.2.2.16794.49600.

[19] K. Buchtela, “RADIOCHEMICAL METHODS | Gamma-Ray Spectrometry,” *Encyclopedia of Analytical Science: Second Edition*, pp. 72–79, Jan. 2005, doi: 10.1016/B0-12-369397-7/00525-2.

[20] Δ. Χιώνης, “ΥΠΟΛΟΓΙΣΜΟΣ ΣΥΝΤΕΛΕΣΤΩΝ ΔΙΟΡΘΩΣΗΣ ΤΟΥ ΦΑΙΝΟΜΕΝΟΥ ΠΡΑΓΜΑΤΙΚΗΣ ΣΥΜΠΤΩΣΗΣ ΜΕ ΧΡΗΣΗ ΤΕΧΝΙΚΩΝ ΠΡΟΣΟΜΟΙΩΣΗΣ ΜΟΝΤΕ-CARLO,” ΕΜΠ-Μηχανολόγων Μηχανικών, 2011.

[21] J. Al-Tuweity *et al.*, “Determination of correction factor of self-absorption for lead-210 in environment samples using spike method,” in *E3S Web of Conferences*, EDP Sciences, Feb. 2021. doi: 10.1051/e3sconf/202123400051.

[22] A. Chouak, P. Vuister, G. Paic, M. Berrada, and J. Csikai, “Determination of U and Ra in rock samples by gamma-spectrometric method,” *Journal of Radioanalytical Chemistry*, vol. 45, no. 2, pp. 445–451, 1978, doi: 10.1007/BF02519612.

[23] Epa, “Environment Protection Authority Radiation Information sheet Naturally occurring radioactive material (NORM).” [Online]. Available: www.arpansa.gov.au/understanding-radiation/radiation-sources/more-radiation-sources/ionising-

[24] “Fly ash - Energy Education.” Accessed: May 22, 2024. [Online]. Available: https://energyeducation.ca/encyclopedia/Fly_ash

[25] S. R. Chowdhury, “Recycled Smelter Slags for In Situ and Ex Situ Water and Wastewater Treatment—Current Knowledge and Opportunities,” Mar. 01, 2023, *Multidisciplinary Digital Publishing Institute (MDPI)*. doi: 10.3390/pr11030783.

[26] F. Salvat, J. M. Fernández-Varea, and J. Sempau, “PENELOPE, a code system for Monte Carlo simulation of electron and photon transport.”

[27] Σ. Μηχανολόγων, Μ. Τομέας, and Π. Τεχνολογίας, “ΕΘΝΙΚΟ ΜΕΤΣΟΒΙΟ ΠΟΛΥΤΕΧΝΙΟ ΠΡΟΣΟΜΟΙΩΣΗ ΤΗΣ ΑΛΛΗΛΕΠΙΔΡΑΣΗΣ ΦΩΤΟΝΙΑΚΩΝ ΑΚΤΙΝΟΒΟΛΙΩΝ ΚΑΙ ΥΛΗΣ ΜΕ ΧΡΗΣΗ ΤΟΥ ΚΩΔΙΚΑ PENELOPE-ΕΦΑΡΜΟΓΗ ΣΕ ΠΡΟΒΛΗΜΑΤΑ ΥΠΟΛΟΓΙΣΜΟΥ ΘΩΡΑΚΙΣΕΩΝ ΚΑΙ ΒΑΘΜΟΝΟΜΗΣΗΣ ΑΝΙΧΝΕΥΤΙΚΩΝ ΔΙΑΤΑΞΕΩΝ ΔΙΠΛΩΜΑΤΙΚΗ ΕΡΓΑΣΙΑ ΤΟΥ.”

[28] Δ. Μηχανολόγου Μηχανικού ΕΜΠ, “ΑΝΑΠΤΥΞΗ ΚΑΙ ΕΦΑΡΜΟΓΗ ΤΕΧΝΙΚΩΝ ΠΡΟΣΔΙΟΡΙΣΜΟΥ ΠΟΛΥ ΧΑΜΗΛΩΝ ΣΥΓΚΕΝΤΡΩΣΕΩΝ ΡΑΔΙΕΝΕΡΓΩΝ ΙΧΝΟΣΤΟΙΧΕΙΩΝ ΣΕ ΔΕΙΓΜΑΤΑ ΠΕΡΙΒΑΛΛΟΝΤΙΚΗΣ ΣΗΜΑΣΙΑΣ ΔΙΔΑΚΤΟΡΙΚΗ ΔΙΑΤΡΙΒΗ ΜΑΡΙΛΙΑΣ Ι. ΣΑΒΒΑ ΕΘΝΙΚΟ ΜΕΤΣΟΒΙΟ ΠΟΛΥΤΕΧΝΕΙΟ ΣΧΟΛΗ ΜΗΧΑΝΟΛΟΓΩΝ ΜΗΧΑΝΙΚΩΝ ΤΟΜΕΑΣ ΠΥΡΗΝΙΚΗΣ ΤΕΧΝΟΛΟΓΙΑΣ.”

[29] K. L. Karfopoulos and M. J. Anagnostakis, “Parameters affecting full energy peak efficiency determination during Monte Carlo simulation,” *Applied Radiation and Isotopes*, vol. 68, no. 7–8, pp. 1435–1437, Jul. 2010, doi: 10.1016/j.apradiso.2009.11.020.

[30] HORIBA JOBIN YVON, “Table of X-ray Emission Lines.” Accessed: Jul. 16, 2024. [Online]. Available: www.jobinyvon.com/xray

Appendix

Original Matlab code

```
% EFFICIENCY CORRECTION FACTOR
% 1. Source - detector setup
d=2; % Fictitious source-to-detector distance [cm]
% 2. Sample geometry
prompt='Geometry [2/8] : ';
geom=input(prompt);
if geom==8
r=3.6; % Radius of the sample [cm]
t=1.077; % Thickness of the sample [cm]
end
if geom==2
r=3.6; % Radius of the sample [cm]
t=6.9; % Thickness of the sample [cm]
end
if geom~=2 && geom~=8
fprintf('ERROR: the requested geometry does not exist. Please, insert
2 or 8.')
return
end
% 3. Sample material
prompt='\n MATERIAL \n\n 1:Soil \n 2:Red Mud \n 3:Fly Ash \n 4:SF
Slag \n 5:Phosphogypsum \n 6:G Slag \n 7:L Slag \n\n';
mat=input(prompt);
if mat==1 % Soil
ro=1.000; % Density of the sample [g/cm^3]
x_en=[30 40 50 60 80 100 150 200 300 400 500 600 800 1000];
v_mi=[1.3647 0.67714 0.42883 0.31624 0.2212 0.18221 0.14283 0.12509
0.10562 9.40E-02 8.59E-02 7.98E-02 7.12E-02 6.54E-02];
A=0.265;
B=-3.4735;
C=8.79645;
end
if mat==2 % RM
ro=1.735; % Density of the sample [g/cm^3]
x_en=[30 40 50 60 80 100 150 200 300 400 500 600 800 1000];

v_mi=[2.3833 1.1128 0.65302 0.44617 0.27595 0.21015 0.15105 0.12856
0.1066 9.43E-02 8.58E-02 7.95E-02 7.06E-02 6.45E-02];
A=0.3423;
B=-4.4342;
C=11.758;
end
if mat==3 % FA
ro=0.97; % Density of the sample [g/cm^3]
x_en=[30 40 50 60 80 100 150 200 300 400 500 600 800 1000];
v_mi=[1.303 0.65079 0.4151 0.30808 0.21748 0.18011 0.14199 0.1246
0.1053 9.37E-02 8.55E-02 7.94E-02 7.08E-02 6.49E-02];
A=0.2572;
B=-3.3855;
C=8.5359;
end
if mat==4 % SF Slag
```

```
ro=1.981; % Density of the sample [g/cm^3]
x_en=[30 40 50 60 80 100 150 200 300 400 500 600 800 1000];
v_mi=[2.0893 0.98742 0.58836 0.40853 0.2599 0.20184 0.14848 0.12738
0.10614 9.40E-02 8.56E-02 7.94E-02 7.05E-02 6.45E-02];
A=0.3247;
B=-4.214;
C=11.07;
end
if mat==5 % PG
ro=0.931; % Density of the sample [g/cm^3]
x_en=[30 40 50 60 80 100 150 200 300 400 500 600 800 1000];
v_mi=[1.7362 0.83582 0.511 0.36429 0.24186 0.19295 0.14608 0.12648
0.10609 9.43E-02 8.62E-02 8.01E-02 7.17E-02 6.60E-02];
A=0.3013;
B=-3.9132;
C=10.125;
end
if mat==6 % G Slag
ro=1.657; % Density of the sample [g/cm^3]
x_en=[30 40 50 60 80 100 150 200 300 400 500 600 800 1000];
v_mi=[1.9894 0.94384 0.56592 0.39565 0.25471 0.19941 0.14809 0.12748
0.10646 9.43E-02 8.59E-02 7.96E-02 7.07E-02 6.46E-02];
A=0.3172;
B=-4.1203;
C=10.785;
end
if mat==7 % L Slag
ro=2.645; % Density of the sample [g/cm^3]
x_en=[30 40 50 60 80 100 150 200 300 400 500 600 800 1000];
v_mi=[2.8348 1.3072 0.75301 0.50389 0.30434 0.22218 0.15429 0.12966
0.10659 9.40E-02 8.54E-02 7.90E-02 7.01E-02 6.39E-02];
A=0.3645;
B=-4.7186;
C=12.66;
End

if mat<1
fprintf('ERROR: the requested material does not exist. Please, enter
a number in the range [1,7]')
return
end
if mat>7
fprintf('ERROR: the requested material does not exist. Please, enter
a number in the range [1,7]')
return
end
% 4. Calibration material: 4M HCl
ro_cal=1.059;
x_en_cal=[30 40 50 60 80 100 150 200 300 400 500 600 800 1000];
v_mi_cal=[0.65694 0.38878 0.28935 0.24176 0.19693 0.17476 0.14622
0.13034 0.11146 0.10012 9.24E-02 8.68E-02 7.93E-02 7.45E-02];
A_cal=0.1518;
B_cal=-2.1001;
C_cal=4.7583;
% 5. Linear attenuation coefficient
prompt='\n ENERGY [keV] \n\n ';
energy=input(prompt);
```

```
if energy<30
fprintf('\n ERROR: the energy range is [30, 1000] keV \n\n ');
return
end
if energy>1000
fprintf('\n ERROR: the energy range is [30, 1000] keV \n\n ');
return
end
Lia_cal = ismember(energy, x_en_cal);
Lia=ismember(energy, x_en);
if Lia_cal==1
mi_m_cal=interp1(x_en_cal, v_mi_cal, energy);
else
mi_m_cal=exp(A_cal*(log(energy))^2+B_cal*log(energy)+C_cal);
end
if Lia==1
mi_m=interp1(x_en, v_mi, energy);
else
mi_m=exp(A*(log(energy))^2+B*log(energy)+C);
end
mi_cal=mi_m_cal*ro_cal;
mi=mi_m*ro;

% 6. Integral method
J_cal=integral2(@(x,y)(y.*exp(-
mi_cal.*(x.*(y.^2+(x+d).^2).^1/2)./(x+d))./(y.^2+(x+d).^2),0,t,0,r);
J=integral2(@(x,y)(y.*exp(-
mi.*(x.*(y.^2+(x+d).^2).^1/2)./(x+d))./(y.^2+(x+d).^2),0,t,0,r);
% 7. Efficiency correction factor
ECF=J/J_cal
```

Upgraded Matlab code

```
unction varargout = GUI_ECF(varargin)
% GUI_ECF MATLAB code for GUI_ECF.fig
% GUI_ECF, by itself, creates a new GUI_ECF or raises the
existing
% singleton*.
%
% H = GUI_ECF returns the handle to a new GUI_ECF or the handle
to
% the existing singleton*.
%
% GUI_ECF('CALLBACK',hObject,eventData,handles,...) calls the
local
% function named CALLBACK in GUI_ECF.M with the given input
arguments.
%
% GUI_ECF('Property','Value',...) creates a new GUI_ECF or
raises the
% existing singleton*. Starting from the left, property value
pairs are
% applied to the GUI before GUI_ECF_OpeningFcn gets called. An
% unrecognized property name or invalid value makes property
```

```
application
% stop. All inputs are passed to GUI_ECF_OpeningFcn via
varargin.
%
% *See GUI Options on GUIDE's Tools menu. Choose "GUI allows
only one
% instance to run (singleton)".
%
% See also: GUIDE, GUIDATA, GUIHANDLES
% Edit the above text to modify the response to help GUI_ECF
% Last Modified by GUIDE v2.5 04-Jun-2020 13:46:11
% Begin initialization code - DO NOT EDIT
gui_Singleton = 1;
gui_State = struct('gui_Name', mfilename, ...
'gui_Singleton', gui_Singleton, ...
'gui_OpeningFcn', @GUI_ECF_OpeningFcn, ...
'gui_OutputFcn', @GUI_ECF_OutputFcn, ...
'gui_LayoutFcn', [] , ...
'gui_Callback', []);
if nargin && ischar(varargin{1})
gui_State.gui_Callback = str2func(varargin{1});
end
if nargout
[varargout{1:nargout}] = gui_mainfcn(gui_State, varargin{:});
else
gui_mainfcn(gui_State, varargin{:});
end
% End initialization code - DO NOT EDIT

% --- Executes just before GUI_ECF is made visible.
function GUI_ECF_OpeningFcn(hObject, eventdata, handles, varargin)
% This function has no output args, see OutputFcn.
% hObject handle to figure
% eventdata reserved - to be defined in a future version of MATLAB
% handles structure with handles and user data (see GUIDATA)
% varargin command line arguments to GUI_ECF (see VARARGIN)
% Choose default command line output for GUI_ECF
handles.output = hObject;
% Update handles structure
guidata(hObject, handles);
% UIWAIT makes GUI_ECF wait for user response (see UIRESUME)
% uiwait(handles.figure1);
% --- Outputs from this function are returned to the command line.
function varargout = GUI_ECF_OutputFcn(hObject, eventdata, handles)
% varargout cell array for returning output args (see VARARGOUT);
% hObject handle to figure
% eventdata reserved - to be defined in a future version of MATLAB
% handles structure with handles and user data (see GUIDATA)
% Get default command line output from handles structure
varargout{1} = handles.output;
function d_Callback(hObject, eventdata, handles)
% hObject handle to d (see GCBO)
% eventdata reserved - to be defined in a future version of MATLAB
% handles structure with handles and user data (see GUIDATA)
% Hints: get(hObject,'String') returns contents of d as text
% str2double(get(hObject,'String')) returns contents of d as a
double
```

```
% --- Executes during object creation, after setting all properties.
function d_CreateFcn(hObject, eventdata, handles)
% hObject handle to d (see GCBO)
% eventdata reserved - to be defined in a future version of MATLAB
% handles empty - handles not created until after all CreateFcns
called
% Hint: edit controls usually have a white background on Windows.
% See ISPC and COMPUTER.
if ispc && isequal(get(hObject,'BackgroundColor'),
get(0,'defaultUicontrolBackgroundColor'))
set(hObject,'BackgroundColor','white');
end

function geom_Callback(hObject, eventdata, handles)
% hObject handle to geom (see GCBO)
% eventdata reserved - to be defined in a future version of MATLAB
% handles structure with handles and user data (see GUIDATA)
% Hints: get(hObject,'String') returns contents of geom as text
% str2double(get(hObject,'String')) returns contents of geom
as a double
% --- Executes during object creation, after setting all properties.
function geom_CreateFcn(hObject, eventdata, handles)
% hObject handle to geom (see GCBO)
% eventdata reserved - to be defined in a future version of MATLAB
% handles empty - handles not created until after all CreateFcns
called
% Hint: edit controls usually have a white background on Windows.
% See ISPC and COMPUTER.
if ispc && isequal(get(hObject,'BackgroundColor'),
get(0,'defaultUicontrolBackgroundColor'))
set(hObject,'BackgroundColor','white');
end
function energy_Callback(hObject, eventdata, handles)
% hObject handle to energy (see GCBO)
% eventdata reserved - to be defined in a future version of MATLAB
% handles structure with handles and user data (see GUIDATA)
% Hints: get(hObject,'String') returns contents of energy as text
% str2double(get(hObject,'String')) returns contents of energy
as a double
% --- Executes during object creation, after setting all properties.
function energy_CreateFcn(hObject, eventdata, handles)
% hObject handle to energy (see GCBO)
% eventdata reserved - to be defined in a future version of MATLAB
% handles empty - handles not created until after all CreateFcns
called
% Hint: edit controls usually have a white background on Windows.
% See ISPC and COMPUTER.
if ispc && isequal(get(hObject,'BackgroundColor'),
get(0,'defaultUicontrolBackgroundColor'))
set(hObject,'BackgroundColor','white');
end
function mat_Callback(hObject, eventdata, handles)
% hObject handle to mat (see GCBO)
% eventdata reserved - to be defined in a future version of MATLAB
% handles structure with handles and user data (see GUIDATA)
% Hints: get(hObject,'String') returns contents of mat as text
```

```
% str2double(get(hObject,'String')) returns contents of mat as
a double
% --- Executes during object creation, after setting all properties.
function mat_CreateFcn(hObject, eventdata, handles)
% hObject handle to mat (see GCBO)
% eventdata reserved - to be defined in a future version of MATLAB
% handles empty - handles not created until after all CreateFcns
called
% Hint: edit controls usually have a white background on Windows.
% See ISPC and COMPUTER.
if ispc && isequal(get(hObject,'BackgroundColor'),
get(0,'defaultUicontrolBackgroundColor'))
set(hObject,'BackgroundColor','white');
end
% --- Executes on button press in pushbutton_ECF.
function pushbutton_ECF_Callback(hObject, eventdata, handles)
% hObject handle to pushbutton_ECF (see GCBO)
% eventdata reserved - to be defined in a future version of MATLAB
% handles structure with handles and user data (see GUIDATA)
global ECF
d=str2double(get(handles.d,'String'));
geom=str2double(get(handles.geom,'String'));
mat=str2double(get(handles.mat,'String'));
energy=str2double(get(handles.energy,'String'));
r=str2double(get(handles.r,'String'));
t=str2double(get(handles.t,'String'));
ro=str2double(get(handles.r0,'String'));
if geom==8
r=3.6; % Radius of the sample [cm]
t=1.077; % Thickness of the sample [cm]
end
if geom==2
r=3.6; % Radius of the sample [cm]
t=6.9; % Thickness of the sample [cm]
end
if mat==1 % Soil
%ro=1.000; % Density of the sample [g/cm^3]
x_en=[30 35 40 45 50 60 80 100 150 200 300 400 500 600 800 1000];
v_mi=[1.3986 0.94829 0.69336 0.53746 0.43687 0.32054 0.22286 0.18346
0.14449 0.12715 0.1078 0.09582 0.08719 0.080498 0.070568 0.063378];
if energy<150
A=-0.1166;
B=2.23;
C=-13.91;
D=26.45;
End

if energy>150
A=-0.009175;
B=0.1466;
C=-1.194;
D=1.518;
end
if energy == 150
mi_m = 0.14449;
end
end
```

```
%----------------------%
if mat==2 % RM
%ro=1.735; % Density of the sample [g/cm^3]
x_en=[30 35 40 45 50 60 80 100 150 200 300 400 500 600 800 1000];
v_mi=[2.4322 1.6057 1.136 0.84954 0.6646 0.45251 0.27827 0.21156
0.15243 0.13019 0.10832 0.095736 0.086904 0.080133 0.070162
0.062977];
if energy<150
A=0.05843;
B=0.03045;
C=-5.118;
D=15.65;
end
if energy>150
A=-0.01837;
B=0.3375;
C=-2.511;
D=4.532;
end
if energy == 150
mi_m = 0.15243;
end
end
if mat==3 % FA
%ro=0.97; % Density of the sample [g/cm^3]

x_en=[30 35 40 45 50 60 80 100 150 200 300 400 500 600 800 1000];
v_mi=[1.3293 0.90393 0.66316 0.51594 0.42092 0.31096 0.21839 0.18083
0.14326 0.1263 0.1072 0.095314 0.086741 0.08009 0.070214 0.063062];
if energy<150
A=-0.1312;
B=2.41;
C=-14.61;
D=27.27;
end
if energy>150
A=-0.008551;
B=0.1338;
C=-1.107;
D=1.316;
end
if energy == 150
mi_m = 0.14326;
end
end
if mat==4 % SF Slag
%ro=1.981; % Density of the sample [g/cm^3]
x_en=[30 35 40 45 50 60 80 100 150 200 300 400 500 600 800 1000];
v_mi=[2.1344 1.4182 1.0111 0.76188 0.60103 0.41581 0.26279 0.20354
0.14988 0.12899 0.10784 0.095452 0.086701 0.079972 0.070045
0.062882];
if energy<150
A=0.0233;
B=0.4741;
C=-6.893;
D=17.81;
end
```

```
if energy>150
A=-0.01615;
B=0.2912;
C=-2.189;
D=3.788;
end
if energy == 150
mi_m = 0.14988;

end
end
if mat==5 % PG
%ro=0.931; % Density of the sample [g/cm^3]
x_en=[30 35 40 45 50 60 80 100 150 200 300 400 500 600 800 1000];
v_mi=[1.788 1.1929 0.8559 0.65158 0.51956 0.36841 0.24326 0.19421
0.14812 0.12903 0.1087 0.09643 0.087671 0.080905 0.070893 0.063656];
if energy<150
A=-0.04834;
B=1.394;
C=-10.68;
D=22.69;
end
if energy>150
A=-0.01202;
B=0.2064;
C=-1.611;
D=2.488;
end
if energy == 150
mi_m = 0.14812;
end
end
if mat==6 % G Slag
%ro=1.657; % Density of the sample [g/cm^3]
x_en=[30 35 40 45 50 60 80 100 150 200 300 400 500 600 800 1000];
v_mi=[2.0355 1.3532 0.96602 0.72969 0.57714 0.40182 0.25697 0.20074
0.14933 0.12897 0.10807 0.095716 0.086964 0.080226 0.070275
0.063093];
if energy<150
A=0.003599;
B=0.7292;
C=-7.954;
D=19.19;
End

if energy>150
A=-0.01488;
B=0.2652;
C=-2.013;
D=3.393;
end
if energy == 150
mi_m = 0.14933;
end
end
if mat==7 % L Slag
%ro=2.645; % Density of the sample [g/cm^3]
```

```
%x_en= [30 35 40 45 50 60 80 100 150 200 300 400 500 600 800 1000];
%v_mi= [2.8873 1.9 1.3376 0.99276 0.77023 0.51427 0.30434 0.22462
0.15579 0.13119 0.10815 0.095316 0.086421 0.079639 0.06969 0.062537];
x_en=[30 35 40 45 50 55 60 65 70 75 80 85 90 95 100 110 120 130 140
150 200 300 400 500 600 800 1000];
v_mi=[2.8873 1.9 1.3376 0.99276 0.77023 0.61962 0.51427 0.43773
0.38099 0.33781 0.30434 0.2778 0.25643 0.239 0.22462 0.2023 0.18594
0.17349 0.16371 0.15579 0.13119 0.10815 0.095316 0.086421 0.079639
0.06969 0.062537];
if energy<150
A=0.0935;
B=-0.4211;
C=-3.292;
D=13.46;
end
if energy>150
A=-0.023;
B=0.433;
C=-3.167;
D=6.022;
end
if energy == 150

mi_m = 0.15579;
end
end
if mat==8 % Water
%ro=1.000; % Density of the sample [g/cm^3]
x_en=[30 35 40 45 50 60 80 100 150 200 300 400 500 600 800 1000];
v_mi=[0.37808 0.30952 0.27011 0.24513 0.22824 0.20686 0.18425 0.17113
0.15067 0.13711 0.11866 0.10614 0.096845 0.89541 0.078607 0.070644];
if energy<150
A=-0.2567;
B=3.54;
C=-16.56;
D=24.49;
end
if energy>150
A=7.263e-05;
B=-0.0478;
C=0.1627;
D=-1.517;
end
if energy == 150
mi_m = 0.15067;
end
end
% 4. Calibration material: 4M HCl
ro_cal=1.059;
x_en_cal=[30 35 40 45 50 60 80 100 150 200 300 400 500 600 800 1000];
v_mi_cal=[0.66261 0.48741 0.38816 0.32701 0.28709 0.23968 0.1966
0.1763 0.1507 0.13599 0.11712 0.10458 0.095361 0.088137 0.077348
0.069501];
if energy<150
A_cal=-0.2998;
B_cal=4.347;
C_cal=-21.38;
```

```
D_cal=33.82;
End

if energy>150
A_cal=-0.002213;
B_cal=0.000239;
C_cal=-0.1725;
D_cal=-0.757;
end
if energy == 150
mi_m_cal = 0.1507;
end
%Lia_cal = ismember(energy, x_en_cal);
%Lia=ismember(energy, x_en);
%if Lia_cal==1
%mi_m_cal=interp1(x_en_cal, v_mi_cal, energy);
%else
if energy ~= 150
mi_m_cal=exp(A_cal*log(energy)^3 + B_cal*log(energy)^2 +
C_cal*log(energy) + D_cal);
end
%end
%if Lia==1
%mi_m=interp1(x_en, v_mi, energy);%it takes the v_mi for the
corresponing energy
%else
if energy ~=150
mi_m=exp(A*log(energy)^3 + B*log(energy)^2 + C*log(energy) + D);% it
calculates the μ
end
%end
mi_cal=mi_m_cal*ro_cal; % this multiplies the μ with density
mi=mi_m*ro; % this multiplies the μ with density
% 6. Integral method
J_cal=integral2(@(x,y)(y.*exp(-
mi_cal.*(x.*(y.^2+(x+d).^2).^1/2)./(x+d))./(y.^2+(x+d).^2),0,t,0,r);
J=integral2(@(x,y)(y.*exp(-
mi.*(x.*(y.^2+(x+d).^2).^1/2)./(x+d))./(y.^2+(x+d).^2),0,t,0,r);

ECF=J/J_cal
set(handles.ECF,'String',ECF);
set(handles.m,'String',mi_m);
function ECF_Callback(hObject, eventdata, handles)
% hObject handle to ECF (see GCBO)
% eventdata reserved - to be defined in a future version of MATLAB
% handles structure with handles and user data (see GUIDATA)
% Hints: get(hObject,'String') returns contents of ECF as text
% str2double(get(hObject,'String')) returns contents of ECF as
a double
% --- Executes during object creation, after setting all properties.
function ECF_CreateFcn(hObject, eventdata, handles)
% hObject handle to ECF (see GCBO)
% eventdata reserved - to be defined in a future version of MATLAB
% handles empty - handles not created until after all CreateFcns
called
% Hint: edit controls usually have a white background on Windows.
% See ISPC and COMPUTER.
```

```
if ispc && isequal(get(hObject,'BackgroundColor'),
get(0,'defaultUicontrolBackgroundColor'))
set(hObject,'BackgroundColor','white');
end
function r_Callback(hObject, eventdata, handles)
% hObject handle to r (see GCBO)
% eventdata reserved - to be defined in a future version of MATLAB
% handles structure with handles and user data (see GUIDATA)
% Hints: get(hObject,'String') returns contents of r as text
% str2double(get(hObject,'String')) returns contents of r as a
double
% --- Executes during object creation, after setting all properties.
function r_CreateFcn(hObject, eventdata, handles)
% hObject handle to r (see GCBO)
% eventdata reserved - to be defined in a future version of MATLAB
% handles empty - handles not created until after all CreateFcns
called
% Hint: edit controls usually have a white background on Windows.
% See ISPC and COMPUTER.
if ispc && isequal(get(hObject,'BackgroundColor'),
get(0,'defaultUicontrolBackgroundColor'))
set(hObject,'BackgroundColor','white');
end

function t_Callback(hObject, eventdata, handles)
% hObject handle to t (see GCBO)
% eventdata reserved - to be defined in a future version of MATLAB
% handles structure with handles and user data (see GUIDATA)
% Hints: get(hObject,'String') returns contents of t as text
% str2double(get(hObject,'String')) returns contents of t as a
double
% --- Executes during object creation, after setting all properties.
function t_CreateFcn(hObject, eventdata, handles)
% hObject handle to t (see GCBO)
% eventdata reserved - to be defined in a future version of MATLAB
% handles empty - handles not created until after all CreateFcns
called
% Hint: edit controls usually have a white background on Windows.
% See ISPC and COMPUTER.
if ispc && isequal(get(hObject,'BackgroundColor'),
get(0,'defaultUicontrolBackgroundColor'))
set(hObject,'BackgroundColor','white');
end
function r0_Callback(hObject, eventdata, handles)
% hObject handle to r0 (see GCBO)
% eventdata reserved - to be defined in a future version of MATLAB
% handles structure with handles and user data (see GUIDATA)
% Hints: get(hObject,'String') returns contents of r0 as text
% str2double(get(hObject,'String')) returns contents of r0 as
a double
% --- Executes during object creation, after setting all properties.
function r0_CreateFcn(hObject, eventdata, handles)
% hObject handle to r0 (see GCBO)
% eventdata reserved - to be defined in a future version of MATLAB
% handles empty - handles not created until after all CreateFcns
called
% Hint: edit controls usually have a white background on Windows.
```

```
% See ISPC and COMPUTER.
if ispc && isequal(get(hObject,'BackgroundColor'),
get(0,'defaultUicontrolBackgroundColor'))
set(hObject,'BackgroundColor','white');
end
function m_Callback(hObject, eventdata, handles)
% hObject handle to m (see GCBO)
% eventdata reserved - to be defined in a future version of MATLAB
% handles structure with handles and user data (see GUIDATA)

% Hints: get(hObject,'String') returns contents of m as text
% str2double(get(hObject,'String')) returns contents of m as a
double
% --- Executes during object creation, after setting all properties.
function m_CreateFcn(hObject, eventdata, handles)
% hObject handle to m (see GCBO)
% eventdata reserved - to be defined in a future version of MATLAB
% handles empty - handles not created until after all CreateFcns
called
% Hint: edit controls usually have a white background on Windows.
% See ISPC and COMPUTER.
if ispc && isequal(get(hObject,'BackgroundColor'),
get(0,'defaultUicontrolBackgroundColor'))
set(hObject,'BackgroundColor','white');
end
```

New Matlab code

```
dsc=app.SourcetodetectordistancedsdccmEditField.Value;
def_EID=app.define_EID.Value;
geom=app.EnterGeometry2580EditField.Value;
mat= app.EditField.Value;
energy=app.EnergyinkeV302000EditField.Value;
r=app.RadiusofthesamplecmEditField.Value;
t=app.ThicknessofthesamplecmEditField.Value;
ro=app.DensityoftheSampleMaterialgcm3EditField.Value;
if def_EID==0
de=app.DetectorEffectiveInteractionDepthdecmEditField.Value;
end


if def_EID==1
if energy <= 1000
de = 0.0000000554*energy.^3-0.0000333964*energy.^2+0.0030357146*energy+
1.67236;
elseif energy > 1000
de = 3.14425;
end
end
```

```
d=dsc+de;



if geom==8
r=3.6; % Radius of the sample [cm]
t=1.077; % Thickness of the sample [cm]
end


if geom==5
r=3.6; % Radius of the sample [cm]
t=2.2; % Thickness of the sample [cm]
end


if geom==2
r=3.6; % Radius of the sample [cm]
t=6.9; % Thickness of the sample [cm]
end


if mat==1 % Soil %ro=1.000 % Density of the sample [g/cm^3]
x_en=[30 35 40 45 50 60 80 100 150 200 300 400 500 600 800 1000];
v_mi=[1.3986 0.94829 0.69336 0.53746 0.43687 0.32054 0.22286 0.18346 0.14449
0.12715 0.1078 0.09582 0.08719 0.080498 0.070568 0.063378];
if energy<150
A=-0.1166;
B=2.23;
C=-13.91;
D=26.45;
end


if energy>150
A=-0.009175;
B=0.1466;
C=-1.194;
D=1.518;
end


if energy == 150
mi_m = 0.14449;
end
end
```

```
%----------------------%
if mat==2 % RM %ro=1.735 % Density of the sample [g/cm^3]
x_en=[30 35 40 45 50 60 80 100 150 200 300 400 500 600 800 1000];
v_mi=[2.4322 1.6057 1.136 0.84954 0.6646 0.45251 0.27827 0.21156 0.15243
0.13019 0.10832 0.095736 0.086904 0.080133 0.070162 0.062977];
if energy<150
A=0.05843;
B=0.03045;
C=-5.118;
D=15.65;
end
if energy>150
A=-0.01837;
B=0.3375;
C=-2.511;
D=4.532;
end


if energy == 150
mi_m = 0.15243;
end
end
%----------------------%


if mat==3 % FA %ro=0.97 % Density of the sample [g/cm^3]
x_en=[30 35 40 45 50 60 80 100 150 200 300 400 500 600 800 1000];
v_mi=[1.3293 0.90393 0.66316 0.51594 0.42092 0.31096 0.21839 0.18083 0.14326
0.1263 0.1072 0.095314 0.086741 0.08009 0.070214 0.063062];
if energy<150
A=-0.1312;
B=2.41;
C=-14.61;
D=27.27;
end
if energy>150
A=-0.008551;
B=0.1338;
C=-1.107;
D=1.316;
end
if energy == 150
mi_m = 0.14326;
end
end
%----------------------%
```

```
if mat==4 % SF Slag %ro=1.981 % Density of the sample [g/cm^3]
x_en=[30 35 40 45 50 60 80 100 150 200 300 400 500 600 800 1000];
v_mi=[2.1344 1.4182 1.0111 0.76188 0.60103 0.41581 0.26279 0.20354 0.14988
0.12899 0.10784 0.095452 0.086701 0.079972 0.070045 0.062882];
if energy<150
A=0.0233;
B=0.4741;
C=-6.893;
D=17.81;
end
if energy>150
A=-0.01615;
B=0.2912;
C=-2.189;
D=3.788;
end
if energy == 150
mi_m = 0.14988;
end
end
%----------------------%


if mat==5 % PG %ro=0.931 % Density of the sample [g/cm^3]
x_en=[30 35 40 45 50 60 80 100 150 200 300 400 500 600 800 1000];
v_mi=[1.788 1.1929 0.8559 0.65158 0.51956 0.36841 0.24326 0.19421 0.14812
0.12903 0.1087 0.09643 0.087671 0.080905 0.070893 0.063656];
if energy<150
A=-0.04834;
B=1.394;
C=-10.68;
D=22.69;
end
if energy>150
A=-0.01202;
B=0.2064;
C=-1.611;
D=2.488;
end
if energy == 150
mi_m = 0.14812;
end
end


%----------------------%
```

```
if mat==6 % G Slag %ro=1.657 % Density of the sample [g/cm^3]
x_en=[30 35 40 45 50 60 80 100 150 200 300 400 500 600 800 1000];
v_mi=[2.0355 1.3532 0.96602 0.72969 0.57714 0.40182 0.25697 0.20074 0.14933
0.12897 0.10807 0.095716 0.086964 0.080226 0.070275 0.063093];
if energy<150
A=0.003599;
B=0.7292;
C=-7.954;
D=19.19;
end
if energy>150
A=-0.01488;
B=0.2652;
C=-2.013;
D=3.393;
end

if energy == 150
mi_m = 0.14933;
end
end

            %----------------------%

if mat==7 % L Slag %ro=2.645 % Density of the sample [g/cm^3]%x_en= [30 35 40
45 50 60 80 100 150 200 300 400 500 600 800 1000];%v_mi= [2.8873 1.9 1.3376
0.99276 0.77023 0.51427 0.30434 0.22462 0.15579 0.13119 0.10815 0.095316
0.086421 0.079639 0.06969 0.062537];
x_en=[30 35 40 45 50 55 60 65 70 75 80 85 90 95 100 110 120 130 140 150 200
300 400 500 600 800 1000];
v_mi=[2.8873 1.9 1.3376 0.99276 0.77023 0.61962 0.51427 0.43773 0.38099
0.33781 0.30434 0.2778 0.25643 0.239 0.22462 0.2023 0.18594 0.17349 0.16371
0.15579 0.13119 0.10815 0.095316 0.086421 0.079639 0.06969 0.062537];

if energy<150
A=0.0935;
B=-0.4211;
C=-3.292;
D=13.46;
end

if energy>150
A=-0.023;
B=0.433;
C=-3.167;
D=6.022;
end
```

```
if energy == 150
mi_m = 0.15579;
end
end

            %----------------------%

if mat==8 % Water %ro=1.000 % Density of the sample [g/cm^3]
x_en=[30 35 40 45 50 60 80 100 150 200 300 400 500 600 800 1000];
v_mi=[0.37808 0.30952 0.27011 0.24513 0.22824 0.20686 0.18425 0.17113 0.15067
0.13711 0.11866 0.10614 0.096845 0.89541 0.078607 0.070644];

if energy<150
A=-0.2567;
B=3.54;
C=-16.56;
D=24.49;
end

if energy>150
A=7.263e-05;
B=-0.0478;
C=0.1627;
D=-1.517;
end

if energy == 150
mi_m = 0.15067;
end
end

% 4. Calibration material: 4M HCl
ro_cal=1.059;
x_en_cal=[30 35 40 45 50 60 80 100 150 200 300 400 500 600 800 1000];
v_mi_cal=[0.66261 0.48741 0.38816 0.32701 0.28709 0.23968 0.1966 0.1763
0.1507 0.13599 0.11712 0.10458 0.095361 0.088137 0.077348 0.069501];

if energy<150
A_cal=-0.2998;
B_cal=4.347;
C_cal=-21.38;
D_cal=33.82;
end

if energy>150
A_cal=-0.002213;
```

```
B_cal=0.000239;
C_cal=-0.1725;
D_cal=-0.757;
end


if energy == 150
mi_m_cal = 0.1507;
end
%Lia_cal = ismember(energy, x_en_cal);
%Lia=ismember(energy, x_en);
%if Lia_cal==1
%mi_m_cal=interp1(x_en_cal, v_mi_cal, energy);
%else

if energy ~= 150
mi_m_cal=exp(A_cal*log(energy)^3 + B_cal*log(energy)^2 + C_cal*log(energy) +
D_cal);
end
%end
%if Lia==1
%mi_m=interp1(x_en, v_mi, energy);%it takes the v_mi for the corresponing
energy
%else


if energy ~=150
mi_m=exp(A*log(energy)^3 + B*log(energy)^2 + C*log(energy) + D);% it
calculates the μ
end
%end
mi_cal=mi_m_cal*ro_cal; % this multiplies the μ with density
mi=mi_m*ro; % this multiplies the μ with density

% 6. Integral method
J_cal=integral2(@(x,y)(y.*exp(-
mi_cal.*(x.*(y.^2+(x+d).^2).^1/2)./(x+d))))./(y.^2+(x+d).^2),0,t,0,r);
J=integral2(@(x,y)(y.*exp(-
mi.*(x.*(y.^2+(x+d).^2).^1/2)./(x+d))))./(y.^2+(x+d).^2),0,t,0,r);
ECF=J/J_cal;

app.EFCEditField.Value=ECF;
app.MassAttenuationCoefficientEditField.Value=mi_m;
app.EIDcmEditField.Value=de;
```

--- Τέλος εγγράφου ---